Daniela Friedl, BSc

Deep-seated gravitational slope deformations and their possible influence on the drainage system - Examples from the Niedere Tauern Range, Austria

MASTER'S THESIS

to achieve the university degree of

Master of Science

Master's degree programme: Earth Sciences

submitted to

Graz University of Technology

Supervisor

Univ.-Ass. Mag. Dr.rer.nat. Gerfried Winkler

Institut of Earth Sciences (University of Graz)

Graz, March 2017

AFFIDAVIT

I declare that I have authored this thesis independently, that I have not used other than the declared sources/resources, and that I have explicitly indicated all material which has been quoted either literally or by content from the sources used. The text document uploaded to TUGRAZonline is identical to the present master's thesis.

_____
Date

_____
Signature

ACKNOWLEDGEMENT

ABSTRACT

Deep-seated gravitational slope deformations (DSGSD) gained in importance in the past and were often focus of scientific research. For this reason they were chosen as the superior issue of this master thesis. The first aim of this work was to detect existing DSGSDs throughout the entire styrian part of the Niedere Tauern Range and to collect information concerning factors which influence DSGSDs. Water in general is often discussed as triggering factor, though still research is required according to the influence of mass movements, in particular DSGSDs, on the drainage system. Thus, the second objective focusses on the creation of data which give an approach concerning this complex question. As local test sites 4 examples of DSGSDs within the Niedere Tauern Range were chosen. Based on a digital elevation model with a resolution of 1 m (airborne laserscan (ALS) – data) the DSGSDs were marked within a GIS platform to blend and analyse the obtained information with parameters/informations such as lithology, maximum glacier extent or elevation data. The investigation was supplemented with information acquired by field work in 4 local test sites. Within the regional investigation area 135 DSGSDs, exceeding 0.3 km² in extent, were detected. The results of the analysis reveal that rock properties are more important regarding the formation of DSGSDs than glacial processes. Furthermore, it was determined that the length/width ratio correlates with the increase of the area and therefore a law of proportionality exists between the area and the elongation. Concerning the influence of the DSGSDs on the drainage system it was observed that springs within 3 of 4 local test sites preferentially occur as spring horizons in the intermediate and lower part of the DSGSD. Within the fourth DSGSD the spring horizons are situated in the upper and intermediate part. Thus, it can be assumed that the underground condition of 3 of 4 DSGSDs are similar while the 4th DSGSD shows a different internal structure.

ZUSAMMENFASSUNG

Tiefgreifende Massenbewegungen wurden in der vergangenen Zeit immer wichtiger und oft Ziel von wissenschaftlichen Untersuchungen. Aus diesem Grund wurden sie als übergeordnetes Thema dieser Masterarbeit gewählt. Das erste Ziel dieser Arbeit war es, vorhandene tiefgreifende Massenbewegungen der steirischen Niederen Tauern flächendeckend zu erheben und Informationen in Bezug auf Faktoren, die die Bildung solcher Hangdeformationen beeinflussen, zu ermitteln. Wasser im Allgemeinen ist als Auslöser für Massenbewegungen ein viel diskutiertes Thema, jedoch ist noch großer Forschungsbedarf betreffend des Einflusses von Massenbewegungen, im Speziellen tiefgreifende, auf das Entwässerungssystem. Deshalb konzentriert sich der zweite Bearbeitungsschwerpunkt auf die Erstellung von Daten, die einen Ansatz in Bezug auf diese komplexe Fragestellung liefern. Als lokale Bearbeitungsgebiete wurden 4 Beispiele von tiefgreifenden Massenbewegungen innerhalb der Niederen Tauern gewählt. Basierend auf einem Höhenmodell mit 1 m Auflösung (airborne laser scan (ALS) – Daten) wurden die Massenbewegungen in einer GIS Plattform ausgewiesen und in weiterer Folge mit den Parametern/Informationen wie z.B. der Lithologie, Gletscherhochständen oder Höheninformationen verschnitten und analysiert. Ergänzt wurden die Untersuchungen durch Geländeaufnahmen der 4 lokalen Testgebiete. Es wurden innerhalb des regionalen Untersuchungsgebiets 135 tiefgreifende Massenbewegungen mit einer Mindestfläche von 0.3 km² erhoben. Die Ergebnisse der Analyse ergaben, dass Gesteinseigenschaften hauptsächlich für das Auftreten von tiefgreifenden Massenbewegungen verantwortlich sind und glaziale Prozesse eine untergeordnete Rolle spielen. Des Weiteren konnte festgestellt werden, dass das Längen-Breiten-Verhältnis mit der Zunahme der Fläche korreliert und dementsprechend eine Gesetzmäßigkeit zwischen der Größe und Längenausdehnung feststellbar ist. In Bezug auf den Einfluss der Massenbewegungen auf das Entwässerungssystem kann festgestellt werden, dass die Quellen in den 4 Testgebieten vorwiegend in Form von Quellhorizonten bei 3 der 4 lokalen Testgebiete im unteren bzw. mittleren Bereich der Massenbewegungen auftreten. Bei der vierten Massenbewegung liegen die Quellhorizonte im oberen und mitteleren Bereich. Aufgrunddessen kann vermutet werden, dass der Untergrundaufbau von 3 der 4 Massenbewegungen ähnlich ist, während die vierte Massenbewegung eine andere interne Struktur aufweist.

TABLE OF CONTENTS

1. LIST OF ABREVIATIONS

ALS	Airborne Laser Scan
Area	horizontal projection of the area
BP	before present
DEM	Digital Elevation Model
DSGSD	DSGSD
LGM	Last Glacial Maximum
m.a.s.l.	meters above sea level
MPa	Megapascal
RoT	Rottenmanner Tauern
ScT	Schladminger Tauern
SeT	Seckauer Tauern
UCS	Unconfined (Uniaxial) compressive strength
WoT	Wölzer Tauern

2. **INDRODUCTION**

Mass movements in their entirety have been a long time focus of many researches. Many classification systems were introduced e.g. by Varnes in 1978 (Cruden and Varnes 1996) which was further developed concerning additional factors such as the rate of movement (Cruden and Varnes 1996) and is still in use by the U.S. Geological Survey (U.S. Geological Survey 2004). In the year 2014, a further development of this classification was introduced by Hungr et al.

The main purpose of such classification systems was not only to find a universally valid way to accurately describe mass movements but also to estimate the hazard risk regarding the safety of the resident population and infrastructure (Hermann 1996). It is evident that loss of human lives and properties caused by mass movements still happen.

The triggering factors for such phenomena are various, to just name one of the problems with the estimation of possible occurrences of mass movements. These factors include seismicity (e.g. earthquake in Nepal 2015), volcanic activity (e.g. eruption of Mt. St. Helens 1980), heavy rainfall events and changes of the groundwater level and therefore alterations of the flow-pressure and the capillary force within the underground (e.g.: Lang, et al. 2007; Zezere, Trigo and Trigo 2005; Zangerl, et al. 2008). Anthropogenic influences also have to be taken into account according the triggering of mass movements. For example, the construction of embankments can change the stable conditions of a slope to a metastable or even worse, to an unstable state.

These examples underline the fact that much research work is still necessary to understand the possible occurrence, the influencing factors, the kinematic and the formation of DSGSDs.

Therefore the first focus of this master thesis is on the existence of DSGSDs (in the following DSGSD) within the Niedere Tauern Range. The first aim of this research is to create an inventory map of existing mass movements of this specific type.

As Hermann (1996) in his publication in course of the international symposium INTRAPRAEVENT mentions, is the fact that DSGSDs are directly and indirectly a potential source of hazard for population and infrastructure. This risk of hazard refers to the possibility that DSGSDs, which are characterized by a very low rate of movement (Ambrosi and Crosta 2006; F. Agliardi, et al. 2013), can turn into catastrophic mass movements (Dramis and Sorriso-Valvo 1994; Hermann 1996). Although DSGSD marked as relict and mostly assumed to be at least metastable or stable under the rectent climate conditions, deformations at infrastructures as dams are occurring due to displacements of about 1 cm/year (Crosta, et al 2013).

Furthermore, existing DSGSDs can induce secondary slope failures (Ambrosi and Crosta 2011; Hermann 1996; Agliardi, Crosta and Zanchi 2001).

As mentioned above, water is the most often mentioned trigger for mass movements in general (Zezere 2000). Various ways exist how water can be responsible for slope failures. Rainfall in particular is very well investigated and it is proven that especially the durance of rainfall events is an influence factor concerning the type of slope failure which is forming (Zezere 2000). Futhermore, increasing and decreasing flow pressure within the ground in particular in relation with water reservoirs due to lowering and rising the water table within the reservoir (Lang, et al 2007) can further induce landslides. Increasing pore water pressure caused by infiltrating water (precipitation, snowmelt, rising water table) and therefore a decrease in effective stress within the ground is named also as triggering factor (Maatsura, et al 2008; Huang, et al 2012). In the meanwhile monitoring programmes with the purpose to observe the behaviour of landslides especially concerning the reactivation of already existing landslides are not uncommon anymore and often described within existing literature (Zezere 2000; Huang, et al 2012).

Water as triggering factor of mass movements is already very well investigated but still large gaps exist in the knowledge of the influence of mass movements, especially DSGSDs, on the drainage system. Thus, the second aim of this master thesis focusses on the creation of data which give a approach concerning the possible influence on the underlying drainage system. On this specific issue is barely any information available at the current state of research. To gain a basic understanding in relation to this question, data has to be acquired in the first step and further set into a context. Based on this data, an attempt is to create a relationship between deep-seated gravitational movement and the underlying drainage system.

3. MASS MOVEMENTS

3.1. CLASSIFICATION OF MASS MOVEMENTS

Many classification systems for mass movements or landslides were introduced in the past by several authors. The most common classification was proposed by Varnes in 1978 and was further developed by Cruden & Varnes in 1996. The considered definition for landslides: "*the movement of mass of rock, debris or earth down a slope*" was introduced by Cruden (1991, 27). The classification is based on the involved material and the type of movement. For a more detailed description, further properties such as water content or the rate of movement can be taken into account.

Table 1: The table presents the developed classification system by Hungr et al. (2014) which was modified after Cruden and Varnes (1996). The red rectangle marks the category of deep-seated gravitational slope failures.

Type of movment	Rock	Soil
Fall	1. Rock/ ice fall	2. Boulder / debris /silt fall
Topple	3. Rock block topple 4. Rock flexural topple	5. Gravel/sand/silt topple
Slide	6. Rock rotational slide 7. Rock planar slide 8. Rock wedge slide 9. Rock compound slide 10. Rock irregular slide	11. Clay/silt rotational slide 12. Clay/silt planar slide 13. Gravel/sand/debris slide 14. Clay/silt compound slide
Spread	15. Rock slope spread	16. Sand/silt liquefication spread 17. Sensitive cly spread
Flow	18. Rock/ice avalanche	19. Sand/silt/debris dry flow 20. Sand/silt/debris flowslide 21. Sensitive clay flowslide 22. Debris flow 23. Mud flow 24. Debris flood 25. Debris avalanche 26. Earthflow 27. Peat flow
Slope deformation	28. Mountain slope deformation 29. Rock slope deformation	30. Soil slope deformation 31. Soil creep 32. Solifluction

Hungr, et al (2014) further developed this classification and considers a new system where deep-seated gravitational mass movements are designated as rock flow and can be further differentiated into mountain slope deformations and rock slope deformations (Compare Figure 1). The only difference between the subgroups of slope deformations is the scale of the occurring phenomenon. This classification system is therefore applicable for large sale gravitational slope deformations which are the focus of this work. These are described in detail in the following chapter.

3.2. DEEP-SEATED GRAVITATIONAL SLOPE DEFORMATIONS (DSGSDS)

Since the beginning of the 20th century, DSGSDs gained more and more attention (Crosta 1996). Examples include Ampferer (1939, 1940), Zischinsky (1969a, 1969b) and Hutchinson (1988) who focused on this type of mass movement, to name a few researchers. They tried to characterize and name this phenomenon. Hutchinson (1988) even tried to create a classification which includes DSGSDs as a separate form of mass movement. Although DSGSDs gained in importance within the last century, no universally applicable definition and terminology exist. Within the proposed definitions no clear demarcation was created between DSGSDs and landslides. (Crosta 1996)

Therefore within this work, a DSGSD is referred to as a mass movement which is characterized with relatively low displacement rates of a few millimeters up to tens of meters per year (Ambrosi and Crosta 2006; Crosta et al. 2013; Cruden and Varnes 1996), a huge volume of involved material and "*the lack of a single clearly defined failure plane*" (Kellerer-Pirklbauer et al. 2010, 66). The extent of the affected area can reach up to several square kilometers (Kellerer-Pirklbauer et al. 2010).

Figure 1: Classification of mass movements after their rate of movement corresponding to velocities (modified after: Zangerl et al., 2008 and Cruden and Varnes, 1996)

As mentioned above, they became a greater focus of researchers in the past due to the availability of more accurate datasets and advanced investigation tools. With these new tools it was recognized that DSGSDs occur more often than considered in the past. (Agliardi, et al. 2013)

Features which are representative of this type of mass movement are multiple ridges (Figure 2), trenches, scarps, uphill facing scarps and half-grabens which are usually dominant in the upper sectors of the slope (Agliardi, et al. 2013; Crosta 1996; Agliardi, Crosta and Zanchi 2001). The headscarp can be located in front or behind the crestline (Hutchinson 1988). In the intermediated part, counterscarps are typical (Crosta 1996), while bulging, buckling folds and enhanced rock fracturing are

Figure 2: Double ridge of the DSGSD Kleinsölk. Viewing direction from summit Zinken to Ebeneck (SW to NE)

characteristic for the slope toe (Crosta 1996). A flexural structure which occurs within the slope is as well often described in the literature. The bulging slope toe is often designated in the specific technical literature as *Talzuschub* (Zischinski 1969b from: Crosta 1996). For the middle part which often shows a concave form is in the literature often designated as *Sackung,* or *sagging* in English (Agliardi, et al. 2013; Hutchinson 1988). For better understanding compare Figure 4.

In some cases, particularly in weak rock masses, secondary landslides are present instead of the outward bulging toe (Agliardi, et al. 2013).

Further typical for DSGSDs is that the size of a DSGSD often equates to the size of the slope or is at least comparable to it (Agliardi, et al. 2001).

The formation of DSGSDs is considered to start at the slope toe caused by stresses which are suggested to be the greatest within this zone. A basal shear zone, which can be located in several 10 to 100 meters depth, will be formed. The thickness of such a shear zone can reach up to tens of meters (Crosta, et al. 2013; Strauhal, et al. 2016). This was observed e.g. at the DSGSD Klasgarten located at the Kaunertal (Tyrol) by data aquired from boreholes and the purpose built observation tunnel (Strauhal, et al. 2016). Neveretheless it is believed that the shear zones are not occuring in a distinct way.

As mentioned in the introduction, DSGSDs can induce secondary and even tertiary mass movements (Ambrosi and Crosta 2011; Hermann 1996; Agliardi, Crosta and Zanchi 2001). This segmentation is caused by the formation of further shear zones within the primary phenomenon. Within this context it is important to take into account that these segments are possibly active, although the primary DSGSD shows no further activity. (Zangerl 2017)

In the literature, many different triggering factors are suggested. These factors include deglaciation of glacial influenced valleys, topographic and tectonic stresses as well as seismic events (Agliardi, et al. 2013). These factors are described in more detail in the following.
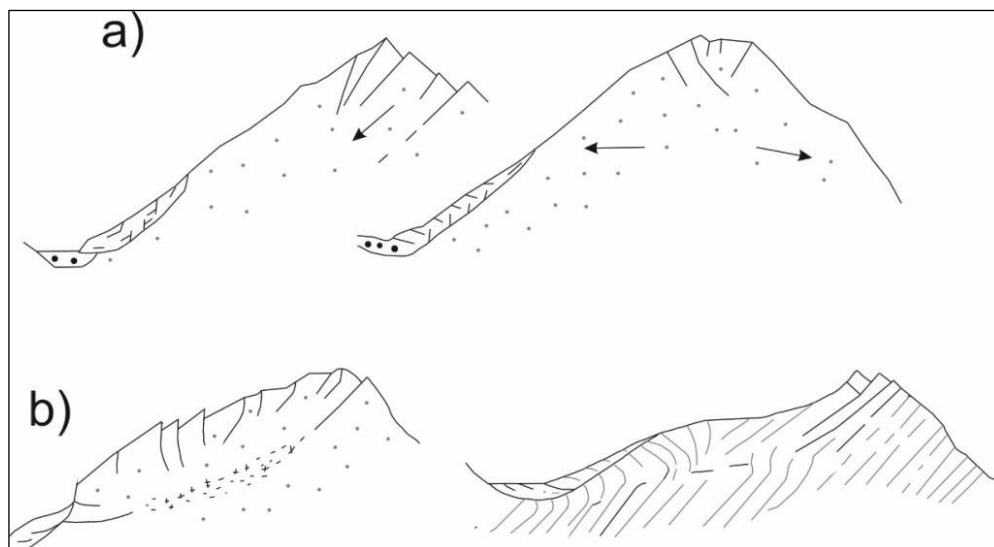
Figure 3: Examples of deep-seated slope failures. a) Initial and b) advanced stages (modified after: Nemcok 1972)

Hermann (1996) introduces and describes furthermore the different stages of the development of DSGSDs. He considers three stages - an initial state, a more developed stage and a final "mature" stage. According to Hermann (1996) each of these shows specific features which distinguish them from each other. They are described as follows:

(1) Initial stage: well developed headscarp, missing bulging slope toe, already distorted bedrock within the loosened material of the mass movement; Figure 3
(2) Developed stage: distinct double ridges often with offsets of 50 m and more, initial segmentation of the mass movement, the bulging slope toe is already slightly visible; Figure 3
(3) Final "mature" stage: typical pattern of the classical *Sackung;* heavy distorted bedrock as completely loosened material; shows typical concave-convex appearance by missing material in the upper part and excess material in the toe segment (bulging slope toe); Compare Figure 4.
(Hermann 1996)
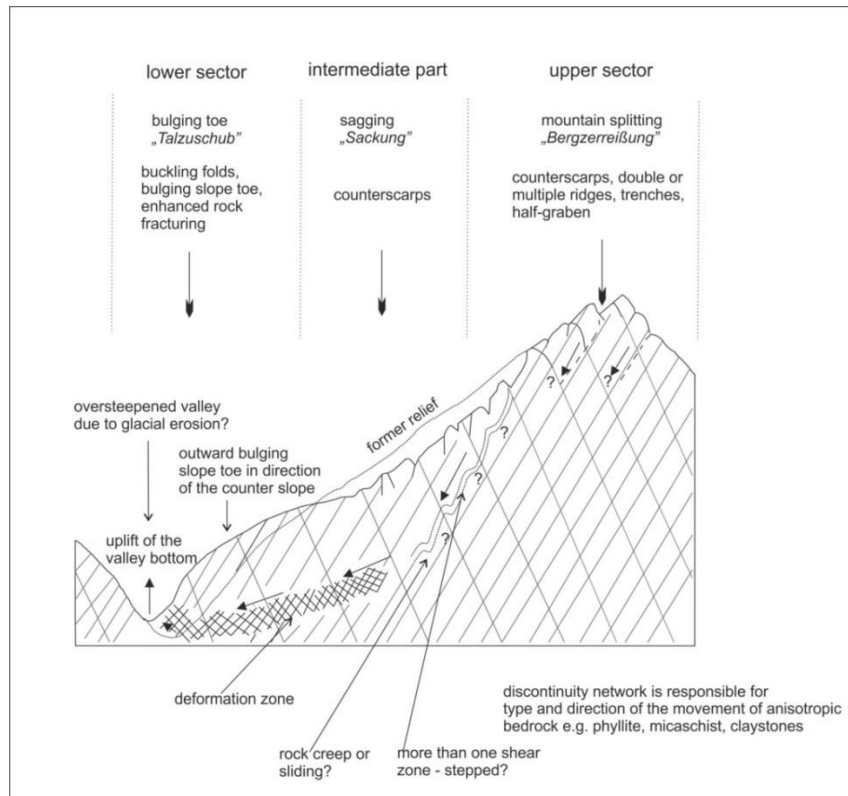
Figure 4: Schematic representation of the morphologic features of a DSGSD in final stage (modified after: Weidner, Moser and Lang, 2011)

According to the data acquired by Strauhal, et al. (2016) it can be assumed that in general, the moved material within a deep-seated gravitational mass movement has a higher hydraulic conductivity than the underlying bedrock due to the heavy disintegration of the moved rocks. The basal shear zone is assumed to have a very low value for hydraulic conductivity caused by the occurrence of fault gauge and / or fault breccia, which is characterized by a higher amount of fine components, such as clay or silt. Caused by the confining properties, the infiltrated water would move along fractures but atop of the shear zone in a downwards movement. (Strauhal, et al. 2016; Crosta, et al. 2013)

The possible groundwater flow within DSGSDs was assumed by Crosta, et al (2013) by performing a steady-state finite model simulations. The aim was to distinguish possibilities of groundwater flow caused by differences in the formation of shear zones. An ideal slope and disingtegrated rock masses within the DSGSD as well as shear zones which were characterized by low permeabiltiy were the model framework. The results are displayed in Figure 5.
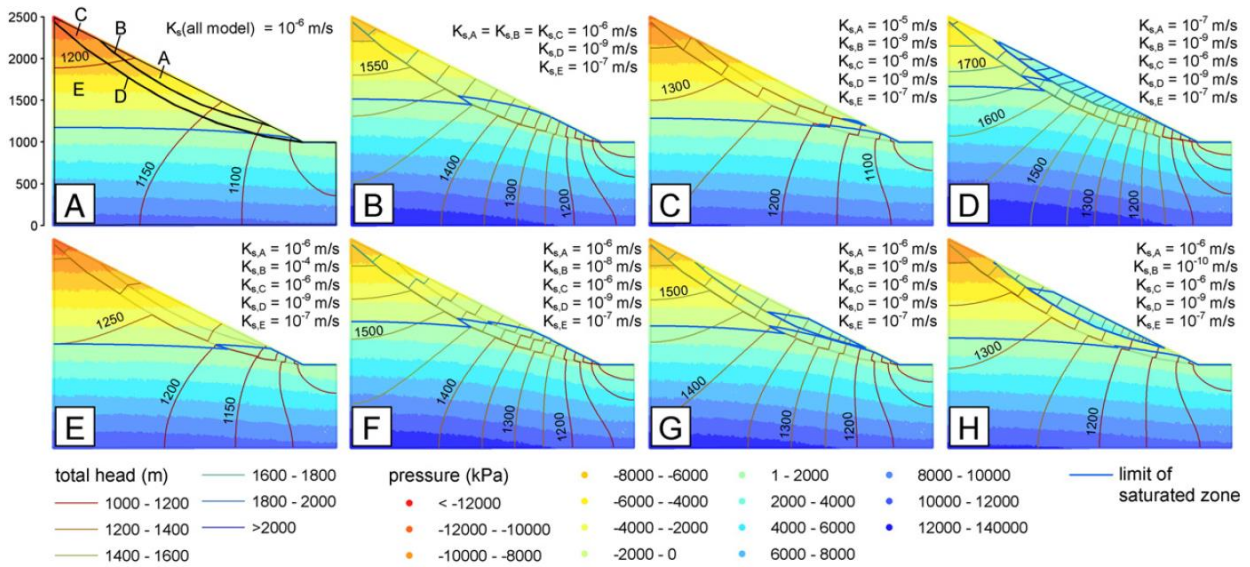
Figure 5: Results of the model simulation concerning the groundwater flow within DSGSDs performed by Crosta, et al. (2013) – A: homogeneous underground with two shearzones; B – one shear zone; D to G – two shearzones, varying values for hydraulic conductivity (K-values within the figure) within area A (compare model A). E to H have as condition varying hydraulic conductivity in zone B (compare model A) and two shear zones again.

Based on the results obtained by the simulation Crosta, et al (2013) considered that "*the presence of low permeable shear bands causes the formation of complex and superimposed groundwater tables.*" (Crosta, et al 2013, 15) Therefore, the groundwater regime depends mainly on the hydraulic conductivity of the involved shear zones.

3.3.   FACTORS PROMOTING AND TRIGGERING SLOPE INSTABILITIES

To make a proper statement regarding the probability of the occurrence of a slope failure, it is fundamental to understand the underlying kinematics and factors which provoke instabilities.

Glade and Crozier (2005) consider three types of factors which promote the destabilizing of slopes and therefore slope failures. These are "*preconditioning, preparatory and triggering factors*" (McColl 2012, 6 from: Glade and Crozier 2005). These are listed in Table 2. The underlying concept is displayed in Figure 6.
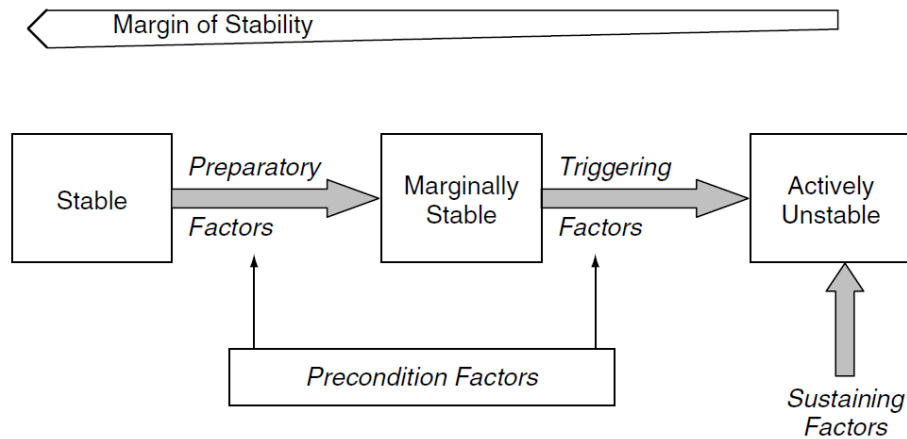
Figure 6: Concept of preconditioning, preparatory and triggering factors according to stability states (Glade and Crozier, 2005 after: Crozier, 1989)

Preconditioning factors are identified as properties which are inherent and inactive and can be understood as a form of catalyst (Glade and Crozier 2005). Preparatory factors are influencing over a long time and consequently reducing the stability of the slope. They are not meant to activate movement, but to be responsible for the change of the stability state from stable to marginally stable (Glade & Crozier, 2005; Figure 6). Triggering Factors are per definition processes which initiate the slope failure. (Glade and Crozier 2005; McColl 2012)

Table 2: Preconditioning, preparatory and triggering factors (modified after McColl, 2012 from Glade and Crozier, 2005)

	Factors	Preconditioning	Preparatory	Trigger
	Lithology	Always		
	Intact rock strength	Always		
	Rock mass quality	Always		
	Joint characteristics	Often		
	Structure (e.g. bedding)	Often		
	Pre-glacial erosion	Often		
	Pre-existing stresses	Often		
	Debuttressing		Sometimes	Sometimes?
	Glacial erosion		Often	Unknown
	Sheet jointing		Often	Often
	Static fatigue		Always	Unknown
	Seismicity		Unknown	Often
Climatic change	Water		Unknown	Often
	Permafrost		Sometimes	Often?
	Weathering		Always?	Unknown

The main message of this concept is that mass movements seldom have one specific cause. It is mostly a combination of influencing factors and processes. Hence it is important to take more than the obvious triggering factor into account. (McColl 2012)

The following describes the causes and triggering factors in more detail which is discussable according to the available data which are collected in course of this master thesis.

3.3.1. GLACIAL EROSION AND DEBUTTRESSING

The present geomorphologic appearance of areas, which were affected by glaciation, was formed by glacial / interglacial cycles during the Quaternary. Therefore the definition of "paraglacial" by Ballantyne (2002, p.1938) is appropriate. He defines it as "*nonglacial earth-surface processes, sediment accumulation, landforms, landsystems and landscapes that are directly conditioned by glaciation and deglaciation.*" (Ballantyne 2002 1938)

In different publications, the retreat of glaciers is believed to be a triggering factor of rock slope instabilities (Ballantyne 2002; McColl 2012). However, Crosta, et al. (2013) considers that glaciation and deglaciation processes are merely a preparatory factor and its effect is minor in relation to the influence of rock erosion.

Ballantyne (2002) considers three different modes as a consequence of loss of mass of former glaciers. These are "(1) *large-scale, catastrophic rock slope failure, […]; (2) large-scale rock mass deformation in form of progressive slow movements […]; and rapid adjustment of rock faces by frequent discrete rockfall events*" (Ballantyne 2002, 1938). Therefore DSGSDs are part of the second postulated mode.

Due to deglaciation, landscapes are exposed which are susceptible to changes (Ballantyne 2002). Examples for influencing factors include ice mass distribution, glacial erosion, seismicity, and others (McColl 2012). In mountain ranges the retreat of glaciers result in the exposure of U-shaped oversteepened valleys or steep rock walls. (Ballantyne 2002; D. Van Husen 1987)

Two kinds of effects of rock slopes on glaciation and deglaciation processes are considered. The first takes the increasing self-weight of oversteepened slopes into account. Due to this weight tensile stresses are occurring at the toe of the slope. According to this stress condition, slope failures along pre-existing joint sets or new occurring zones of weakness are possibly forming. (McColl 2012; Ballantyne 2002)

The second describes effects due to the loss of weight which was formerly brought up by the ice cover. This results in the loss of support of the former glacier and therefore leads to stress-release of the underground. This effect is often named as *debuttressing* in literature. Hence within the rock mass, internal stress-relaxation occurs and joint sets propagate and therefore cause rock damage (Ballantyne 2002; McColl 2012; Cossart, et al. 2008). The concentration of

rock damage is localised mainly at the slope toe caused by the highest stress level due to loading by ice masses. (Cossart, et al. 2008)

3.3.2. INFLUENCE OF THE VALLEY SHAPE

According to a numerical modelling performed by Ambrosi and Crosta (2011), the valley shape has a relevant influence on the formation of DSGSDs. They showed that the development of DSGSDs is also controlled by the existing geometry of the valley (main or tributary) in combination with the orientation of structural features such as schistosity or bedding planes. Unstable slopes according to the numerical models mostly have planes of anisotropy which are oriented subvertical to vertical. (Ambrosi and Crosta 2011). Compare Figure 8.

"*Linear slope profiles with constant inclination are less unstable than broken slope profiles*" (Ambrosi and Crosta 2011, 229). The so called broken profiles describe slopes which show different inclinations along the slope. This is typical for valley affected by glacial erosion or as suggested, successive phases of erosion. Not only superimposed glacial erosional processes can form broken profiles, but also a rapid incision by river erosion, for example, can possibly lead to such phenomena (Ambrosi and Crosta 2011). As mentioned above (Chaper 3.3.1), U-shaped oversteepened valleys were formed due to glacial erosion (Ambrosi and Crosta 2011; Van Husen 1987; Ballantyne 2002). The U-shape is a result of broadening at the bottom due to higher erosion rates along the valley sides (after Harbor 1995, 1992 in Ambrosi and Crosta 2011).
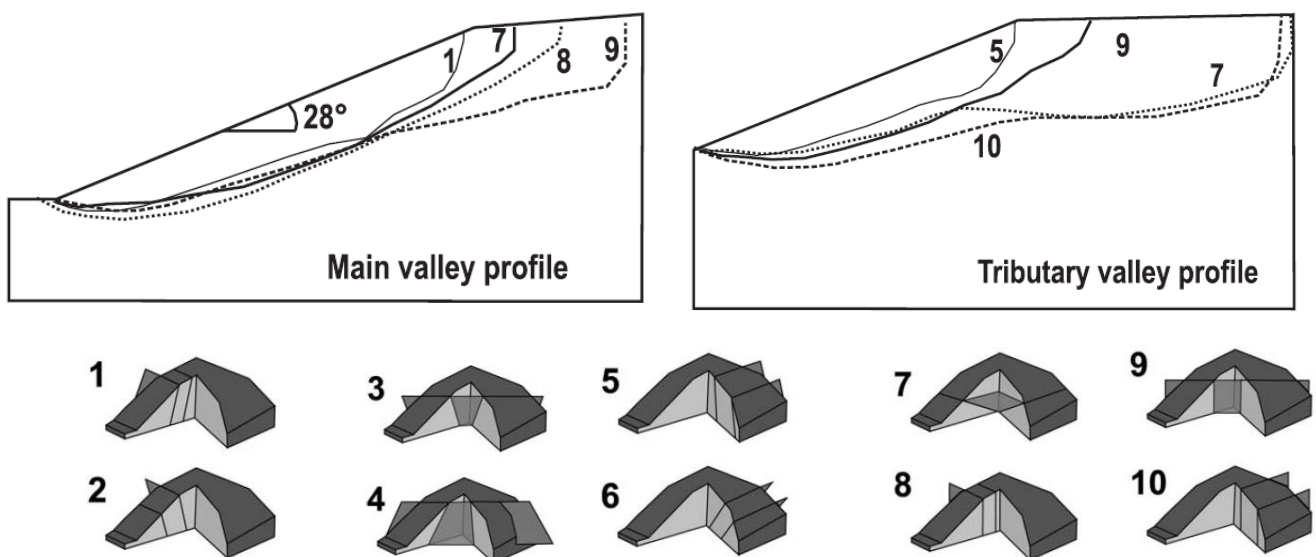

Figure 7: Schematic sketch of the influence of the different orientations of anisotropy planes. The isocontour lines refer to the result of some models of the numerical simulation. (From Ambrosi & Crosta, 2011)

3.3.3. DEGRADATION OF PERMAFROST AND PORE WATER PRESSURE

Water in the form of cleft and / or pore water which is permanently frozen is referred to as permafrost. It occurs mostly in areas of higher altitude, for example within the Alps. The degradation of this phenomenon due to warmer climatic conditions is considered to influence the formation of mass movements. (McColl 2012; Kellerer-Pirklbauer, et al. 2010)

Permafrost is responsible for higher bonding action within the soil and rock mass and therefore a higher rock strength. Because of the warmer conditions while deglaciation periods the lower permafrost level (altitude) rises. Below this level the rock strength decreases and discontinuity networks possibly develop caused by mechanical wheatering due to alternating thaw and frost conditions. (McColl 2012)

Joint networks and existent discontinuities not only weaken the intact rock and provide possible zones of weakness where slope failures can occur. Due to their persistence and aperture they form possible pathways for water and therefore for erosional and weathering processes. Thus, pore water pressure can develop due to rainfall events and melting of snow and ice for example. Different types of joints can be present within an intact rock mass. They are differentiated according to their origin as are tectonic processes for example. (McColl 2012)

3.3.4. ROCK MASS CHARACTERISTICS

Rock slope failures are not just dependent on external processes but also on the involved rock mass. Properties such as lithology and its specific geomechanic properties, existing discontinuities (e.g. joints, schistosity and foliation) and their corresponding properties, including orientation, roughness and cohesion influence mainly the rock strength. (Ballantyne 2002)

According to these properties, a rock mass can be classified as isotropic or anisotropic. "*Anisotropy is defined as variations of properties with respect to the directions concerned in design and analysis of rock structures*" (Bidgoli and Jing 2014, 156). Rock masses which contain discontinuities such as schistosity, foliation and bedding planes for example are often considered as anisotropic.

Agliardi et al. (2013) determined that DSGSDs occur more often in anisotropic rock masses than in isotropic ones. According to Weidner, Moser & Lang (2011) in anisotropic rocks the discontinuity network determines the type and the direction of movement of the slope deformation. Ambrosi and Crosta (2011) were performing a numerical model by using different input parameters including geological and geomechanical properties. These were related to different valley profiles (main and tributary). The purpose was to determine factors which influence the possible displacement and occurring stress conditions within the ground, the most.

Based on the results of this numerical model, Ambrosi and Crosta (2011) consider that *"most unstable slopes are those containing vertical – subvertical ubiquitous planes."* (Ambrosi and Crosta 2011, 229) Compare Figure 7.
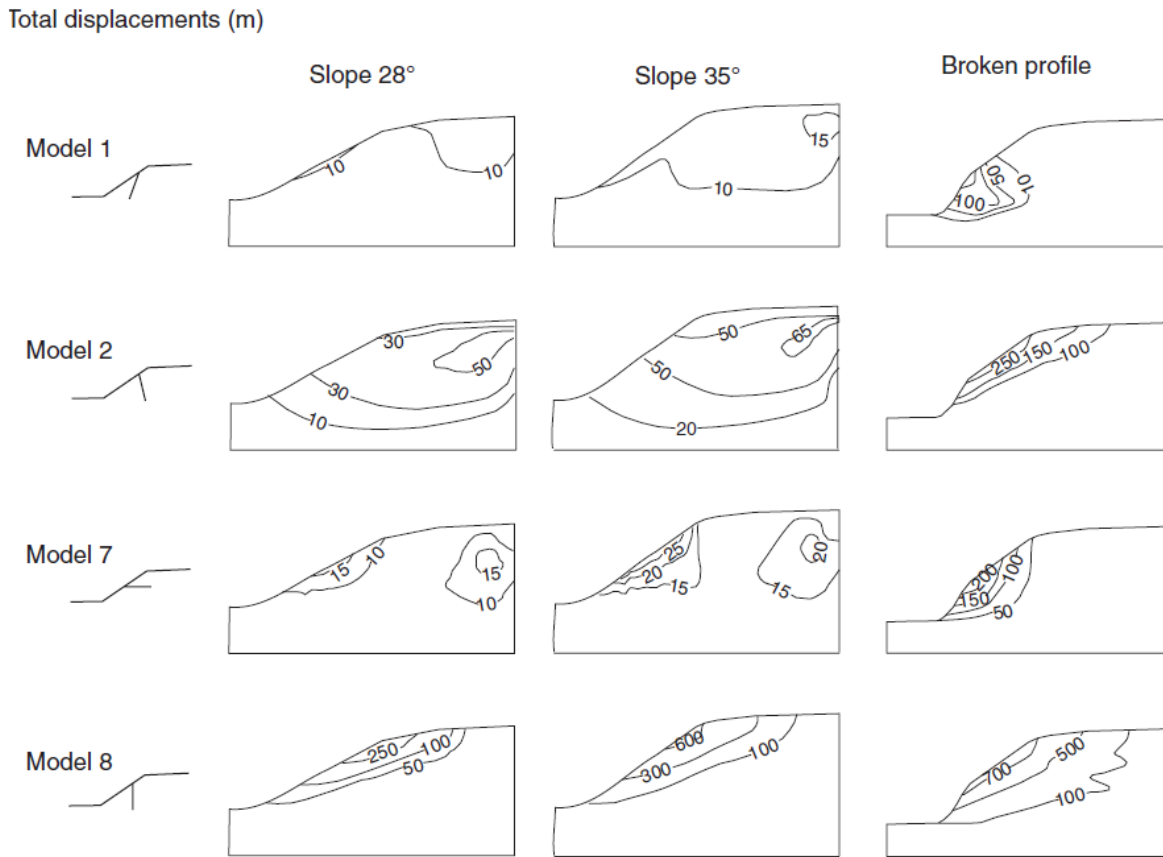
Figure 8: Displacement is presented as isocontour-lines given in [m] as a function of the valley shape and the orientation of the anisotropy planes by varying K-values. The parameter K is referred to as the ratio of vertical to horizontal stresses (from Ambrosi and Crosta, 2011). The models this figures refers to, are presented in Figure 7.

Therefore it can be assumed that rock control is an important factor according to slope instabilities.

The rock strength is commonly expressed as the uniaxial or unconfined compressive strength (UCS), measured in Megapascal (MPa). It is a measure for a material to withstand external stresses from one direction under unconfined conditions. The tensile strength (TS) is related to the UCS and is an indicator for the bonding strength of the components of a material. Both parameters are dependent on the isotropy / anisotropy of the specific material. The tensile strength typically increases if the uniaxial compressive strength of a material increases – although this relation is not linear. (Prinz and Strauß 2006)

$$TS = \frac{UCS}{10} \, up \, to \, \frac{UCS}{25}$$

The UCS which is typically for the in the investigation area existing lithologies are used to classify them according to their rock strength. (Compare chapter 8.4) For lithologies, where no typical values are available within the literature, the UCS can be estimated after Hoek and Brown (1997). The table which is commonly used for field estimations is presented below.

Table 3: Field estimates of UCS modified after Hoek and Brown (1997)

Grade*	Term	UCS [MPa]	Examples
R6	extremely strong	> 250	fresh basalt, chert, diabase, gneiss, granite, quarzite
R5	very strong	100 - 250	Amphibolite, sandstone, basalt, gabbro, gneiss, granodiorite, limestone, marble, rhyolite, tuff
R4	strong	50 - 100	Limestone, marble, phyllite sandstone, schist, schale
R3	medium strong	25 - 50	Claystone, coal, concrete, schist, shale, siltstone
R2	weak	5 - 25	Chalk, rocksalt, potash
R1	very weak	1 - 5	highly wheatered or altered rock
R0	extremely weak	0.25 - 1	stiff fault gauge

* grade (after Brown 1981 in: Hoek and Brown 1997)

4. SPRINGS AND HYDROGEOLOGIC PARAMETERS

4.1. TYPES OF SPRINGS

Springs are generally to be found in locations where groundwater discharges from the underground. The duration of how long the water stayed in the underground is referred to as the residence time. Springs can be classified according to the reason why water discharges at specific locations. Different types of springs are described in the literature (Hölting and Coldewey 2013; Mattheß and Ubell 2003; Bryan 1919). In the course of this master thesis, contact springs, barrier springs and fracture springs are the most important types based on the classification summarized in Hölting & Coldewey (2013). Springs can occur side by side in spring horizons. (Compare Figure 9)

Contact springs (Figure 10-2) occur typically at the border lines between different geologic units. The water table ends naturally according to Hölting and Coldewey (2013) and often forms

—— Isohypsen (groundwater) – – Flowdirection ⚲ Spring
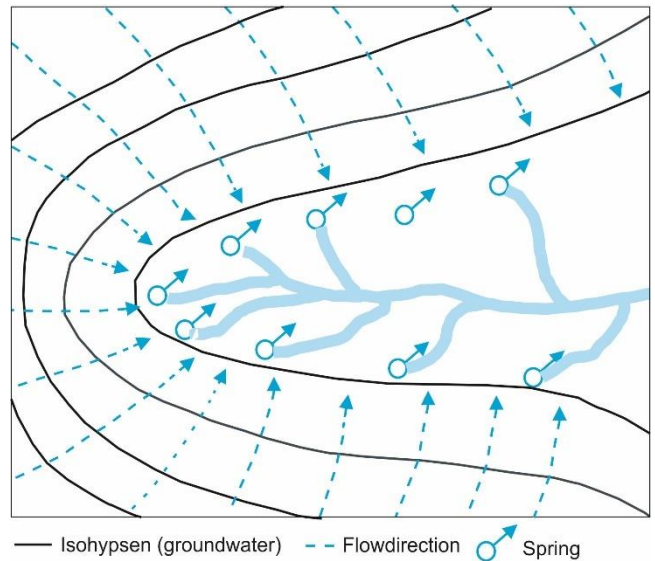
Figure 9: Spring horizon (Modified after Hölting and Coldewey, 2013)

spring horizons. Barrier springs (Figure 10-3, 4) occur if the water encounters layers with a lower hydraulic conductivity. Regarding DSGSDs this can possibly occur where the part where the extension regime dominates (high permeablitiy, disintegrated rock) and the part of compressional regime (lower permeability) coming together. Hence the water discharges at such boundaries. In crystalline areas, fracture springs are also important. The water in the

16
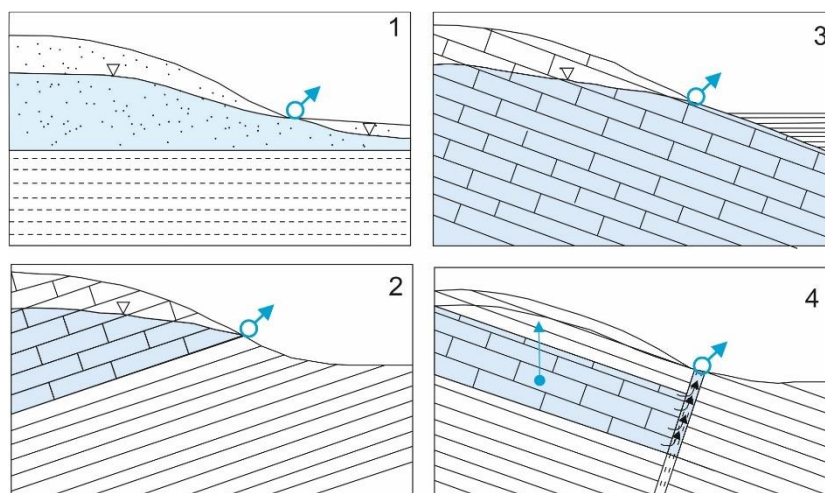
Figure 10: Types of springs. (Modified after Hölting and Coldewey, 2013)
1) springs due to reduction of the crosssection, 2) contact spring, 3) barrier spring, 4) barrier spring due to an existing fault

underground flows along discontinuities e.g. fractures, joints or bedding planes. The water flow within discontinuity networks depend on the specific properties such as persistence, aperture and possible infillings for example. Due to these properties of the discontinuity network, the water discharges at the surface as spring. According to Mattheß & Ubell (2003), the springs discharge in crystalline areas where the porous media (e.g. moraine material, erosion product of the bedrock) which typically overlies the crystalline bedrock ends in steep slope areas.

4.2. HYDROGEOLOGICAL PARAMETERS

To characterize spring water or water in general, several hydrologic field parameters are measured. This includes at least the electric conductivity, the discharge of the spring and the water temperature. Sampling for hydrochemical analysis is often undertaken in addition. The following describes the parameters which are measured within the field investigation in more detail.

4.2.1. ELECTRIC CONDUCTIVITY

The electric conductivity is normally provided in microsiemens (µS) or millisiemens (mS) per centimeter (cm). This value is an indicator for the degree of mineralization and therefore a first impression of the residence time of the water in the ground. Normally, the higher the electric conductivity, the higher the amount of dissolved ions within the water. This is not necessarily valid for fluids showing a high pH-value. Furthermore, a high value for electric conductivity indicates a longer residence time within the ground although the expected values depend on the lithology which the water passed through. Thus, the measured electric conductivity has to set in context with the underlying lithology and geology.

Within the crystalline area of the Niedere Tauern Range, the electric conductivity of springs of rock glaciers lies typically in a range between 20 µS/cm and 70 µS/cm (Untersweg und Schwendt 1995). Higher values indicate the presence of geologic units which contain more soluble rock masses such as marble and limestone. For example within the local test site Hauser Kaibling marble seams (higher soluble) strike through and therefore the electric conductivity shows values >100 µS/cm.

Due the possible influence of meteoric water (precipitiation) a dilution effect can occur. The values for electric conductivity are possibly below the expected values within the investigated area. Therefore it is again an indicator for the residence time of the water within the ground In this case low values indicate that the water hadn't enough time to solve ions from the lithology which was passed through.

4.2.2.   WATER TEMPERATURE

The water temperature is measured in this case in degree Celsius [°C]. It is a method to distinguish between water which circulates through shallow depth and water from deeper ground. Water which passed through shallow depth of the ground reflects the impact of solar radiation on the surface. Caused by thermal conduction the ground is heated up or cooled down depending on the insolation on the surface. This effect influences a depth of up to 20 m. The water temperature of shallow depth reflects this influence and shows in long observation measurements seasonal fluctuations.

Water which passed through deeper ground (deeper than ca. 20 m) shows typically a water temperature of groundwater which is around 5°C. This water temperature stays constant irrespective of the season and therefore solar radiation.

The water temperature has always to set in context to seasonal time respectively the solar insolation while measuring.

4.2.3.   DISCHARGE

The discharge of a spring is a very important parameter and is dependent on the infiltration and the precipitation conditions within the catchment area.

The discharge of a spring or a surficial water channel is usually measured in l/s. To acquire data, different measurement methods are available. During field work, the water flow is usually determined as the water amount (measure beaker) over time (stop watch) or is simply estimated.

The discharge can be perennial or intermittent. Perennial refers to springs or surficial water channels which contain water year-round. If discharge only occurs episodically (e.g. seasonal or after precipitation events) the springs or surficial water channels are designated as intermittent. (Hölting and Coldewey 2013)

5. REGIONAL INVESTIGATION AREA: NIEDERE TAUERN RANGE

5.1. GEOGRAPHIC BOUNDARY AND DIVISION

The Niedere Tauern Range is part of the Eastern Alps in Austria and includes an area of 2438 km². It is located in the northwestern part of Styria and the easternmost area of Salzburg. The small part of the Niedere Tauern Range which is located in Salzburg is neglected within the performed analysis. Therefore for this work the western border is chosen as the federal border between the federal state of Styria and the federal state of Salzburg. The northern border is formed by the Enns Valley in the west, the Liesing Valley and the Palten Valley in the east. The boarder in the east and south until Murau is represented by the Mur Valley.

The Niedere Tauern Range is subdivided from east to west into the Seckauer Tauern, Rottenmanner Tauern, Wölzer Tauern and the Schladminger Tauern. Compare Figure 11.

The surrounding valleys of the Niedere Tauern Range are longitudinal valleys (Enns Valley, Mur
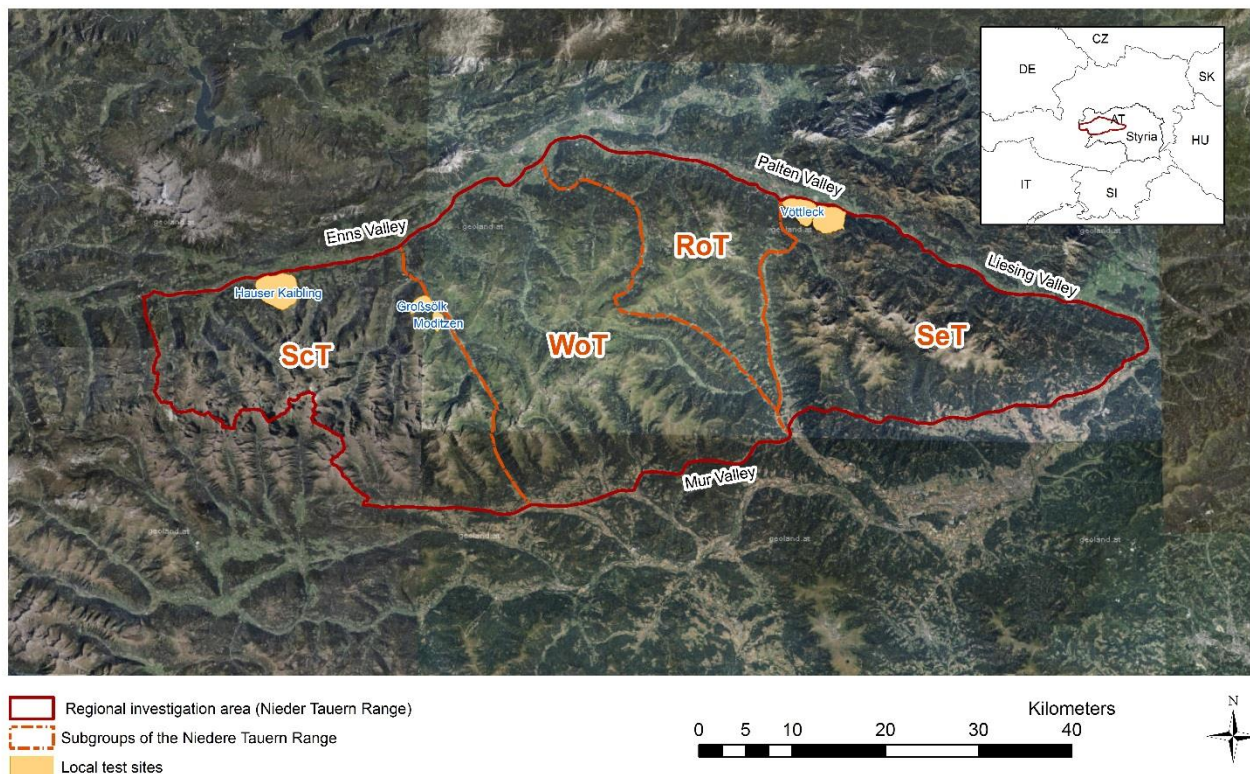

Figure 11: Position and Subdivision of the Niedere Tauern Range. (Map sources: © GIS Steiermark; © EuroGeographics for the administrative boundaries)

Valley). Within the Niedere Tauern Range, the main valleys have an orientation dominating from north to south and form a herringbone pattern.

The elevation generally decreases from west to east. The area of highest elevation is located in the southwest of the Niedere Tauern Range.

5.2. GEOLOGICAL SETTING

5.2.1. TECTONICS AND GENERAL DESCRIPTION

The Niedere Tauern Range is part of the Upper Austroalpine basement nappes (Gaidies, et al. 2006) and of the Greywacke Zone in the north.

The Austroalpine Unit was divided by Tollmann (1977) into three subunits, the Lower, the Middle and the Upper Austroalpine nappes. Therefore the Niedere Tauern Range was part of the Middle Austroalpine. Based on current scientific knowledge, the Austroalpine Unit is divided into the Lower Austrolalpine subunit and the Upper Austroalpine subunit, which now includes the formerly Middle Austrolapine. (Pfingstl, et al. 2015; Froitzheim, Plasienka and Schuster 2008; Schmid, et al. 2004)

The Upper Austroalpine is further subdivided from the structurally highest to the structurally lowest into the Drauzug-Gruktal Nappe System, Ötztal – Bundschuh Nappe System, Koralpe – Nappe System and Silvretta – Seckau Nappe System and

Figure 12: Tectonic sequences of the Upper Austroalpine (UAA) and the Lower Austroalpine (LAA) Nappes (Gasser, et al. 2009)

a Mesozoic cover (Gaidies, et al. 2006; Pfingstl, et al. 2015). The structurally lowermost unit is the Silvretta-Seckau Nappe System (Pfingstl, et al. 2015; Froitzheim, Plasienka and Schuster 2008; Schmid, et al. 2004). It directly overlies the Lower Austroalpine subunit (Froitzheim, Plasienka and Schuster 2008) and can be encountered in the west of the Niedere Tauern

Range as the Schladming complex and in the eastern part as Seckau Complex (Gaidies, et al. 2006; Pfingstl, et al. 2015)

In the south of the Niedere Tauern Range, Koralpe-Wölz Nappe System lies structurally above the Silvretta-Seckau Nappe System (Pfingstl, et al. 2015). According to Schmidt et al. (2004) it represents a metamorphic extrusion wedge correlated with an Eo-Alpine event. The Koralpe-Wölz Nappe System is disclosed as Wölz Complex in the central area (Gaidies, et al. 2006) and the Rappold-Complex in the southeast part of the Niedere Tauern Range. Corresponding to Pfingstl et al. (2015) the grade of metamorphosis can reach from diagentic conditions at the top to epidote-amphibolite facies at the bottom of the pile. Therefore the highest grades of metamorphosis occur in the Koralpe-Wölz Nappe System of the Upper Austroalpine subunit. In the north, the geologic units reach up to lower-greenschist-facies.

In the north of the Niedere Tauern range, the Silvretta-Seckau Nappe System is overlain by rock masses of the Noric Nappe which can be assigned to the Greywackezone. These lithologies mainly consist of sediments of Paleozoic age siliciclastic development which can reach up to greenschist-facies. (Pfingstl, et al. 2015; Gasser, et al. 2009)

The geologic Nappes are displayed in Figure 13, the vertical arrangement in Figure 12.
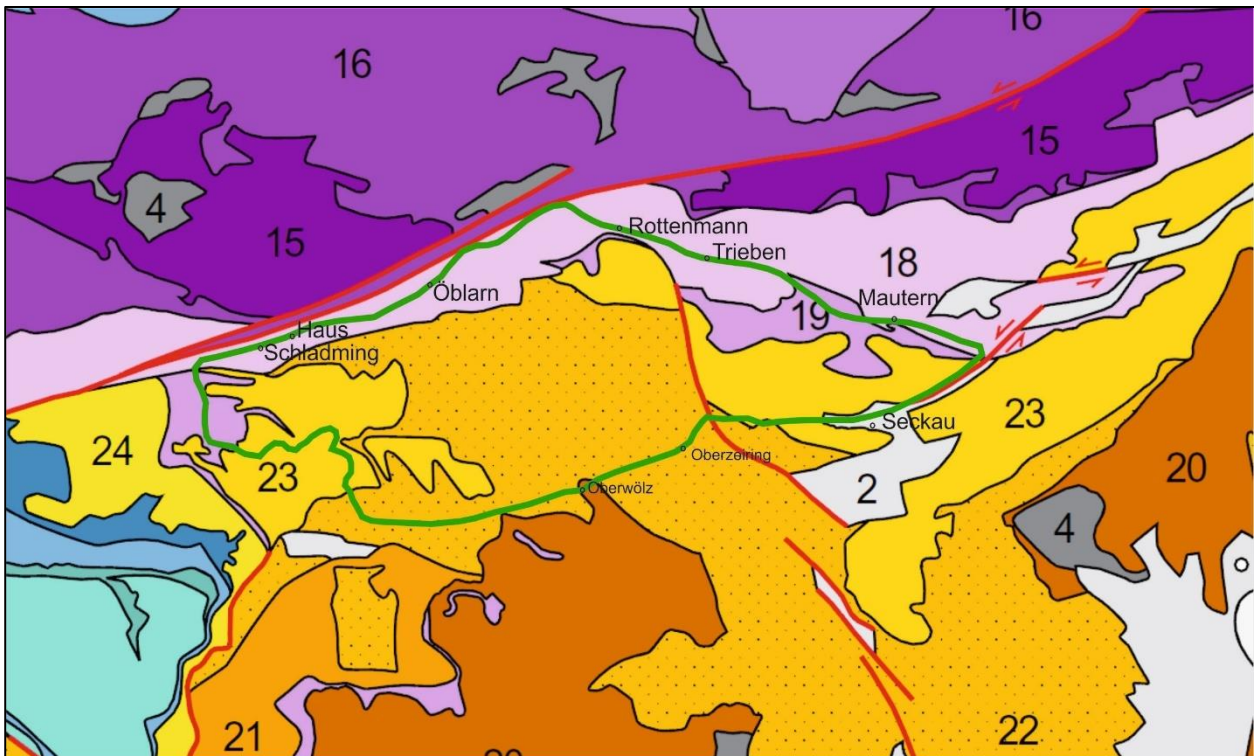
Austroalpine Nappes:

Northern Calcareous Alps and Grauwackenzone (Upper Austroalpine):

15 — Juvavic nappes (Mesozoic cover)

16 — Tirolian nappes (Mesozoic cover)

17 — Bavarian nappes (Mesozoic cover)

18 — Grauwackenzone (Paleozoic, stratigraphic base of Tirolian nappes)

Upper Austroalpine basement nappes:

19 — Mesozoic cover of Upper Austroalpine basement nappes

20 — Drauzug-Gurktal nappe system
(Tonale series, Steinach nappe, basement of Drauzug, Gurktal nappe, Graz Paleozoic)

21 — Ötztal-Bundschuh nappe system
(Ötztal and Bundschuh nappes)

22 — Koralpe-Wölz high pressure nappe system
(Schneebergzug, Millstatt, Wölz, Saualpe-Koralpe crystalline units)

23 — Silvretta-Seckau nappe system
(Campo-Sesvenna-Silvretta nappes, Innsbrucker Quarzphyllit, Schladming, Seckau, Semmering nappes)

☐ Niedere Tauern (Schematic)

Figure 13: Tectonic map of the area of the Niedere Tauern Range. The legend just includes the geologic units which are present within the Niedere Tauern Range. (Section after: Schmid, et al. 2004)

In the Enns Valley which represents the northern border of the Niedere Tauern Range, one of the biggest faults of Austria, the Salzach-Ennstal-Mariazell-Puchberg (SEMP) fault, is located. It is a sinistral fault system which extends from the Tauern Window until the Vienna basin (Hausegger and Kurz 2013). It is considered that it was formed in the Miocene while lateral extrusion (Hausegger and Kurz 2013; Keil und Neubauer 2009). Simultaneously to the formation of the SEMP several other faults (striking mainly from NE to SW or E to W) have developed in addition. (Hausegger and Kurz 2013)

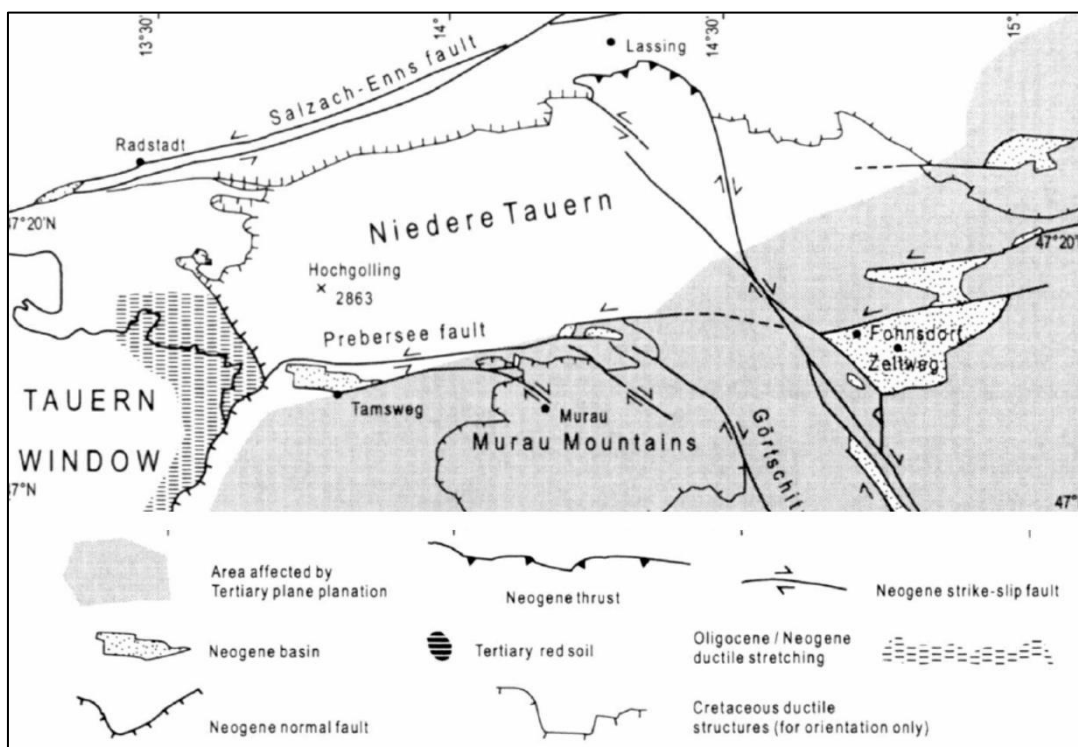Figure 14: Tectonic map of the Niedere Tauern Range. (Modified after: Neubauer and Eder, 2000)

Further faults in the Niedere Tauern Range exist with a striking direction of NW to SE and NNW to SSW (Hermann and Becker 2003). These are described due to their dextral strike slip movement as antiriedl faults of the SEMP. An overview of the main faults occuring within the Niedere Tauern Range are visible in Figure 14.

5.2.2.   ROCK DESCRIPTION

The general setting according to the occurring rock series was described by Tollmann in (1977) as well as by Becker (1981). According to both descriptions, the deepest part consists of granitic gneisses followed by an amphibolite-complex which is built up by different types of amphibolites, hornblende gneisses, augengneisses and serpentinites. The amphibolite series is overlain by a complex mainly consisting of micaschist, which is forming the main part of the Rottenmanner Tauern (Rappolder Complex) as well as of the Wölzer Tauern (Wölzer Complex). The series of micaschist mainly consists of garnet micaschist and achieves its maximum thicknesses in the Wölzer Tauern. Furthermore, this series can contain intercalations of quartzite, carbonate schist, amphibolites and dark carbonates which are designated by Karl Metz (1976) as "*Schwarze Serie*". At different locations marbles of high thickness occur, mostly accessorized with pegmatites (Metz 1976). The carbonate-rich complex of marble, named as "Almhausserie" by Tollmann (1977) occurs at the top. (Tollmann 1977; Becker 1981; Pfingstl, et al. 2015)

5.3.   THE NIEDERE TAUERN RANGE AND THE GLACIATIONS DURING THE QUATERNARY

The Niedere Tauern Range, as part of the European Alps, has been affected by four glaciation stages and the so called lateglacial in the Quaternary. Within Europe, the four big glaciations are known as Günz, Mindel, Riss and Würm. The extents of these four phases are presented in Figure 15. The Last Glacial Maximum (in the following referred to LGM) was part of the Würm glaciation period and took place "*about 21 to 18 – 17 ka BP*" (Kellerer-Pirklbauer, et al 2010, 69).

As visible in Figure 15 and Figure 16, the Niedere Tauern range was not completely covered by an ice sheet during the LGM. According to the paleogeographic map created by Van Husen (1987), the Schladminger Tauern were entirely covered by the ice sheet of the LGM. Only the highest summits reached above the glacier as so called Nunataker. The Wölzer Tauern, as well as the Rottenmanner Tauern, were nearly completely covered by the ice shield, although the glacier in the RoT didn't achieve a thickness as high as within the WoT and ScT. The Seckauer Tauern remained nearly unglaciated, with high altitude glaciers only forming in the valleys. (Compare Figure 16)
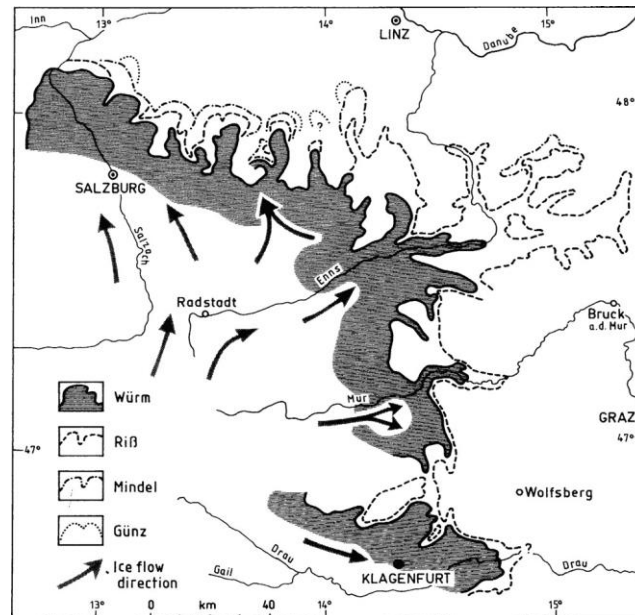
Figure 15: Extent of the four big glaciation periods in Austria (Van Husen, 2011)

The ice sheet during the glaciation period of Riss had the biggest spatial extent while the glacier during the other glaciation stages of the quaternary, Günz and Mindel, is not entirely traceable. The spatial extent of the different glaciation stages is based on glacial deposits which can referred to a specific period, for example, the Würm glaciation deposits named *Niederterrasse* (Van Husen 2011). According to Figure 15 and Figure 16, parts of the Niedere Tauern Range were not covered by the continuous ice sheet during all glaciation periods of the Quaternary.

The LGM was followed by the so called the Alpine Lateglacial. It is referred to as the period between the withdrawal of the glaciers of the LGM until the glaciers reached their extent within the Holocene and therefore the start of the postglacial. (Lieb 1987; Ivy-Ochs, et al. 2008) The Lateglacial is subdivided into 5 stages, namely Gschnitz, Clavadel or Senders, Daun, Egesen and Kartell (Ivy-Ochs, et al. 2008).

The glaciation periods were interrupted by warmer times which are referred to as interglacial stages. These interglacial periods were characterized by ice decay due to the glacier retreat. The present geomorphologic appearance of the Niedere Tauern Range was mainly formed due to these glaciation and interglaciation cycles, especially within the cycles of the Alpine Lateglacial (Lieb 1987).

In the whole Niedere Tauern Range, characteristic features of former glaciation are present as deposits of terminal or lateral moraines, oversteepened side walls of the valley and U-shaped overdeepended valleys, amongst others. (Van Husen 1987; Lieb 1987)
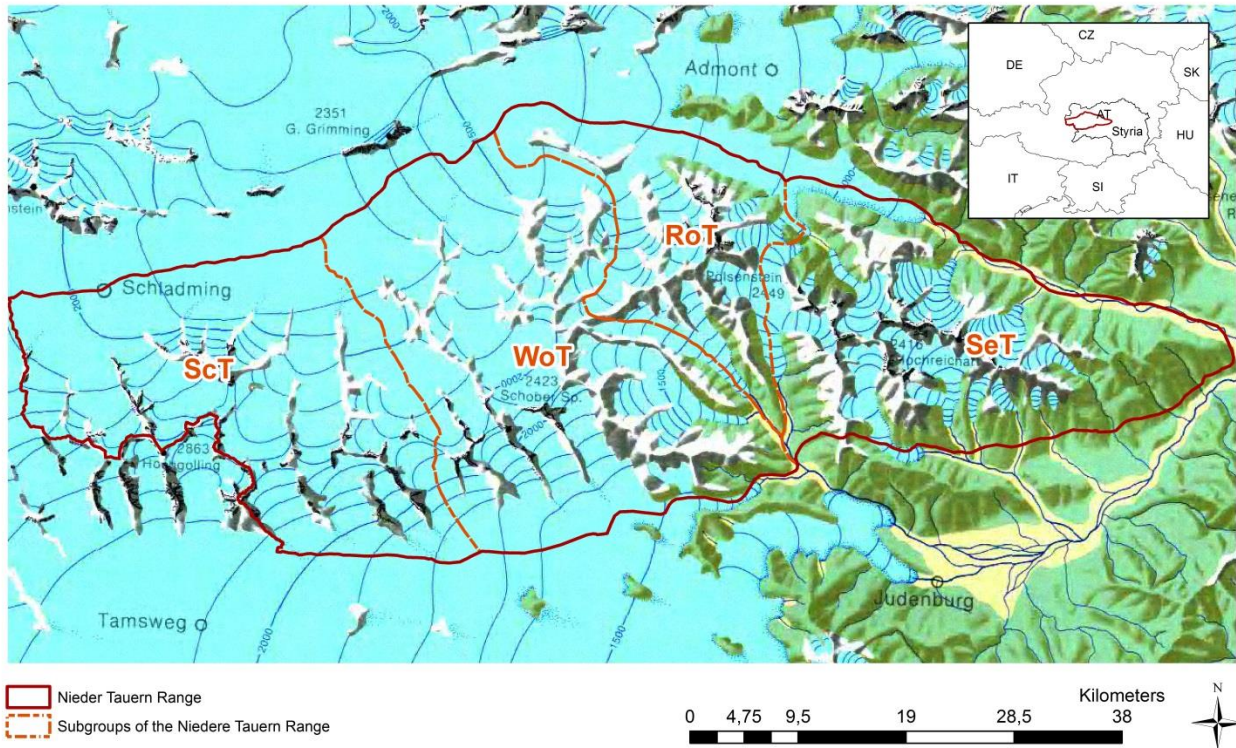
Figure 16: Extent of the glacier during LGM (map sources: paleogeographic map M 1 : 500.000 after Van Husen (1987); © EuroGeographics for the administrative boundaries)

The main valleys of the Niedere Tauern Range were affected by the main glaciers through glacial erosion. Therefore these valleys are formed as oversteepened U-shaped valleys. The tributary valleys which have an orientation of N-S within the Niedere Tauern Range appear as hanging valleys. (Hermann 1997) The infilling of the oversteepened U-shaped valleys can reach up to several hundreds meters in depth in the middle of the valley bottom. (Ivy-Ochs, et al. 2008; Van Husen, 2000)

As explained in the previous section (Chapter 3.3), glacial processes are supposed to be factors influencing the forming of deep seated gravitational slope deformations. These processes are assumed to be triggering as well as preparatory factors. (Glade and Crozier 2005; McColl 2012). Compare Table 2.

6. METHODOLOGY

This thesis is mainly based on four work steps.

- GIS Analysis
- Field Investigation
- Data Analysis

The ALS-Data was provided by the Federal Government of Styria. The hillshades, reliefs and slope maps were previously calculated and provided by researchers of the Institute of Earth Sciences – University of Graz.

The analysis according to existing mass movements within the RoT and the SeT was performed in course of two bachelor theses (Bevilaqua 2015; Oberbichler 2016) and fully implemented into the GIS-model of this master thesis. This data included geomorphologic parameters (e.g. area, headscarps) of mass movements generated by GIS Analysis within their regional test sites (RoT and SeT) as well as field data from their local test sites such as the locations of springs and hydrologic parameters e.g. electric conductivity measurement. Therefore the DSGSD Vöttleck was chosen as first local test site of this master thesis.

Literature research within existing literature was performed to get an overview of the regional investigation site mainly concerning already described DSGSDs. The research included publications, master theses and dissertations, as well as information provided within the "*Massenbewegungen"* web application of the Geological Survey of Austria. The main aim of this research was not only to get an overview of previous research but to choose appropriate local test sites. For this decision, it was necessary that the optional DSGSDs are already well described according to their geological and geomorphological features.

Another aspect of this step was to find data of existing springs within the chosen mapping sites. This includes an internet research on the platform *GIS Steiermark - Gewässer und Wasserinformationen* where the Federal Government of Styria provides information of springs and riparian rights. The collected data of mass movements and springs were incorporated into a GIS platform for further analysis.

6.1. GIS ANALYSIS

This step was performed over the entire regional investigation site, the Niedere Tauern Range. The evaluation is based on a digital elevation model (DEM) which was initially incorporated into

a GIS platform to generate the following analysis for helpful datasets such as hillshades and slope maps. These generated datasets have a resolution of 1 m.

The mapping of possible DSGSDs was based on their characteristic geomorphologic features (Figure 4), such as multiple ridges. These properties are visible in the prepared datasets under permission that they exceed the resolution accuracy of the underlying DEM. The GIS Analysis of the subgroups SeT and RoT was performed by two students in course of their bachelor theses (Oberbichler 2016; Bevilaqua 2015). The evaluation of the missing parts of the Niedere Tauern Range, ScT and WoT, was performed within this master thesis.

The final datasets were cross-referenced with information from previously described DSGSDs within literature.

6.2. FIELD INVESTIGATION

The field investigation was done in total on 11 days in July and August 2016.

At this point, it has to be explicitly indicated that the first part (July) of the field investigation in the course of this master thesis took place in a very wet period with heavy precipitation events. Therefore the measured parameters and the observation of existing springs and surficial water channels have to be considered within this context.

Figure 17: Portable Device (Photo: Daniela Friedl)

The chosen mass movements were mapped according to their hydrological characteristics with the main focus on springs. The main aim was to generate data that allow an interpretation of the influence of DSGSDs on the underlying drainage system.

With a portable measurement device (Figure 17), the electric conductivity and the water temperature was measured and documented for each spring which was found in course of the field investigation. At selectively chosen locations, the same procedure was applied on surficial water channels. The discharge was either estimated or measured by measuring the water flow with a measuring beaker over time. This procedure was repeated at least three times to receive a significant result.

In summary the received data included electric conductivity, water temperature, discharge (mainly estimated) and if possible, the location (X-, Y- and Z-data) of the mapped springs. Additionally, the same information was noted for some water channels in the investigation area.

To confirm the information provided in the corresponding literature of each mapping site, geologic data such as azimuth and dip angle of the schistosity and, if available, joint sets, were measured and cross-referenced with data presented in the corresponding literature. The geomorphologic information was also verified according to their existence.

6.3. DATA ANALYSIS

The dataset of the mapped mass movements during GIS Analysis independently of size and type of the mass movements is further processed within this work step. It has to emphasized that the term *area* used within the analysis always corresponds to the horizontal projection of the area not the real surface area.

The data which was generated by field investigation, as well as data provided by the Federal Government of Styria (Federal Government of Styria, 2016), were incorporated into a GIS platform where each point corresponds to an existing spring. Each corresponding attribute table contains the specific information (field data) within an attribute table. The accurate location, if not collected during field investigation, was assigned within the GIS platform.

The following methods were applied on the dataset created by GIS Analysis.

1)   Spatial distribution

The first objective of this work step was to generate a dataset which just contains the mass movements which are classified as DSGSD or at least as assumed DSGSD. Therefore a threshold value concerning the size of the mass movements was chosen. Within this work this threshold value equals 0.3 km² and was selected independently of literature to limit the dataset to a size which is manageable within the given time and in relation to the needed processing power of the used computers. By applying this threshold value on the generated dataset, mass movements smaller than 0.3 km were excluded from further processing. The remaining dataset was then visually classified according to their type of movement and the order of formation. The mass movements which are not assigned as DSGSD were within this step excluded from further processing.

At this point it has explicitly mentioned that just this dataset containing DSGSDSs was used for the further analysis. The only exceptions constitute the visual interpretation of the spatial

distribution of mass movements within the regional investigation area and the calculation and interpretation concerning possible segmentation, based on the formation order, of the DSGSDs.

2)   _Exposition_

To receive information about a preferred exposition of the hillsides affected by DSGSDs in the regional investigation area, further steps were necessary. For each DSGSD which was drawn as polygon, a line segment had to be constructed corresponding to the mean direction of its exposition. These lines had to be linked with their associated DSGSD by a specific ID. By performing a calculation within the GIS platform, the direction expressed as degrees which therefore corresponds to a geographic direction was obtained and dedicated to each DSGSD.

3)   _Comparison distribution of DSGSDs with the extent of the LGM_

To gain information according to the thickness of the ice cover of the LGM above the DSGSDs it was crucial to introduce parameters which are used as reference points for the calculation. These are presented in Figure 18 below. The elevation of the glacier surface given in m.a.s.l. was obtained for each DSGSD from the paleogeographic map created by Van Husen (1987).
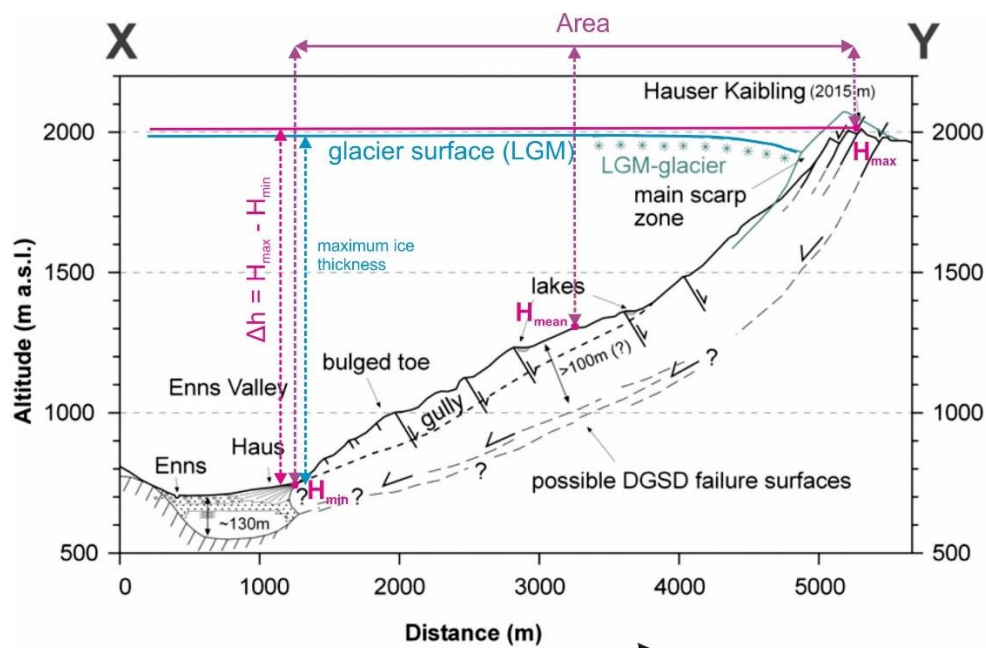
Figure 18: Simplified slope section of the DSGSD Hauser Kaibling (vertically exaggerated by a factor of two. The parameters displayed within the section are used for further analysis. (Modified after Kellerer-Pirklbauer, Strasser &, 2010)

To give a proper interpretation of how many mass movements were completely covered or just partly covered by the glacier of the LGM, the mimimum (H_{min}), the maximum (H_{max}) and the mean elevation (H_{mean} - corresponding to the elevation of the centroid of the polygon) of each

assumed DSGSD has been calculated and substracted from the altitude of the surface of the glacier to receive the thickness of the ice sheet above the specific point. For a better understanding, compare Figure 18.

$$Maximum\ ice\ cover\ [m] = glacier\ surface\ [m.a.s.l.] - H_{min}$$

$$Mean\ ice\ cover\ [m] = glacier\ surface\ [m.a.s.l.] - H_{mean}[m.a.s.l.]$$

$$Minimum\ ice\ cover\ [m] = glacier\ surface\ [m.a.s.l.] - H_{max}\ [m.a.s.l.]$$

$$difference\ in\ altitude\ [m] = \Delta h = H_{max}[m.a.s.l.] - H_{min}\ [m.a.s.l.]$$

H_{min}, H_{max}, H_{mean} as well as the affected area of the DSGSDs were related to the calculated ice thickness. To gain information concerning the variations in geometry of the DSGSDs with increasing size, the area was related to the calculated Δh.

4)   *DSGSD in comparison with underlying geology and the corresponding rock properties*

As mentioned in chapter 5.2, various lithologies occur within the Niedere Tauern Range. To gain a visual analysis of the ALS-Data detected DSGSDs in a context with the underlying bedrock, intermediate work steps were again necessary.

It was crucial to create a dataset which contains the whole geological information of the area affected by DSGSDs. This dataset is based on the geologic map provided by the Federal Government of Styria (© GIS Steiermark). To generate interpretable data, a simplification of this dataset had to be performed by categorization into 11 different types of lithologies.

To gain information concerning the influence of rock strength, these categories were further classified according to their typical values for UCS from literature (Schön 2011, 257-258; Eurock 2014 2014, 1129; Button 2004, 3). Because no test could have been performed on rock samples, the field estimation of Hoek and Brown was applied to get values for UCS as well. The estimation of Hoek and Brown (1997) was verified according to its usability by a comparison with UCS values from literature.

For the classification, the grades respectively the strength classes after Hoek and Brown (1997) were used. The whole list was already presented in chapter 3.3.4, the used classes are listed in Table 4 and Table 7 below. These classes just include hard rocks.

The in Figure 45 lithologies assigned as (para)-glacial deposits and other quaternary deposits correspond to soft rocks. Thus, they are excluded from the interpretation based on the assumption that these sediments were deposited after the beginning of the formation of the DSGSDs. Further based on the geologic map (Federal Government of Styria, 2016) no data for the underlying bedrock is available. Although to present the percentage covered by soft rocks a new grade *Rn* and stengthclass *0* was introduced. (Table 7)

Table 4: List of used classification according to the UCS values found within literature.

Grade according to rock strength (UCS)		Summarized strength classes based on rock strength (UCS)	
R3	medium strong	0	Soft rocks - excluded
R4	strong	1	medium strong to strong
R5	very strong	2	very strong to extremely strong
R6	extremely strong		
Rn	Soft rocks – excluded		

As presented in the tables, only 5 grades were used which correspond to medium strong to extremely stong rock masses as well as the excluded soft rocks. These were further summarized into strength classes (compare Table 4) and analyzed by performing a frequencyl analysis.

5)   Evaluation of the influence of DSGSDs on the drainage system

To gain an impression of the influence of DSGSDs on the drainage system it was crucial to receive evaluable data. This was performed by determine the Z-values (absolute altitude) for each spring within the GIS Platform. On the data obtained by this step a frequency analysis was performed to get the preferred ranges of altitude where springs occur.

To gain a visual impression of the arrangement of the springs within the local test sites, profiles (sections) were created and supplemented with further information as the occurring lithology along the profile, if available information about the direction of the foliation of the rock masses, the previous calculated spring horizons and the glacier surface of LGM.

6)   Statistical Analysis

Of the steps described above (1 to 5) of the data analysis, which were mainly performed within the GIS platform resulted in numerical values within the attribute tables of the specific layers. These values were exported and used for statistical analysis. The main statistical tool which was used, was the frequency analysis including absolute, relative and cumulative frequency.

Aim of this step was to make the received data numerically evaluable and possible trends visible.

6.4. LIMITATIONS

Within the previously described workflow which was performed in course of this thesis, the following limitations have to be considered:

(1) Literature research:
Limitations in access of publications or undisclosed research.

(2) Visual Analysis of ALS-Data:
It has to be considered that the analysis of the ALS-Data is just a subjective visual interpretation of the data. Features and structures are possibly interpreted differently due to different researchers.

(3) Field investigation:
Measured parameters are dependent on the weather conditions. This concerns not only the weather condition during field investigations but also the situation in the weeks before. Further limitations due to inaccessibility of some areas caused by dangerous terrain or private property.

7. LOCAL TEST SITES

In the following section, the three chosen investigation areas, where the detail mapping with focus on springs and hydrogeological parameters has been performed, are described. The description comprises the existing literature and the own field observations. The measured parameters summarized are in a table which is presented in the appendix.

7.1. GROßSÖLK

The DSGSD of Großsölk is located in the Sölk Valley which extends from Gröbming in the North to the South. More precisely, it is situated above the small town Fleiß, near the locality of Großsölk.

Due to the investigation of the ALS-Data, the DSGSD Großsölk has a total area of 0.56 km². The mean exposition of the slope is 62° northeast. The bedrock consists mainly of micaschist which is covered in the Valley by (para-) glacial and other quaternary deposits such as moraine material (Compare Figure 23)

7.1.1. DESCRIPTION

The Großsölk slope deformation has been described in detail by Hermann in his dissertation from 1997. It was also mentioned in further publications (Hermann 1997; Hermann, Madritsch, et al. 2000; Hermann and Becker 2003; Hermann 1996)

It is described as a mass movement which forms a sagging-like structure with a distinct bulging slope. (Hermann 1997) The mean slope inclination is approximately 22°, which is in comparison to the inclination of the adjacent slopes (35° to 40°) relatively flat. (Hermann 1996) The general terrain of the mass movement shows a rugged, stepped relief.

Hermann (1997) divides this DSGSD into three parts. He differentiates between a) the zone where the headscarp of the mass movement is located, b) the central part and the c) zone of the bulging slope toe. Referring to the detailed description, Hermann (1997) states the only precisely visible headscarp is located at the crestline between the summits *Zinken* and *Ebeneck* (Figure 2 and Figure 20). It cuts the headscarp of the mass movement Kleinsölk which is located at the back side of the respective mountain range. In the part where the main headscarp is located, tension cracks are present. (Hermann, 1997, 1996) The slope toe is bulged and creeps towards the valley. It already reaches around 300 m into the Großsölk Valley. The arrangement of the two DSGSDs (Kleinsölk and Großsölk) to each other are visible in Figure 19 and in Figure 20.
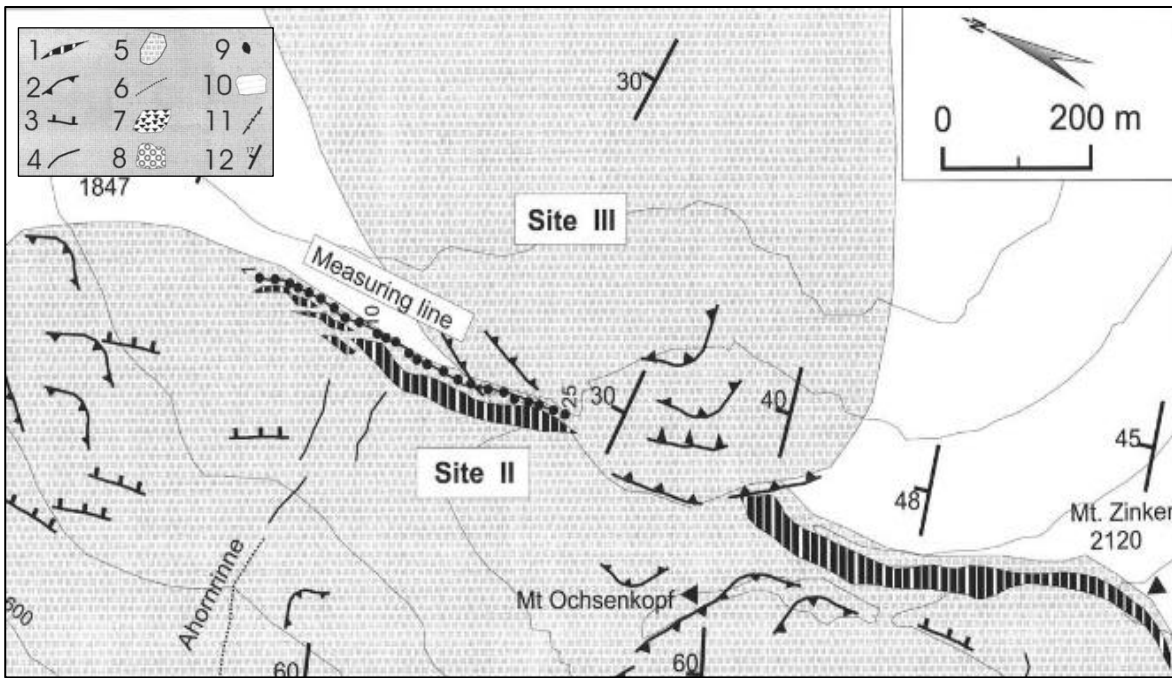
Figure 19: Site III = DGSD Großsölk and Site II = DSGSD Kleinsölk which is responsible for the double ridge at the crestline between Mt. Zinken and the Ebeneck.
Legend: 1 Yielding and dislocation surfaces 2 main scarps, 3 uphill facing scarps, 4 minor scarps and trenches, 5 limitation of spreading slope, 6 avalanche tracks and torrent gullies, 7 rock falls, 8 rotational landslide, 9 ephemeral pond, 10 glacial terrace, 11 brittle fault, 12 strike and tip of schistosity. (Modified after: Becker and Hermann 2003)

The material of the mass movement is described by Hermann (1996) as heavily moist, although it cannot be deduced from this formulation whether the entire material of the DSGSD or simply the topsoil layer is meant. The surficial water channels rising from springs which are located in the upper part of the DSGSD infiltrate into the flat areas in the central part. (Hermann 1996)

The above described observations of Hermann (1996; 1997) could be mostly affirmed through field work, especially the geomorphologic and geologic features (Figure 20). Not everything was totally reproducible, as for example, the infiltration of the water channels couldn't be observed during field work.

Figure 20: View in direction southwest from Ebeneck to the summit Zinken. (Compare Figure 19 and Figure 23) The Double ridge (blue) of the DSGSD Kleinsölk (Hermann, 1996; 1997) which is cut by the headscarp of the DSGSD Großsölk (red) is visible. The arrows mark the moving direction. (Photo: Daniela Friedl)
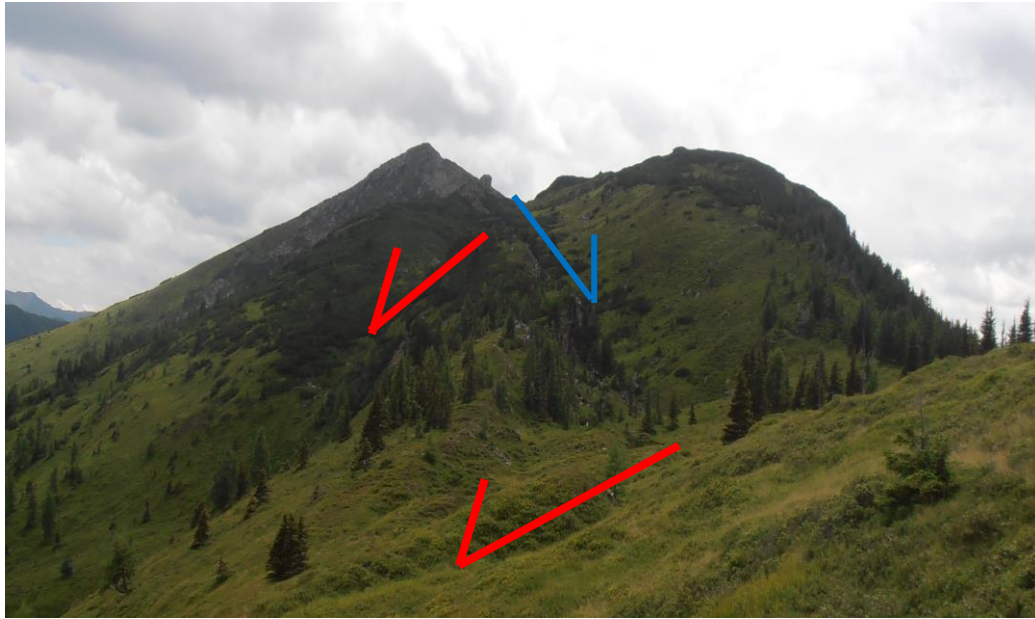
7.1.2. OBSERVATION ACQUIRED DURING FIELD INVESTIAGTION

The field work of the investigation area Großsölk was performed over a total of 6 days in the period from 12.07.2016 to 14.07.2016, on 02.08.2016 and on 04.08.2016. The first investigation period was characterized by heavy precipitation and thunderstorms. The weather during the second field trip was sunny, hot and almost dry. Nevertheless, it has to be considered that the whole summer was relatively wet, which has to be taken into account of interpretation of the measured parameters related to the drainage system.

The area was investigated mainly along forest roads concerning springs. If necessary, surficial water channels were followed until the corresponding spring. For each spring and for selected surficial water channels, data such as electric conductivity, water temperature and discharge were measured and documented.

In total 14 springs were mapped while field investigation. The measured electric conductivity lies in a range between 9 µS/cm and 38 µS/cm. The low electric conductivity is assumed to be as a result of the previous heavy rainfall events and long lasting precipitation periods. The water temperature was mainly between 4°C and 8°C. The water at four springs was higher in water temperature with over 11°C. These high values were measured at springs with a very low discharge which were exposed to the sun for the whole day. The estimated discharge varied from less than 0.2 l/s up to 1 l/s. At two springs the discharge was higher (GS_11, GS_10).

The topsoil layer of most of the lower and the intermediate part of the DSGSD Großsölk can be described as dry notwithstanding the weather situation during the field investigation. The present water was flowing along incised erosion gully's downhill. The majority of the mapped springs were located in the upper part of the mass movement, in this case above 1200 m.a.s.l. (Compare Figure 23)

In the intermediate part of the DSGSD, flat areas and steep parts were observed. The trees within the forest in the central part of the mass movement were not typical a drunken wood – better described as "tipsy". This is an indication for movements which occurred recently at least within the last decades. It is not sure if this movement is due to the primary DSGSD or due to a secondary phenomenon such as soil creep of the overlying quaternary deposits. Maybe even a starting segmentation of the mass movement is visible in this area.

Geomorphologic features such as the headscarp and tension cracks, which are described in the literature, could be affirmed during field investigation.

The locations of the recorded springs are represented in Figure 23 together with the acquired data in the investigation area Moditzen which is described in the following chapter.

7.2. MODITZEN

7.2.1. DESCRIPTION

The investigation area Moditzen is located adjacent to the previous described DSGSD Großsölk in the Sölktal on the boarder to the Wölzer Tauern (Figure 21). The geomorphologic structures and characteristics of this DSGSD were described by Hermann (1996; 1997). His description is supported by maps which visualize the mentioned features.

Figure 21: Picture of the DSGSD Moditzen, taken from adjacent mountain DSGSD Großsölk (viewing direction from NE to SW) (Photo: Daniela Friedl)

According to Hermann (1996), the DSGSD Moditzen is an example of the initial stage (compare chapter 3.2). The DSGSD is built up mainly by micaschist, quaternary and (para-) glacial deposits such as moraine material. The foliation of the bedrock dips in a southern direction while it strikes from east to west. Furthermore, a joint set with an azimuth in a northern direction and a dip angle of about 90° is shown in the morphologic map (Hermann 1997). The terrain is rugged due to the distorted material and flat areas within the mass movements are visible. (Hermann 1996)

7.2.2. OBSERVATIONS AND DATA ACQUIRED DURING FIELD INVESTIGATION

The field investigation of the DSGSD Moditzen took place on the 15th of July and on the 3rd of August 2016. As mentioned above, the first investigation was within a period with heavy precipitation. Therefore it has to be considered again that the observation according hydrogeologic and hydrologic parameters have to be set into this context.

The material of the topsoil of most of the lower and intermediate part of the DSGSD can be described as moisture. Additional many small surficial water channels have been observed. These could be a result of the extremely wet period with high amounts of precipitation although the occurring vegetation in this area indicates that at least the upper zone of the underground is permanently moist.

Figure 22: View in north direction. In the back the Strickertal is visible (Figure 23) Tension Crack observed in the upper part of the DSGSD Moditzen.

Along the forest roads were nearly everywhere road ditches observed which lead the water to drainage pipes which cross the roads below. The purpose of this drainage system is to avoid destruction due to surficial runoff. This could indicate that the surficial water channels are perennial water-leading or at least often existent. Another reason for this observation could be the high surficial runoff of precipitation due to the low permeability of the underground.

In the upper part of the mass movement, above the tree line, the geomorphologic features which were described by Hermann (1996; 1997) as tension cracks (Figure 22) and the headscarp could be affirmed.

Within the investigation area, a total of 16 springs were found in the course of the field work. The measured electric conductivity lies in a range between 18 μS/cm and 43 μS/cm. All but one value of the measured water temperatures was lower than 10°C. The water temperature at only one spring (MOD_16) was a little bit higher with 12°C. The discharge was generally very low with estimated amounts between 0.1 l/s and 0.5 l/s. Only two springs were in an estimated range between 1.0 l/s and 2.0 l/s. The springs were documented in detail on record sheets. The acquired data for discharge, electric conductivity and water temperature are summarized in visualized in Figure 23.
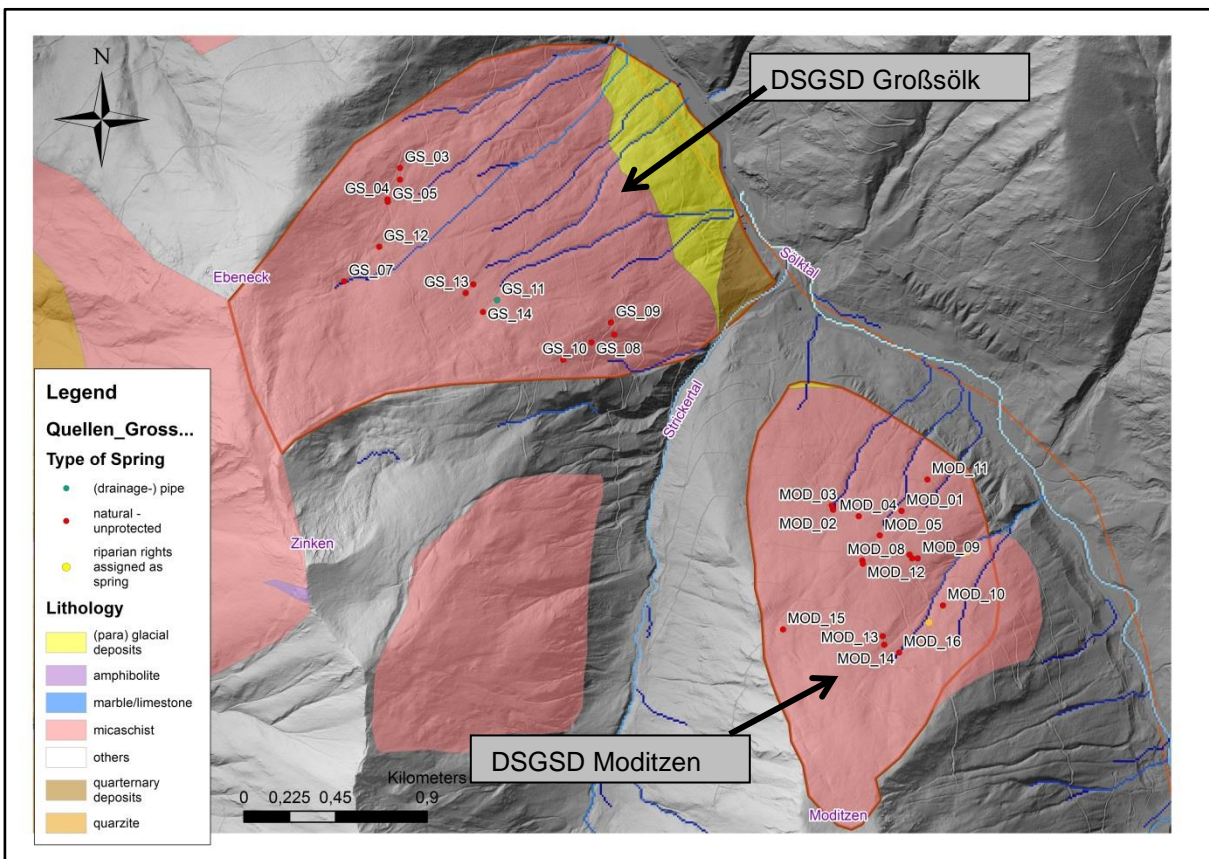
Figure 23: DSGSDs Moditzen and Großsölk: The simplified lithology is presented as well as springs which are colored according to their type. Additional the riparian rights which are assigned as springs are displayed (Federal Government of Styria 2016). (map source: © GIS Steiermark)

7.3. HAUSER KAIBLING

7.3.1. DESCRIPTION

The Hauser Kaibling is located in the northwestern part of the Niedere Tauern Range at its northern border with the Enns-valley. At its toe lies the small town of Haus im Ennstal.

The DSGSD was shortly described by Hermann (1997). Furthermore, the DSGSD Hauser Kaibling was displayed in figures in publications of Hermann and Becker (2001; 2003). A detailed description was done by Kellerer-Pirklbauer, et al. (2010).

As Kellerer-Pirklbauer, et al. (2010) described, the DSGSD Hauser Kaibling involves the whole northern hillside of the Mt. Hauser Kaibling. According to Kellerer-Pirklbauer, et al. (2010) the DSGSD Hauser Kaibling is considered to be inactive.

The profile is described as concave-convex due to missing material in the upper part of the mass movement which is deposited at the slope toe. In the intermediate part – in the transistion zone between the concave and convex form - of the DSGSD, the slope inclination is therefore lower. The mean inclination of the slope is approximately 22.6°. (Kellerer-Pirklbauer, et al. 2010) *"The maximum thickness of the DSGD is assumed to be more than 100 m."* (Kellerer-Pirklbauer, et al. 2010, p. 69)

The geomorphologic features described by Kellerer-Pirklbauer, et al. (2010) in the upper part are tension cracks and multiple ridges (Figure 24). The headscarp zone is located along the crestline with an orientation of NW-SE. The intermediate part is characterized beside its lower slope angle by the existence of smaller scarps, uphill-facing scarps and depression zones which are arranged horizontally. The slope toe is situated within the Enns-valley and is described as steep and outward bulging with a radial drainage system and alluvial fans. It marks the end of the DSGSD in the valley. (Hermann, 1997; Kellerer-Pirklbauer, et al. 2010)

Therefore the features are typical for a DSGSD in the final stage according to Hermann (1996).

The whole hillside is cut by several erosion gullys. This incision already begins in the upper part of the DSGSD. They are arranged in a fan-like way and form the above mentioned radial drainage system. The reasons for the existence of these gullys are erosion processes affecting the disintegrated material of the mass movement. (Kellerer-Pirklbauer, et al. 2010)

Concerning the tectonic environment, the DSGSD Hauser Kaibling is mainly affected by the SEMP fault sytem which is located north of the DSGSD, as well as by the contact zone between the in the chapter 5.2.1 described Greywacke zone and the crystalline basement of the Upper Austroalpine. The mean orientation of the occurring foliation has a *dip direction of 348° (range 295-360°) and for inclination 41° (20-50/75°)* (Kellerer-Pirklbauer, et al. 2010, 69). These values are depending on the altitude. The inclination increases below an elevation of 1000 m.a.s.l., which is referred to as the bulging slope toe (outward creeping) and therefore possibly occurring bending folds. Furthermore, the material affected by the DSGSD is described as intensively distorted and the bedrock as fractured. (Kellerer-Pirklbauer, et al. 2010)
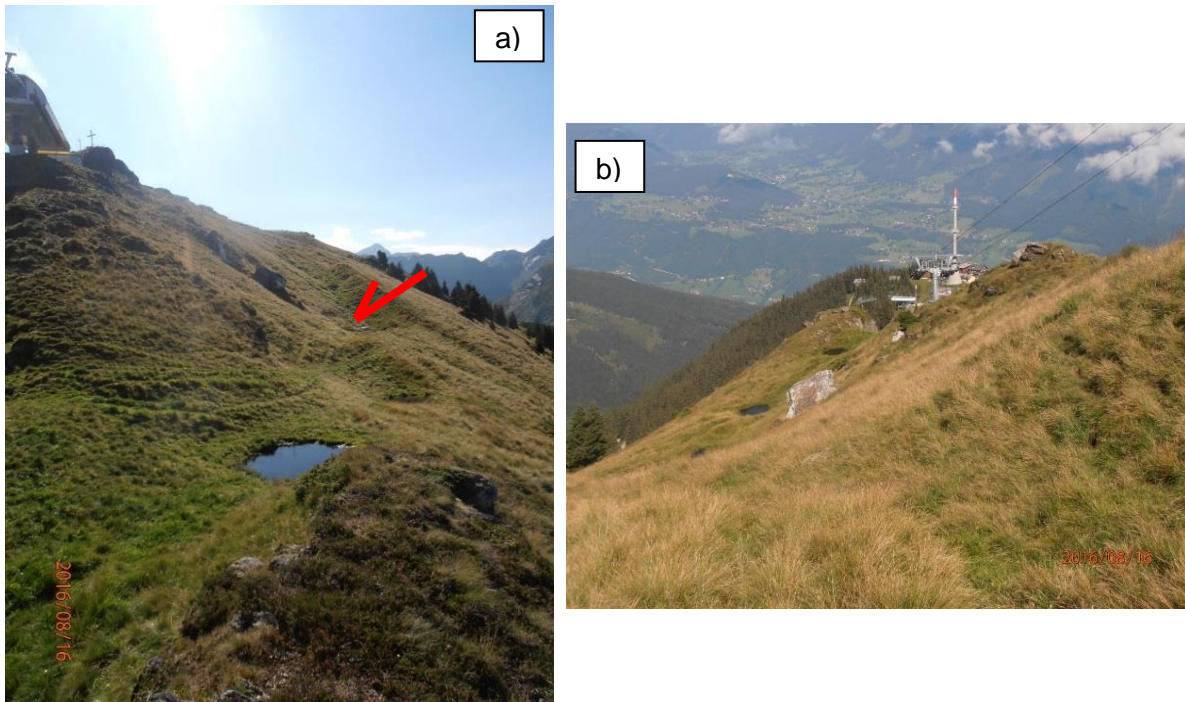
Figure 24: a) Viewing direction: northeastwards, uphill to the summit Hauser Kaibling. The picture shows multiple ridges at the top of the DSGSD Hauser Kaibling with ponds which are typically situated in such grabens. The red arrow marks the direction of movement.
b) View from summit downhill to the Enns Valley in northwestern direction. Again the multiple ridges which are situated at the crestline are visible. (Photos: Daniela Friedl)

The region where the DSGSD Hauser Kaibling is situated was affected by the glaciers occurring during LGM. The surface of this glacier at this glaciation stage was at an altitude of about 1900 m.a.s.l. (Kellerer-Pirklbauer, et al. 2010; Van Husen 1987). This could be affirmed by analysis based on the paleogeographic map of Van Husen (1987).

7.3.2. OBSERVATIONS AND DATA ACQUIRED DURING FIELD INVESTIGATION

The field investigation took place between the 13th and the 16th of August 2016. The weather was continuously sunny and hot. On one day a short thunderstorm passed by.

In total, 55 springs and existing natural and protected springs were documented within the investigation area. The locations with the measured parameters (as a percentage of total) are presented in Figure 25. The measured parameters as values are listed in the appendix.
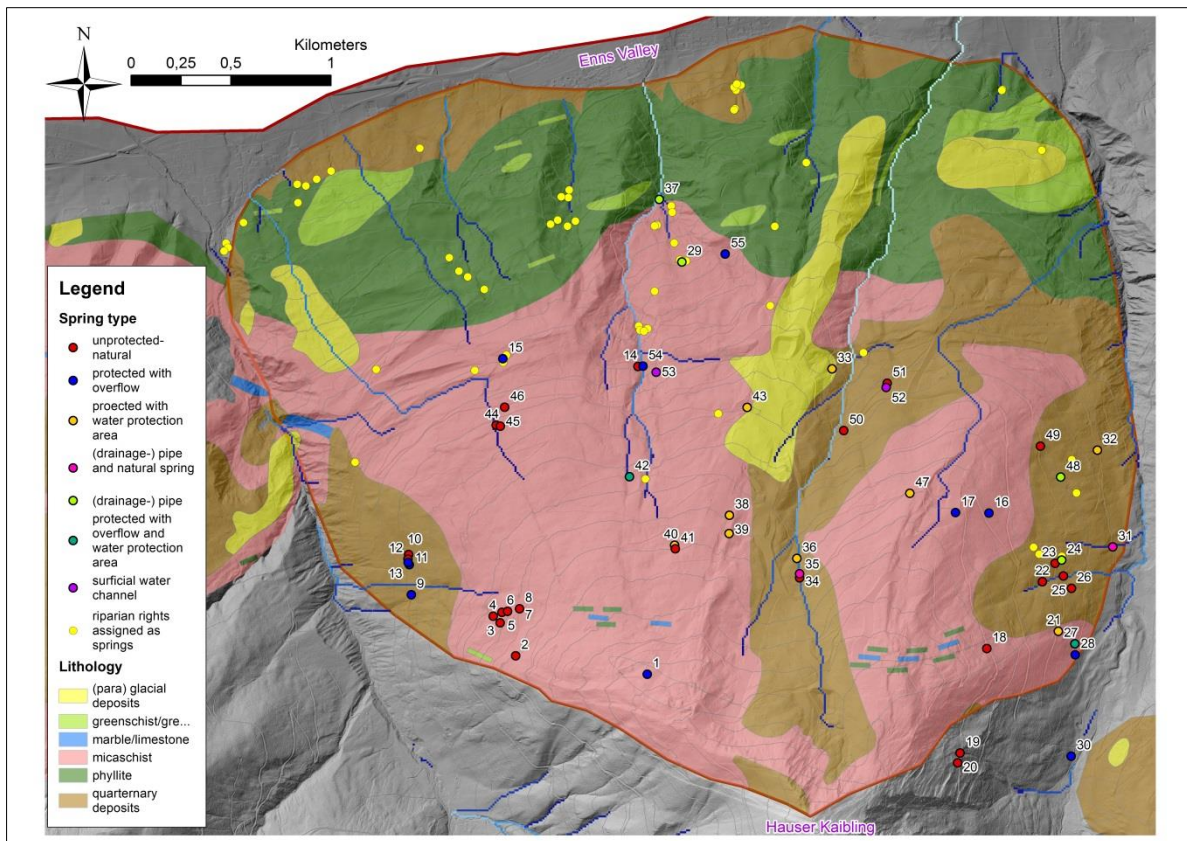
Figure 25: DSGSD Hauser Kaibling: The simplified lithology is presented as well as springs which are colored according to their type. Additional the riparian rights which are assigned as springs are displayed (Federal Government of Styria 2016). (map source: © GIS Steiermark)

The upper part of the DSGSD Hauser Kaibling can be described as dry due to the lack of surficial water channels and springs. The intermediate part as well as the lower part of the hillside was partly wet – at least the surficial soil layer. This observation is supported not only by the existence of springs but also by the occurring vegetation and wet areas. Around the springs, 44 to 46, small ponds were observed.

The measured values for electric conductivity range between 44 µS/cm and 300°µS/cm. The water temperature is generally in a range between 4°C and 10°C. Higher water temperatures were measured at 8 locations as result of the hot and dry weather.

The geomorphologic features described by Kellerer-Pirklbauer, et al. (2010) could be completely affirmed in course of the field investigation.

7.4. VÖTTLECK

The DSGSD Vöttleck is situated at the Palten Valley which is referred to as northern border of the regional investigation site. In detail it is situated within the SeT, the easternmost part of the Niedere Tauern Range.

The DSGSD Vöttleck was described by Fahrnberger (2000). It is mainly built up by rocks of the Greywackezone. These include in this case schists and phyllites of

Figure 26: DSGSD Vöttleck. View from Schwarzkogel to the summit Vöttleck, direction northeast (compare Figure 27). Within the picture, the main headscarp and the multiple ridges are clearly visible. The moving direction (southwards) is marked by the red arrows. (Photo: Gerfried Winkler, from: Oberbichler, 2016)

varying quarz content which are summed up under the term *Greywackeschist*. As visible in Figure 27 the lowermost part of DSGSD is covered by quaternary deposits (brown color). In the southeastern part along the crestline near at the summit of Vöttleck, lithologies which are simplified as *others* and greenschist as well as quartzite occur. The lithology *others* is in this case referred to high crystalline rock masses according to the geologic map (© GIS Steiermark). (Fahrnberger 2000)

The DSGSD Vöttleck has a distinct headscarp with a height of up to 40 m. At the crestline multiple ridges are visible (Figure 26). The terrain can be described as rugged and shows steep parts as well as flat areas where the topsoil is heavily moist. Uphill facing scarps are visible and in their grabens are ponds often located. (Fahrnberger 2000)

The morphology of the DSGSD Vöttleck is heavily influenced by secondary and tertiary movement acitivty. This includes rotational and translational landslides as well as rockfalls. At the lower part a well-developed bulging slope toe is visible. (Oberbichler 2016, Fahrnberger 2000)

The field data, on which the further analysis is based on, was acquired by Oberbichler (2016) and Bevilaqua (2015) in course of their bachelor theses. The field investigation of the DSGSD Vöttleck was not part of this master thesis.
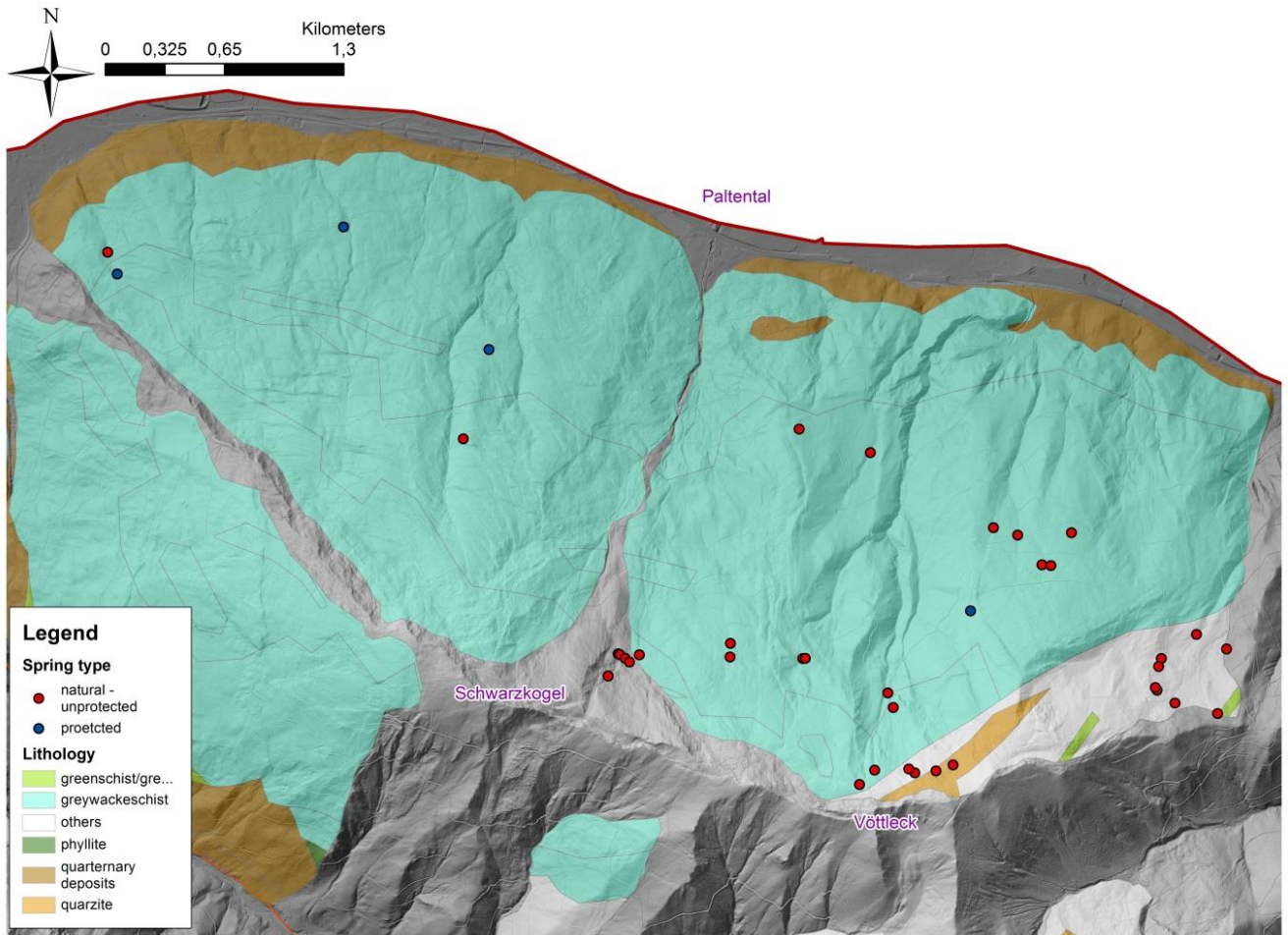
Figure 27 DSGSD Vöttleck. The polygons are referred to the simplified geologic information created from the geologic map (© GIS Steiermark). The springs are displayed according to their type are presented. The location and the type of the springs is based on data acquired by Bevilaqua (2015) and Oberbichler (2016). (Map source: © GIS Steiermark)

8. RESULTS AND DISCUSSION OF ANALYSIS NIEDERE TAUERN RANGE
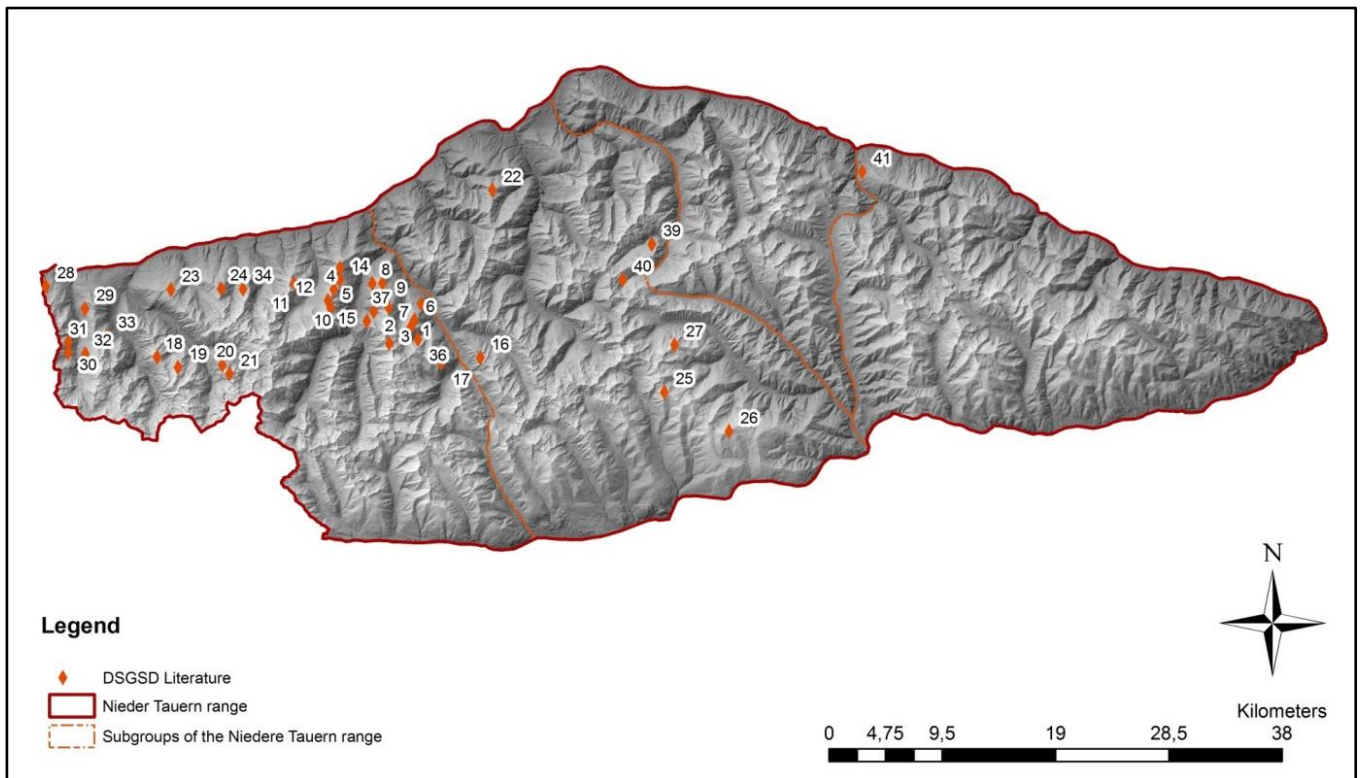
Figure 28: Location of DSGSDs according to literature. The name and the reference are listed in the appendix based on the numbering used in this figure. (Map data source: © GIS Steiermark)

As presented above in Figure 28 in existing literature 41 DSGSDs where found. In some cases, the same mass movements have been described in different publications. In Figure 28 the locations of these DSGSDs are presented. A short description and the corresponding reference based on the numbering used in Figure 28 are presented in the appendix. 8 of total 41 mass movements from literature couldn't be affirmed by visual analysis of the Digital Elevation Model. Although it has to be considered that the size of the characteristic morphologic features didn't exceed the resolution of the DEM.

8.1. DISTRIBUTION OF DSGSDS WITHIN THE NIEDERE TAUERN RANGE

In Figure 29 the results of subdividing the dataset of mass movements in datasets containing mass movements smaller than 0.3 km², respectively which are exceeding 0.3 km² in extent which were further classified as DSGSD and *NO DSGSD,* are presented. As visible just a small amount of the mass movements (exceeding 0.3 km² in extent) was classified as other types of slope failures such as landslides or rockfalls (light green polygons in Figure 29).The resulting

dataset contained in total 135 assumed DSGSDs. Further presented in Figure 29 are line elements visualized which correspond to headscarps (and partly to other features as multiple ridges). These were not explicitly assigned to specific mass movements.
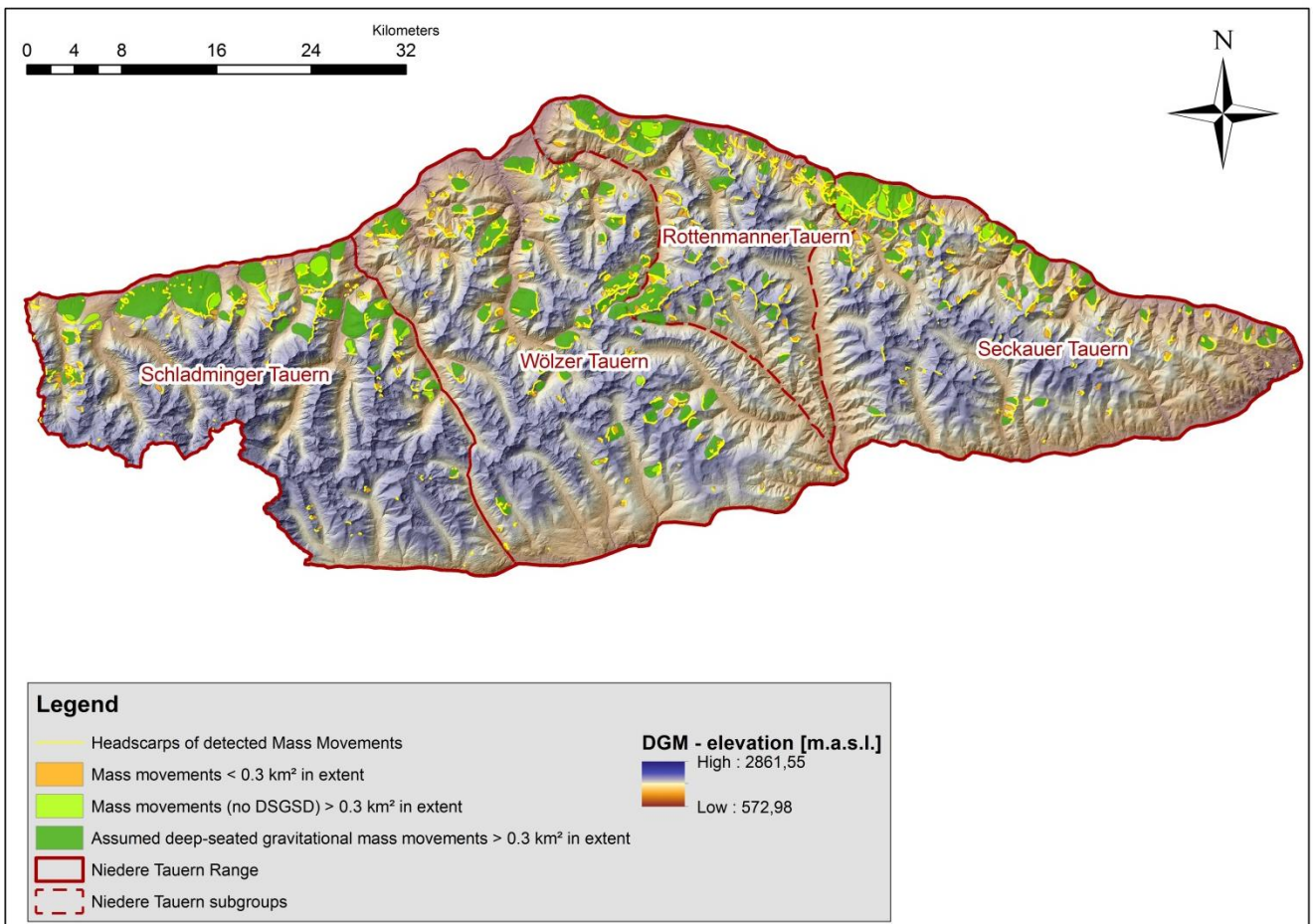
Figure 29: Spatial distribution of the detected mass movements within the Niedere Tauern Range. The dark green polygons represent the dataset of assumed DSGSDs. Therefore the orange polygons are the mass movements with an area smaller than 0.3 km²; the light green polygons refer to mass movements bigger than 0.3 km² but were not classified as DSGSD. (Map source: © GIS-Steiermark)

The assumed DSGSDs cover in total 207 km² of the Niedere Tauern Range. This means that 8.5% of the total area of the regional investigation area is affected by gravitational induced mass movements. By visual interpretation, it seems that in the Niedere Tauern Range the main part of the detected mass movements is located along the northern border (Enns Valley) of the Niedere Tauern Range. This applies for all presented mass movements including the mass movements smaller than 0.3 km² in extent.

For sake of completeness it is mentioned again that just the dataset which contains the assumed DSGSDs was used for the following analysis and the rest of the data (presented as light green and orange polygons in Figure 29) were excluded from further analysis, except the analysis concerning secondary / tertiary movement activity within primary phenomena.

Figure 30: Area of the DSGSDs located in the corresponding subgroup related to the corresponding subgroup. Further the areas of the subgroups as percent related to the total area of the Niedere Tauern Range are displayed.

Table 5: Total area of the Niedere Tauern Range and the different subgroups. Area affected by DSGSDs within the different subgroups. Furter the percentage of the subgroups related to the area of the Niedere Tauern Range and the percentage of area affected by DSGSDs wthin the different subgroups related to the area of the corresponding subgroup.

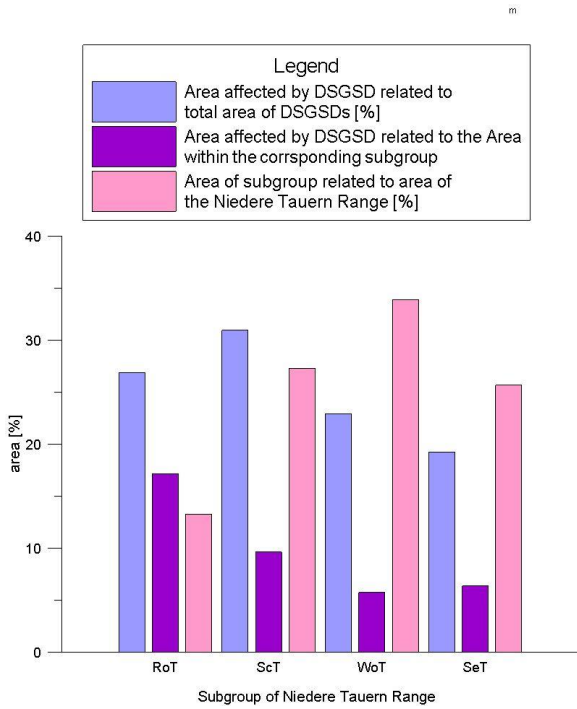|	[km²]	area subgroups related to area of the Niedere Tauern Range [%]
Total area Nieder Tauern Range	2438	100%
Total area DSGSD	207	8%
Total area ScT	665	27%
Total area WoT	826	34%
Total area SeT	626	26%
Total area RoT	324	13%
		area affected by DSGSDS related to area of corresponding subgroup [%]
Area DSGSD ScT	64	10%
Area DSGSD WoT	48	6%
Area DSGSD SeT	40	6%
Area DSGSD RoT	56	17%

As the diagram (Figure 30) reveals, the detected DSGSDs are located in a similar percentage within the different subgroups of the Niedere Tauern Range, varying between 19% and 30%. Related to area of the corresponding subgroup it is visible that within the RoT, which is the smallest of the subgroups of the Niedere Tauern Range, the biggest percentage of the area is affected by DSGSDs (17%) related to its size. The lowest percentage related to its own area has the WoT (6%) as well as the SeT (also 6%).
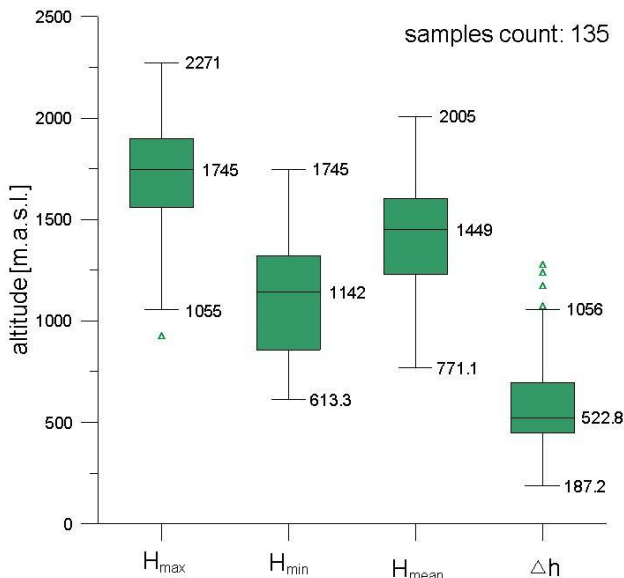
Figure 31: whisker plot of H_{min} (represents the lowest point of the DSGSD), H_{max} (highest point of the DSGSD), Δh (difference between H_{min} and H_{max}) and H_{mean} (refers to the mean elevation of the DSGSD) represented with existing outliers. The mean value is represented by the median of the dataset.

In Figure 31 the values for H_{min}, H_{max}, H_{mean} and Δh are presented as whisker plot with the median and outliers. For the point of highest elevation of DSGSDs the maximum value is at 2271 m.a.s.l. and the lowest value for H_{min} (point of lowest altitude) is 613.3 m.a.s.l. Furthermore as the diagram reveals 50% of the DSGSDs have a difference in altitude between ca. 448 m and 695 m. The range of Δh is between 187 m and 1056 m and shows 4 outliers which

have a higher Δh than the maximum of the range.

Visual interpretation of Figure 29 shows that the DSGSDs occur in areas of lower elevation (brownish color). The blue part, which refers to regions of higher elevation, is mostly free of mass movements. This visual impression is valid for all mass movements (including the mass movements smaller than 0.3 km²) which were marked in course of the GIS Analysis. As Figure 32 presents, the main parts of the analyzed DSGSD have a value of H_{max} (refers to the point of highest altitude of the corresponding mass movement) of about 1800 m.a.s.l. This is in comparison with the maximum value for H_{max} (2271 m.a.s..l.) relatively low (compare Figure 31). Therefore this result underlines the visual impression of Figure 29.
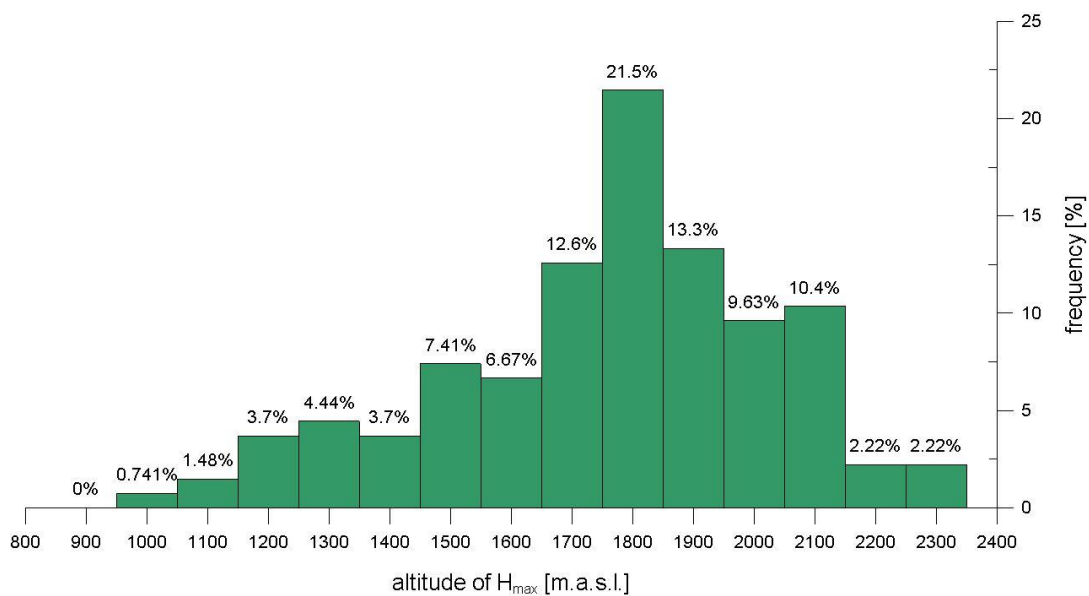
Figure 32: Frequency analysis of H_{max} presented as the percentage of the relative frequency.
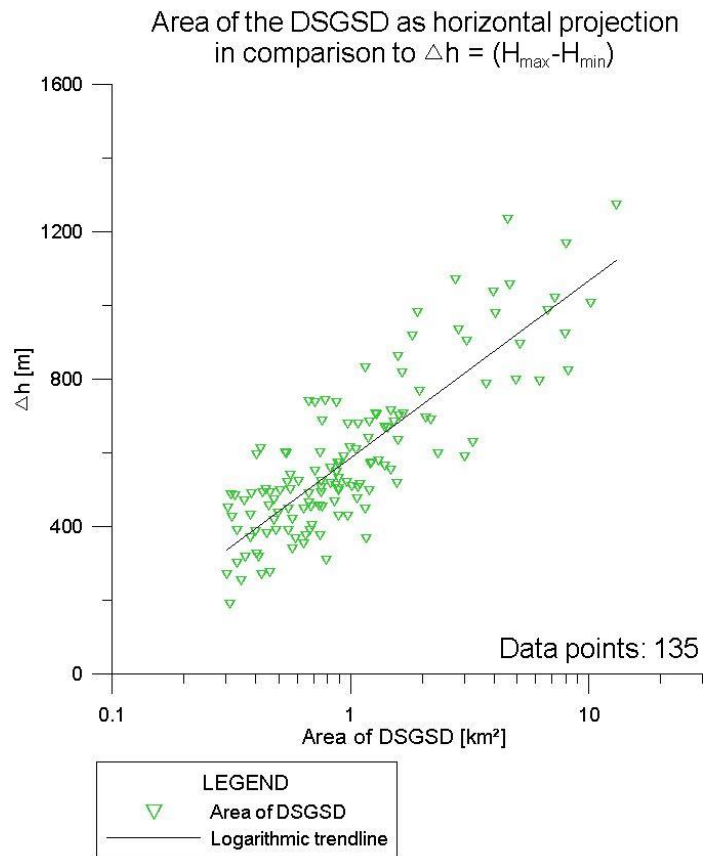
Figure 33: The area of each DSGSD (in logarithmic scale) in relation to Δh (refers to Hmax – Hmin)

- compare Figure 18 (R² of the logartithmic trendline = 0.7)

Figure 33 presents the relationship between the spatial extents (area) of DSGSD to Δh which corresponds to the difference in altitude. It is visible that the length/width ratio correlates with the increase of the affected area by DSGSDs. The diagram reveals that the increase of Δh does not increase at the same scale as the area. Therefore it can be assumed that the majority of the DSGSDs are dominated by its lateral expansion. Once the entire hillside is influenced the area can just increase laterally, if this is possible at all.
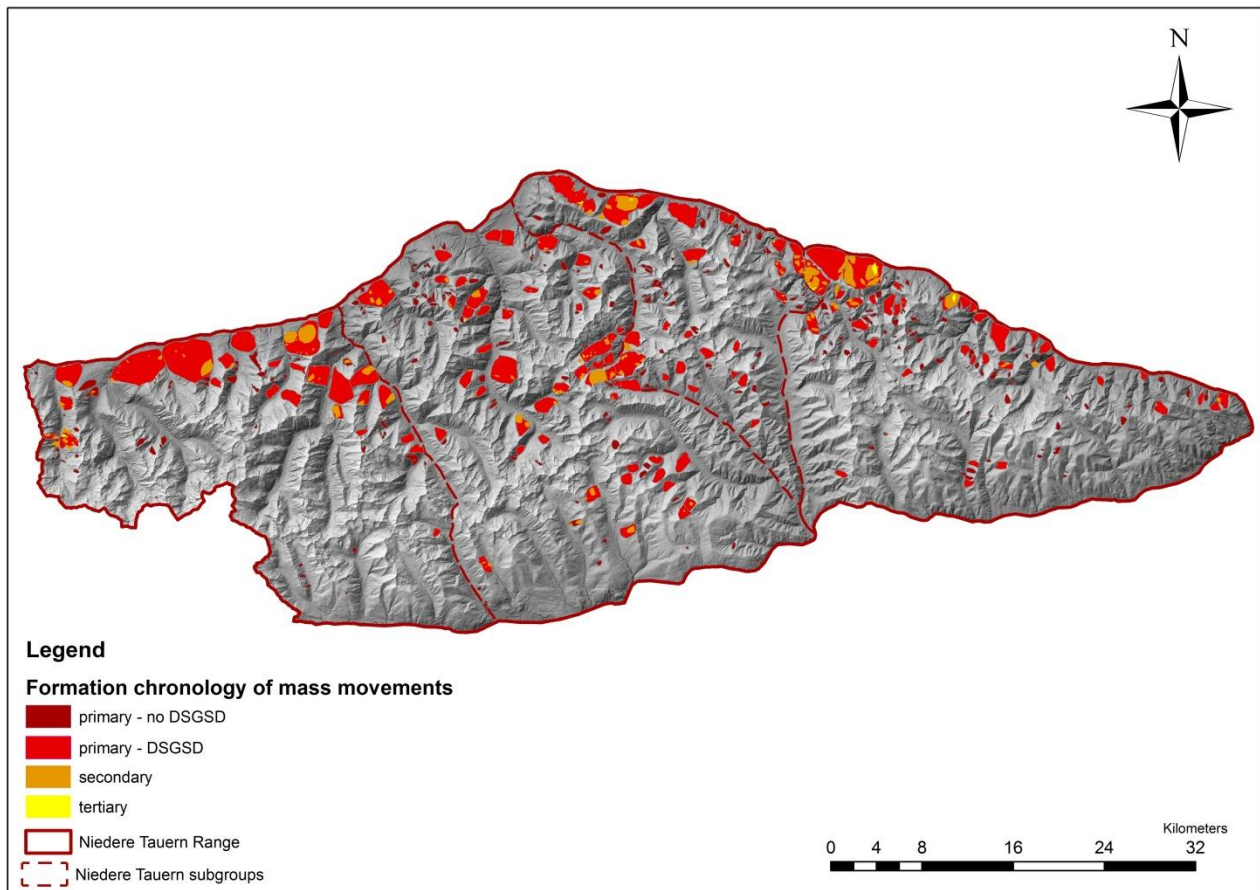
Figure 34: Mass movements colored according to their formation chronology. (Map source: © GIS Steiermark)

Due to the GIS Analysis of the ALS data, 204 km² of the Niedere Tauern Range is covered by primary DSGSDs. Therefore 3 km² of the DSGSDs are secondary movements, but were also classified as DSGSDs. 14.6% of this area is furthermore affected by secondary occurring mass movements, including DSGSDs which are assumed to have formed as secondary mass movement within another DSGSD. The mass movements which are not DSGSDs were not further classified according to their type. 0.4% of the total area (refers to 2.7% of the area of secondary mass movements) show a third movement activity. (Figure 34)

This result underlines the occurrence of secondary / tertiary mass movement events within areas which are already affected by primary gravitational slope deformations. Therefore a segmentation of the involved mass is forming with time.

The analysis according to the segmentation is just an indication according to this phenomenon, due to the fact that the detection of the primary mass movement was of primary importance.

51

8.2. EXPOSITION

By applying the procedure described in chapter 6.3 the angle of the corresponding line segment of the affected hillsides were assigned to each DSGSD. These directions were further subdivided in 8 classes which correspond to the geographic directions north, northeast, east, southeast, south, southwest, west and northwest.

In Figure 35 presents the result obtained from analysis concerning the exposition of the by DSGSDs affected hillsides. The visual impression gained from Figure 35 is that the majority of these hillsides are directed northwards with slight deviations directional east and west. This is referred in the blue, brown and dark violet colored polygons in the representation.
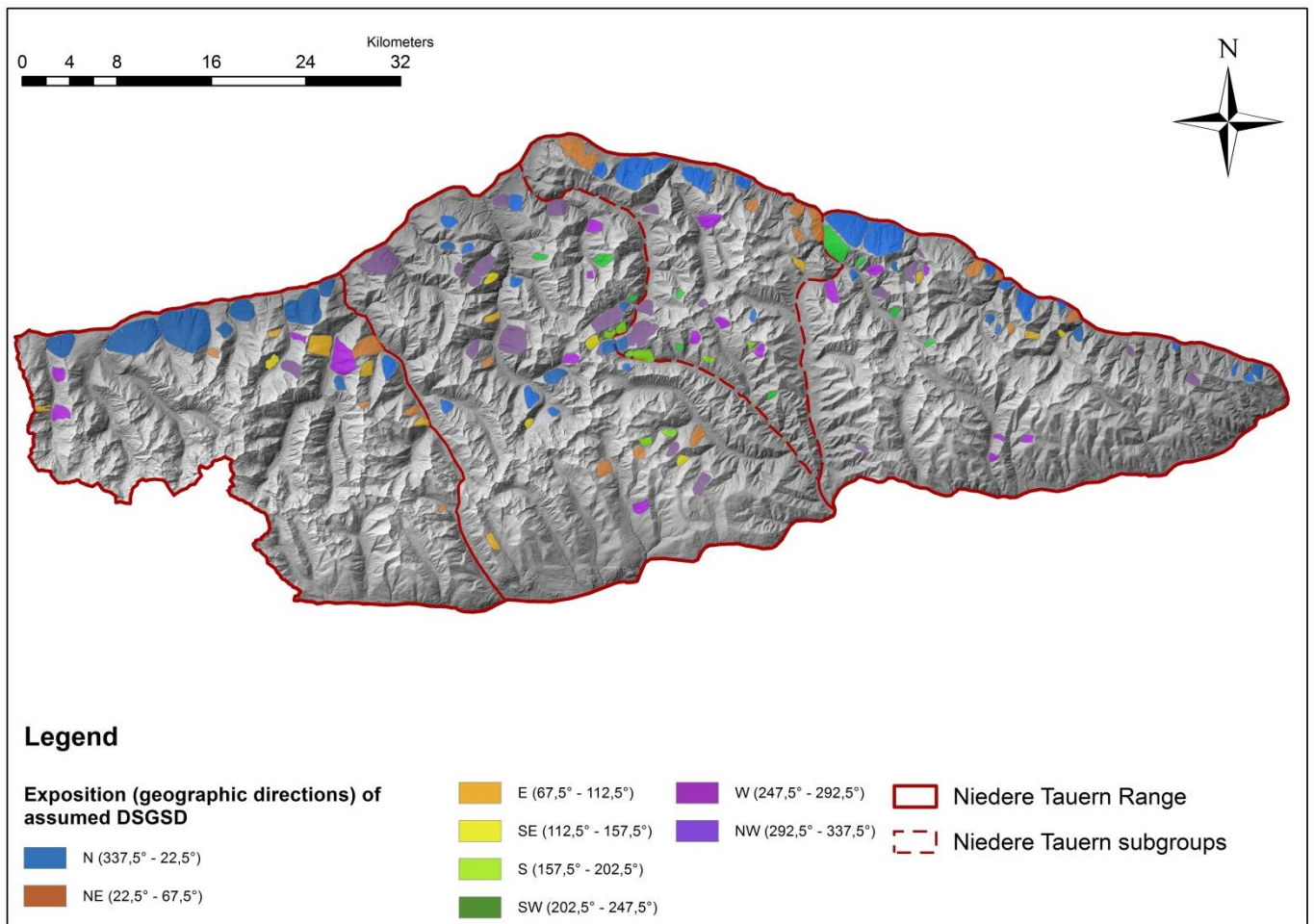
Figure 35: Exposition of the detected mass movements which exceed 0.3 km² in extent.
(Map source: © GIS-Steiermark)

The result of the frequency analysis is presented in Figure 36. The rose diagram shows the absolute frequency as total numbers, the bar chart represents the relative and cumulative frequency as percentage. The diagrams show that the majority of the hillsides affected by DSGSDs have an exposition direction of north (31.1%), northwest (17.0%) or northeast (13.3%).

This corresponds to an angle of the line segment between 292.5° and 67.5°. In total numbers, 83 (61.5%) of the 135 analyzed DSGSDs, which are northwards (N, NE and NW) in direction, are affected by the mass movement. The results of the statistical analysis affirm the visual impression given from Figure 35.

Frequency of assumed DSGSDs ≥ 0.3 km² according to their expositon
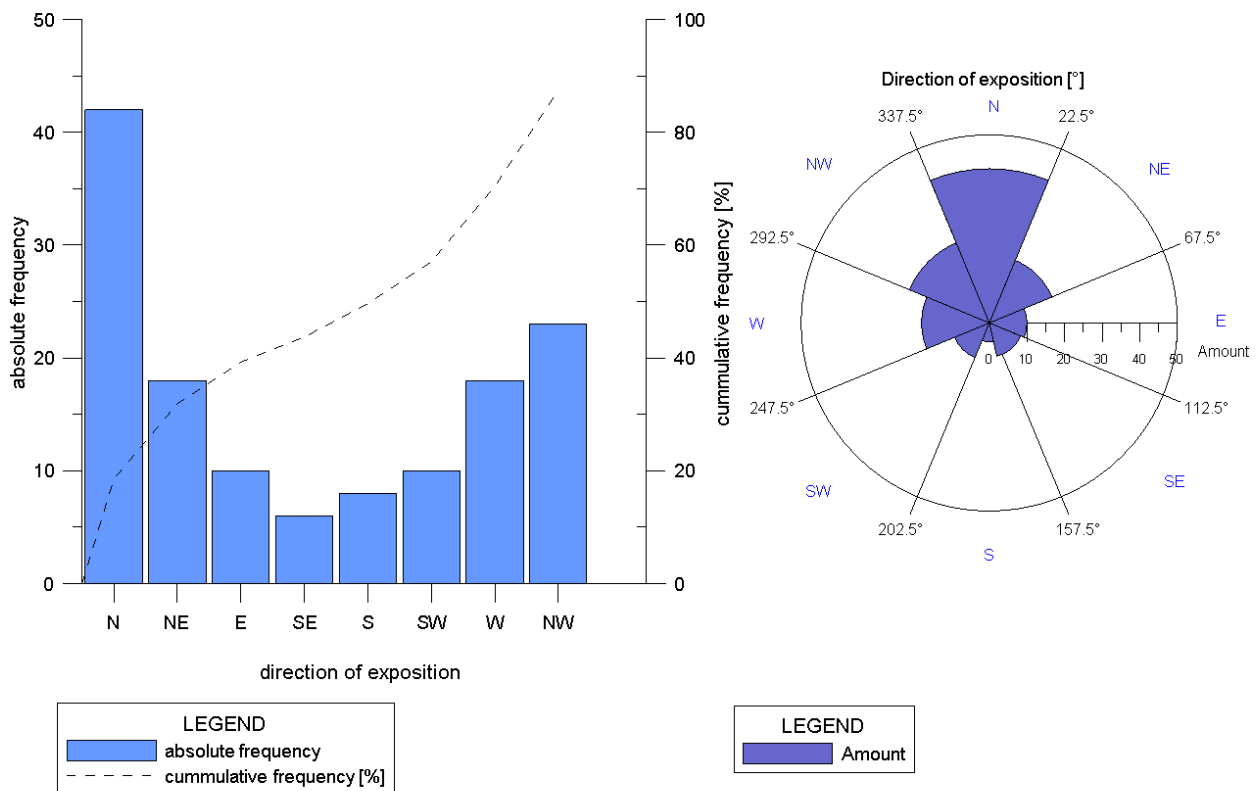
Figure 36: Absolute frequency of the received data visualized as rose diagram. The cumulative frequency in addition to the absolute frequency is presented in the bar chart.

8.3. COMPARISON DISTRIBUTION OF DSGSDS WITH THE EXTENT OF THE LGM

In course of this work phase, an attempt to find a relationship between the assumed DSGSDs and the thickness of the former ice cover during the last glacial maximum. Therefore a visual interpretation was undertaken and further tried to calculate the thickness of the ice sheet above the DSGSDs according to the paleogeographic map from Van Husen (1987) of the last glaciation period (Würm). Within the map, the surface of the ice sheet is expressed as absolute elevation in meters above sea level.

In Figure 37, the overlay of the dataset which contains the assumed DSGSDs is visualized. The map reveals that the areas of the assumed DSGSDs weren't entirely covered by the glaciers of the last glacial maximum. The mass movements situated in the easternmost part of the regional investigation area, the SeT, were just partly affected by this glaciation stage.
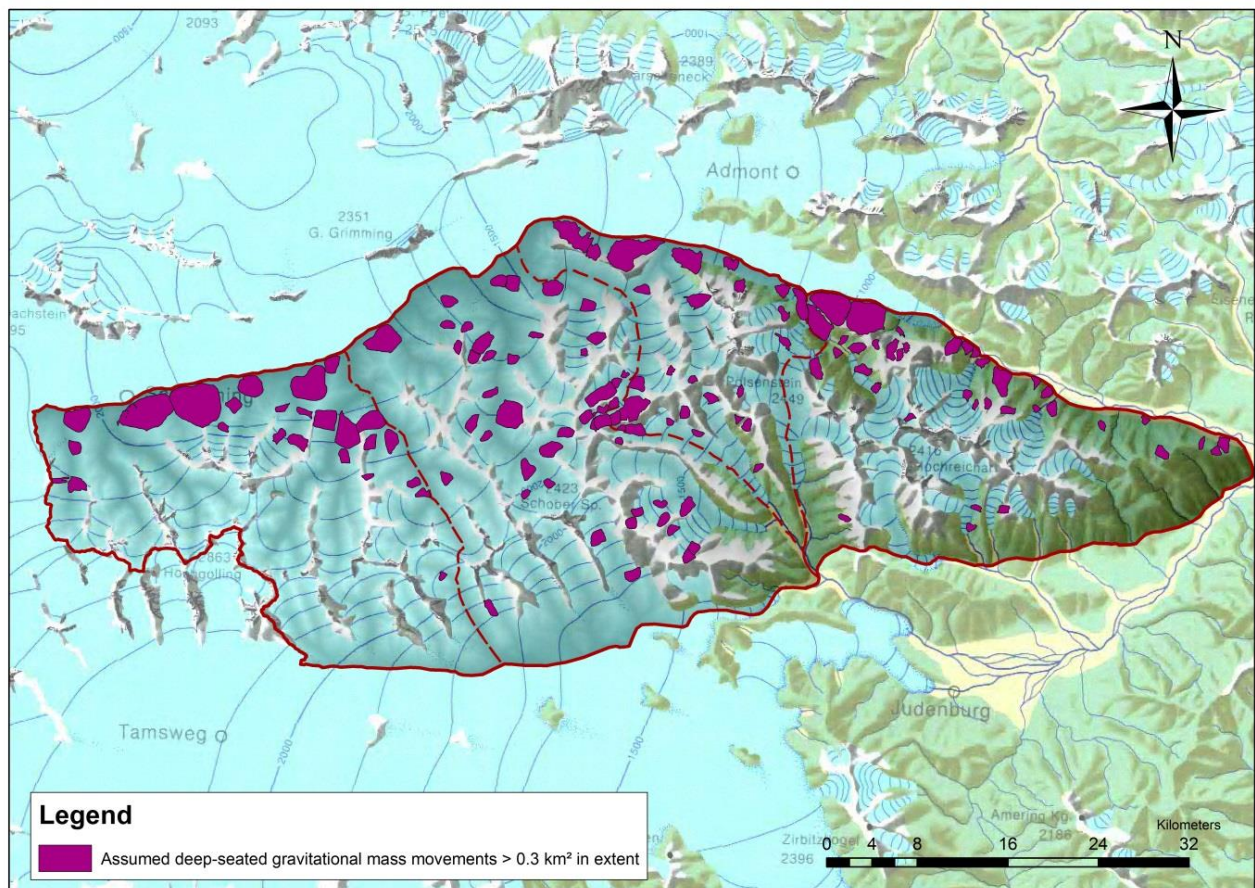
Figure 37: Overlay of the layer containing the assumed DSGSDs over the extent the LGM (map source: Paleogeographic map m 1 : 500.000 (Van Husen,1987))
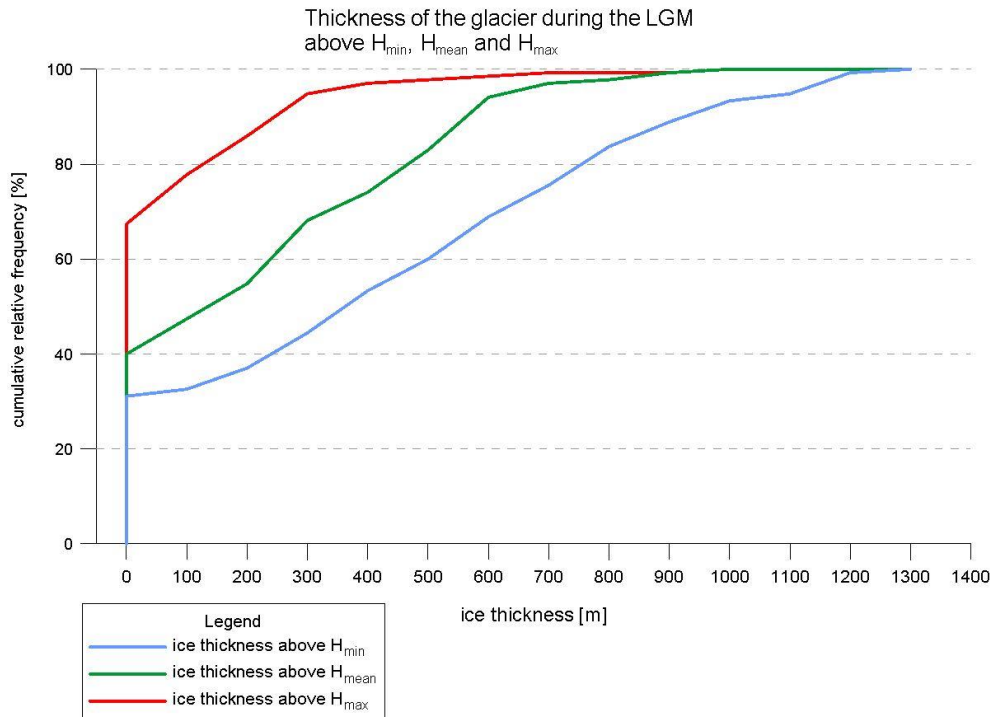
Figure 38: Frequency analysis presented as cumulative frequency in percent of the received data for the ice thickness above H_{min}, H_{mean} and H_{max} (parameters correspond to the minimum, the mean and the maximum elevation of the DSGSDs).

As Figure 38 visualizes, 31% (refers to a total number of 42 DSGSDs) of 135 anazlyzed DSGSDs were not covered by the glacier of the LGM during Würm glaciation stage. 60% (in total numbers 81) of the analyzed DSGSDs were partly covered, means the ice cover reached at least above the mean elevation (Hmean) of the corresponding DSGSD. At least 44 (33%) of the DSGSDs were entirely covered by the ice sheet. This means that the ice cover reached above the highest point H_{max} and therefore covered the whole affected hillside.

In Figure 39 the thickness above the specific points H_{max}, H_{min} and H_{mean} is presented as whisker plot with the corresponding median as mean value, the quantiles and outliers if present. The mean ice thickness (above H_{mean}) above the assumed DSGSDs expressed as a median is 323.2 m. The range lies between 0.16 m. and 906.8 m. The maximum ice thickness related to the lowest point H_{min} of the DSGSDs range between 10.5 m and 1274 m with a median of 565.5 m. 50% of the DSGSDs were covered by an ice shield of at least ca. 380 m up to ca.
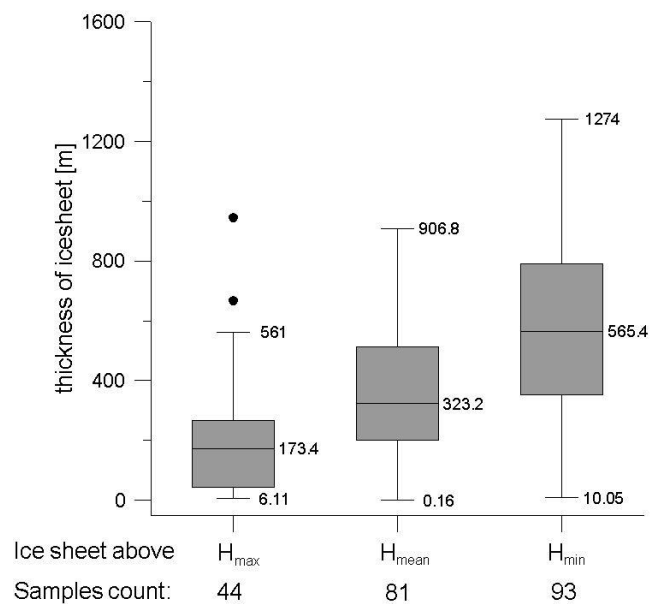
Figure 39: Thickness of the ice sheet above H_{min}, H_{mean} and H_{max} represented as whisker plot with outliers if present. "Null values" were excluded from calculation.

800 m thickness. This is just valid for the DSGSDs which were covered by the glacier.

The following the results, as altitudes of H_{max}, H_{min} and H_{mean}, were related to the thickness of the ice sheet above the corresponding reference point. Furthermore, the area of the specific DSGSD was related to the mean ice thickness of the ice cover (if it was covered) as well as to H_{mean} and Δh to make possible trends visible. "Null values" which correspond to DSGSDs which were not covered by the glacier during the LGM were excluded from the calculation of the line of best fit to avoid falsification of a possible trend. They are only visualized in Figure 40 to gain a visual impression of the amount of mass movements which are not affected by the glacier of LGM.
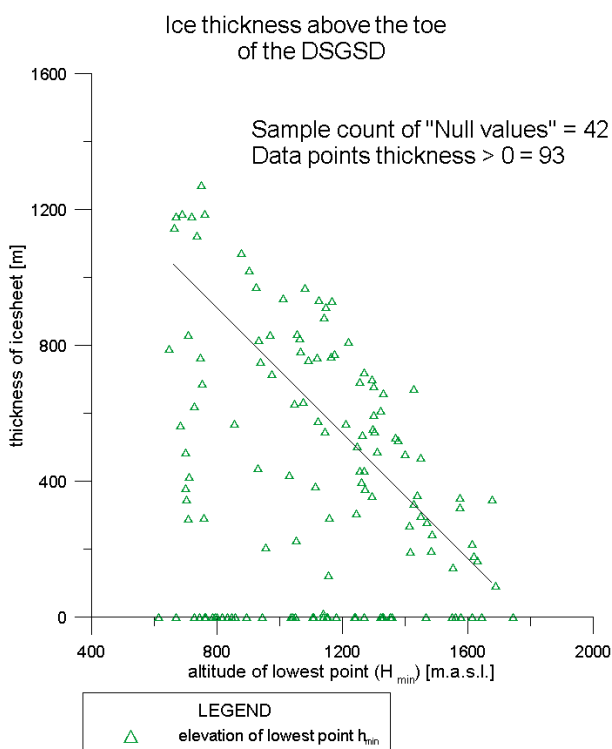
Figure 40: Thickness of the ice cover related to the altitude of the lowest point H_{min}
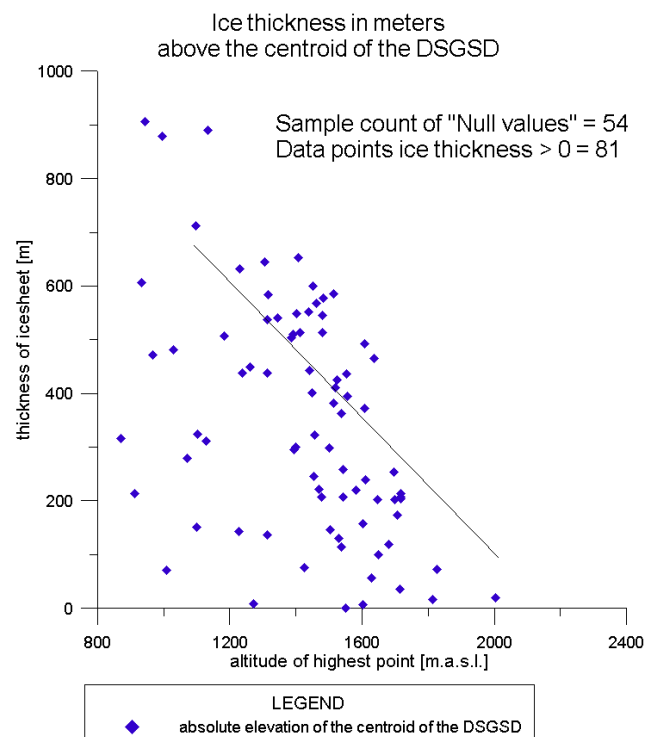
Figure 41: Thickness of the ice sheet during the LGM above the centroid in relation to the elevation of it
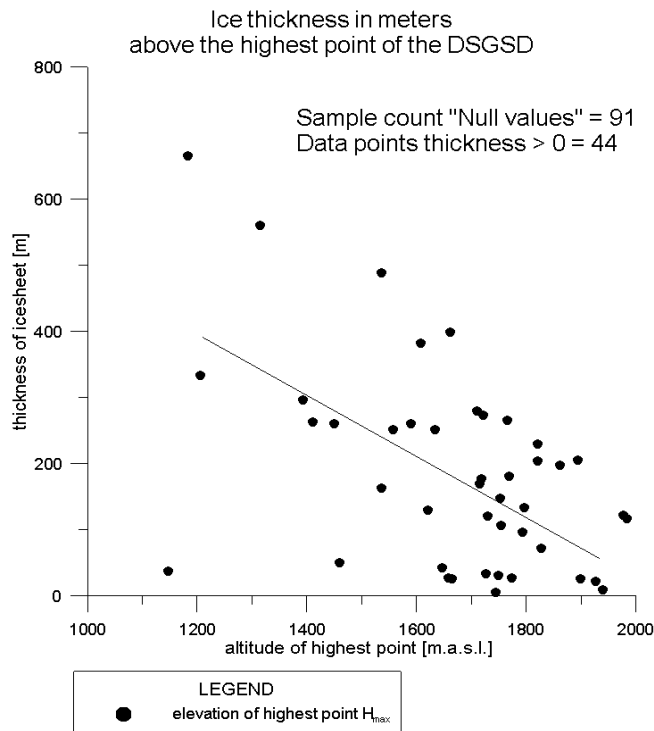
Figure 42: Ice thickness in relation to the point of highest altitude (H$_{max}$) if the DSGSD was covered by an ice sheet during the LGM.

The diagrams Figure 40, Figure 41 and Figure 42 contain information about the possible relationship beween the thickness of the glacier and the altitude of one of the specific points H$_{max}$, H$_{min}$ or H$_{mean}$. They reveal that the lower the altitude of H$_{min}$, H$_{max}$ or H$_{mean}$, the thicker the possible ice sheet above the corresponding reference point. Nevertheless, it is visible that DSGSDs also exist where the lowest point H$_{min}$ is located at a relatively low altitude where the ice cover didn't reach a great thickness.

In Figure 43 and Figure 44 it is visible, that the most assumed deep-seated mass movements involve an area between 0.3 km² (threshold value) and 1.1 km². Just 49 of 135 slope failures are bigger in extent and can reach up to a maximum area of 13.2 km².
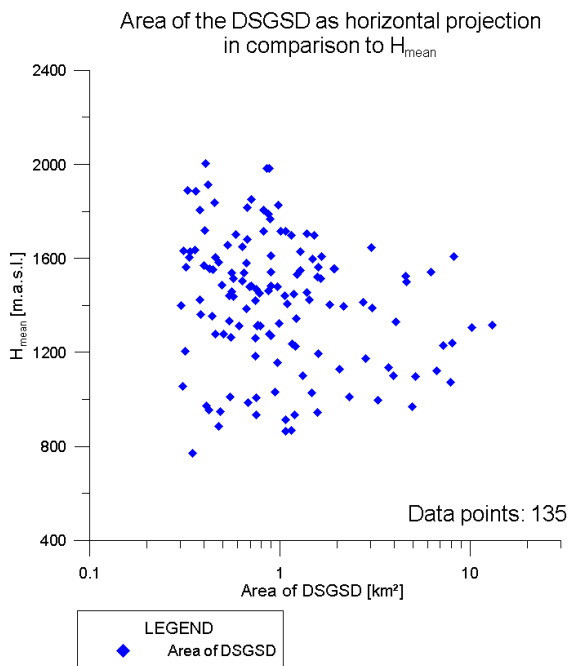
Figure 43: Area of each DSGSD (> 0.3 km²) in relation to the mean elevation (H_{mean}); X-axis (area) plotted in logarithmic scale
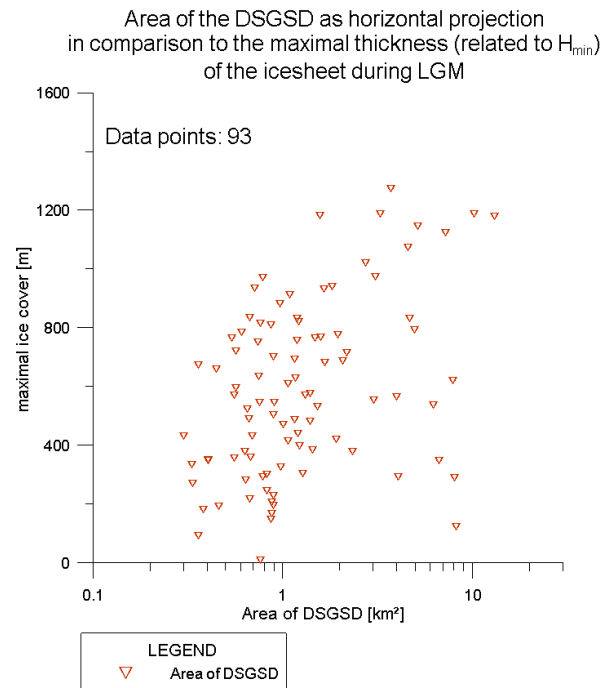
Figure 44: Area of each DSGSD (> 0.3 km²) in relation to the maximal overlay of the glacier (Glacier surface – H_{min}) if it was covered; X-axis plotted in logarithmic scale

Figure 43: The relationship between the spatial extents of DSGSDs and the corresponding mean altitude of the mass movement represented by H_{mean} shows no visible trend. In the range of H_{mean} between 850 m.a.s.l. and 1600 m.a.s.l., the area of the assumed DSGSD cover the entire spectrum from the biggest area to the threshold value of 0.3 km² in extent. The mass movements which show the maximum values for altitude of H_{mean} affect a relatively small area. This has to be seen in relation to the fact that the maximum elevation of the Niedere Tauern Range reaches up to 2800 m.a.s.l. But this is not a trend which can be applied on the entirety of assumed DSGSDs.

Figure 44: The visual impression of the diagram suggests that more DSGSDs which involve a relatively large area were covered by a glacier of great thickness. Slope failures also exist however, which affect a large area, but were just covered by an ice sheet of relatively low thickness (< 400 m). Therefore no explicit trend is visible between the involved area of a DSGSD and the corresponding maximum ice thickness.

8.4. DSGSD IN COMPARISON WITH UNDERLYING GEOLOGY AND

CORRESPONDING ROCK PROPERTIES

As described in chapter 6.3 a categorization into 11 different types of lithologies (compare Table 6) based on the geologic map was done. The result obtained from this work step is presented in Figure 45.
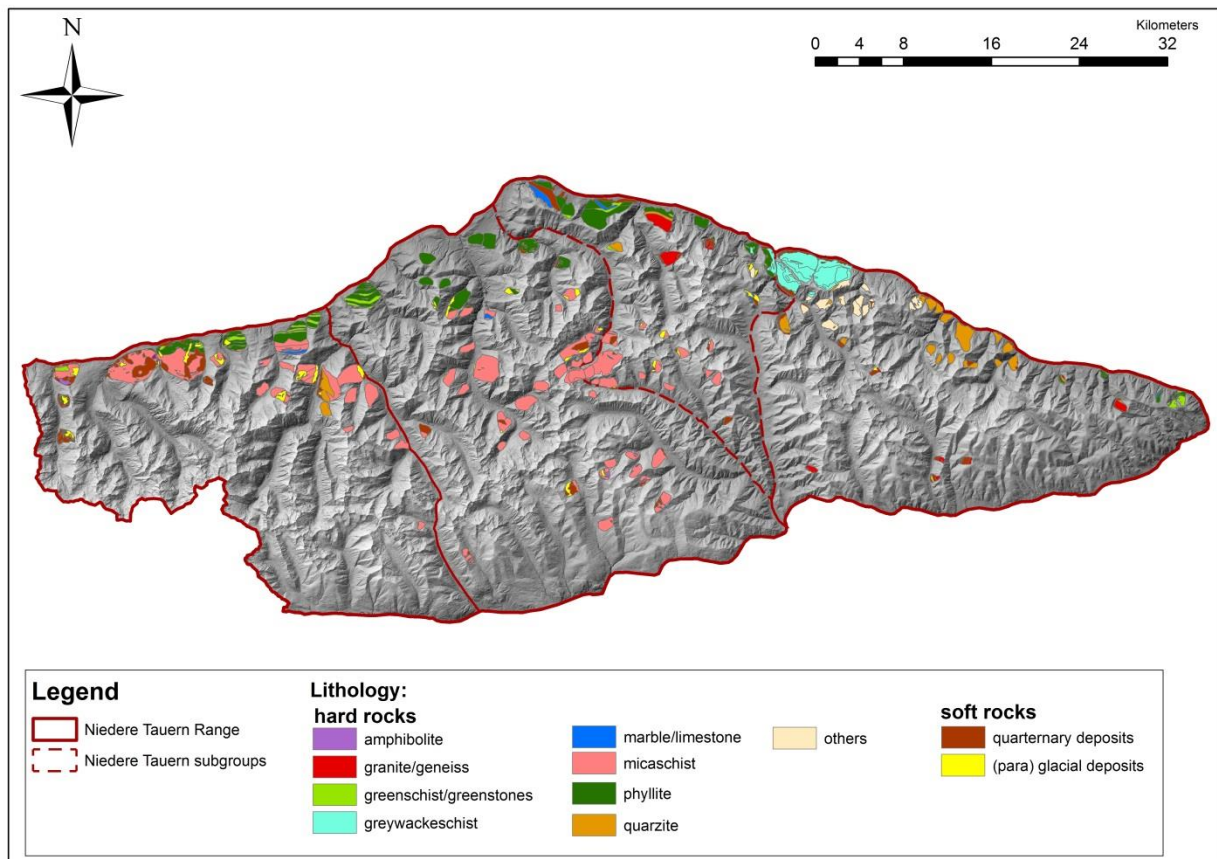
Figure 45: Display of DSGSDs and the simplified lithology occurring within the areas affected by DSGSDs. (Map sources: © GIS Steiermark)

In Figure 45 the simplified lithology for each DSGSD is presented. The visual impression is that the main part of the DSGSDs is built up by micaschist and phyllite.

Granite / Gneiss, Amphibolite, Greenschist / Greenstones and Marble / Limestone seem to be not very relevant according to the formation of this type of mass movement.

As the diagram ( ) and the corresponding Table 6 shows, the main part of the, during GIS-Analysis of ALS-data, detected DSGSDs occur within micaschist (36.1%) and phyllite (18.6%) related to the total area affected by DSGSDs. 11.8% (refers to 24 km²) is covered by other quaternary deposits as (para-) glacial deposits, 9.1% (4.48 km²) by (para-) glacial deposits. For

these areas, data of the underlying bedrock is not available. The results of the frequency analysis (and Table 6) support the above described visual impression although it has to be taken into account that these values are not related to the distribution of each lithology within the whole Niedere Tauern Range. This could relativize this apparently clear result.

Table 6: Results obtained by the frequency analysis.

GeoNr.	Lithology	area [km²]	area [%]
1	micaschist	76	36.6
2	amphibolite	1	0.4
3	granite/geneiss	7	3.2
4	marble/limestone	4	1.8
5	(para) glacial deposits	9	4.4
6	phyllite	38	18.2
7	greywackeschist	19	9.1
8	quarternary deposits	24	11.5
9	quarzite	15	7.3
10	greenschist/greenstones	7	3.5
11	others	8	4.0
	total area	207	
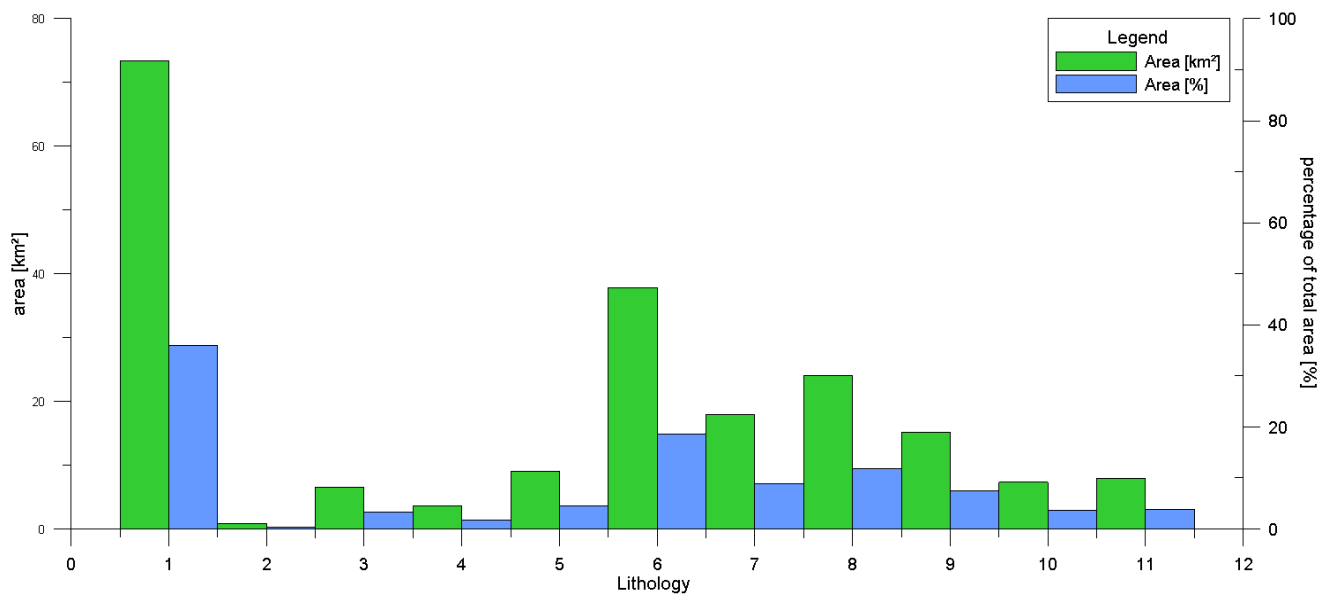
Figure 46: Area as km² and as percentage of the total area for each type of lithology. Each number on X-Axis corresponds to a specific lithology (compare Table 6).

Further the 11 classes of lithology presented previously were further subdivided according to their typical UCS. These are listed in Table 7. This procedure was just applied on hard rocks. Soft rocks as (para-)glacial deposits and other quartenary deposits, were excluded from this classification an marked with *Rn* as grade and *0* as strength class.

Table 7: Classification of the used simplified lithologies according to Table 4. Sources of the values for UCS: A (Schön 2011, 257-258), B – (Eurock 2014 2014, 1129) C- (Button, 2004, 3)

GEO NR	type	UCS	Ref	Grade	Strength class
1	micaschist	5 - 170 MPa (av. 57.8 MPa)	A	R4	1
2	amphibolite	58 - 290 MPa		R5	2
3	granite/gneiss	100 - 325 MPa (av. 181.7 MPa)	A	R5	2
3	granite/gneiss	85 - 250 MPa (av. 174.4 MPa)	A	R5	2
4	marble/limestone	50 - 250 MPa (120.5 MPa)	A	R5	2
4	marble/limestone	85 - 375 MPa (av. 120.9 MPa)	A	R5	2
		50 - 140 MPa (median 95 MPa)	A		
5	(para) glacial deposits	-		Rn	0
6	phyllite	8 - 114 MPa (av. 53 MPa) graphitic	B	R3	1
		14 - 80 MPa (av. 33 MPa) siliceous	B		
		9 - 103 MPa (av. 38 MPa) slaty	B		
		15 - 35 MPa quartz Table 7phyllite, Strenger Tunnel	C		
7	greywackeschist	5 - 170 MPa (av. 57.8 MPa)	A	R4	1
8	quarternary deposits	-		Rn	0
9	quarzite	215 - 310 MPa (av. 288.8 MPa)	A	R6	2
		150 - 300 MPa (median 225 MPa)	A		
10	greenschist/greenstones	5 - 170 MPa (av. 57.8 MPa)	A	R4	1
11	others	-		R5	0
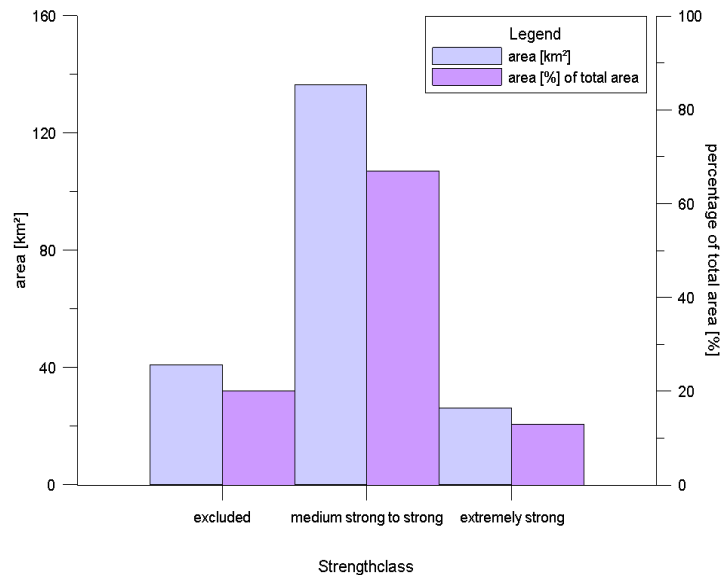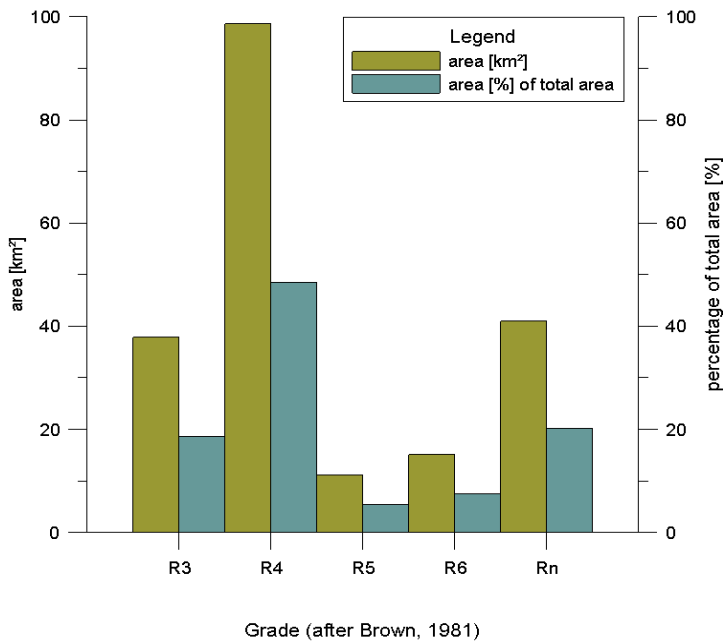
		area	
		[km²]	**[%]of total area**
Grade	R3	37.88	18.22
	R4	102.22	49.17
	R5	11.12	5.35
	R6	15.13	7.28
	Rn	41.54	19.98
strength class	0	41.54	19.98
	1	140.10	67.39
	2	26.24	12.62
lithology	1	75.77	36.45
	2	0.85	0.41
	3	6.59	3.17
	4	3.68	1.77
	5	9.08	4.37
	6	37.88	18.22
	7	19.12	9.20
	8	24.07	11.58
	9	15.13	7.28
	10	7.33	3.52
	11	8.39	4.03
sum		207.87	

Figure 47: Visualization of the percentage of slope deformations occurring in isotropic or anisotropic rock masses. The division into grades was done after Brown, 1981 from Hoek and Brown, 1997. The strength classes in the left diagram are summarized from the first classification in grades. The used classes and grades are listed in Table 7.

The results obtained from this step are displayed in Figure 47. As the diagram reveals (Figure 47), the main part of the analyzed DSGSDs occur within rock masses which are classified as medium strong to strong (67.4%) – grade R4 and R5 according to Hoek & Brown (1997). This refers to an UCS in a range between 5 MPa and 50 MPa and includes lithologies as micaschist, greenschist / greenstones and phyllites. Just 12.6% of the detected assumed DSGSDs occur in areas which are dominated by very strong to extremely strong masses what refers to values for UCS bigger than 50 MPa.

Within this context it is striking that the majority of the DSGSDs have as underlying bedrock rock masses which show typically a high grade of anisotropy. This is valid for all the rock masses which were classified as medium strong and strong.

8.5. SUMMARIZED RESULTS

- As result of the visual analysis of the distribution, the DSGSD within the Niedere Tauern Range occur mainly in the northern part, along the Enns Valley and in several tributary valleys within the Niedere Tauern Range, but not in the same intensity as in the Enns Valley itself. In comparison with the general elevation of the areas where the DSGSDs occur, the visual impression is that the DSGSDs mainly exist in the lower parts of the Niedere Tauern Range.

- The exposition of the hillsides affected by DSGSDs is mostly in a northern, northwestern or northeastern direction.

- The spatial distribution of the detected DSGSDs is consistent with the distribution within the lithologies. Along the Enns Valley, mainly schist and phyllite are present which are classified as rock masses of low rock strength and high anisotropy. As mentioned above 67.4% of the analyzed DSGSDs and therefore the majority are built up by this kind of lithology.

- Furthermore, it was determined that within the primary DSGSDs, secondary or even tertiary mass movements occur. This is considered to be a result of the formation of further shear zones within the primary DSGSD. As mentioned in chapter 3.2 this phenomenon is described as segmentation and was already described by several researchers.

- The results of the analysis according to the ice cover during the LGM show that in total 42 of the in total 135 DSGSDs were entirely covered by the glacier. It is further visible that the lower the altitude of the reference points H_{min}, H_{mean} and H_{max}, the higher the ice cover. The analysis of the relationships between the involved area and the corresponding maximum ice sheet (glacier surface above H_{min}) and the mean elevation of the mass movement do not show an explicit trend.

- The relation of Δh to the involved area of the corresponding DSGSD makes it visible that a relationship (logarithmic) between these parameters exist. It can be assumed that the areas of the DSGSDs are dominated by its lateral extension.

9. RESULTS AND DISCUSSION OF THE ANALYSIS OF THE DATA AQUIRED DURING FIELD INVESTIGATION

Based on the data acquired during the field investigation, the absolute elevation of the springs was calculated within the GIS platform. The same procedure was applied on the data which was acquired for springs which are registered as riparian rights within the *GIS Steiermark* (Federal Government of Styria 2016). A frequency analysis has been performed on the received Z-data [m.a.s.l.]. The results are presented for each mapping area in the following.

9.1. DSGSD HAUSER KAIBLING
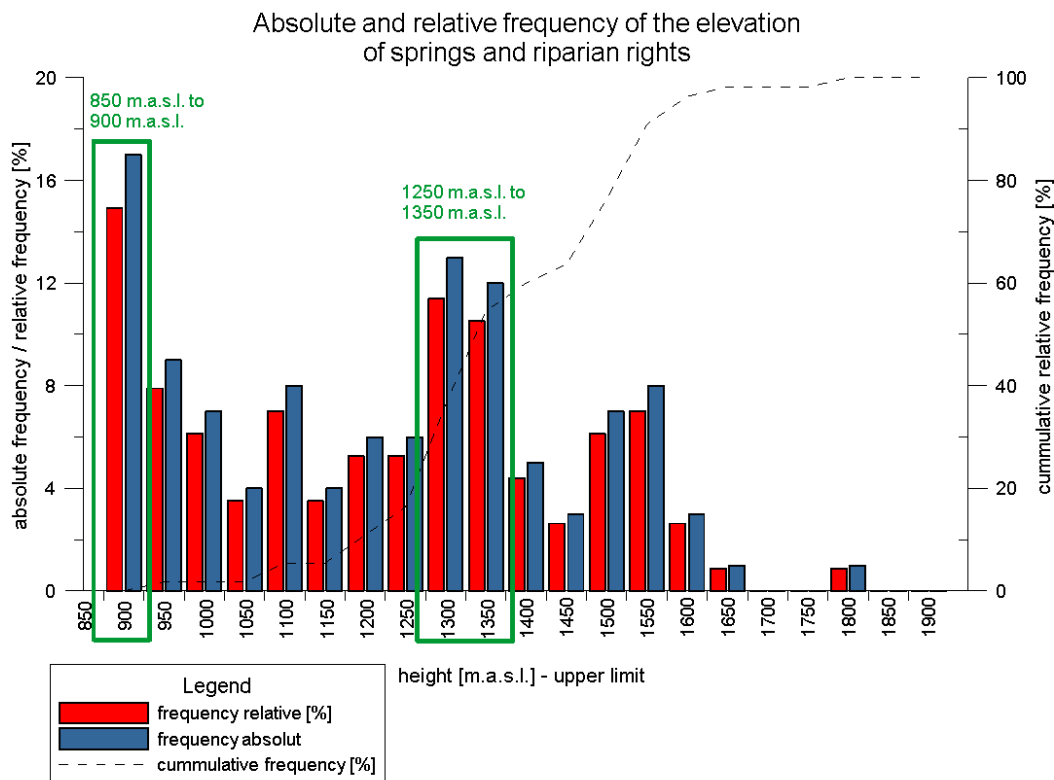
Figure 48: DSGSD Hauser Kaibling: Springs and riparian rights assigned as springs (Federal Government of Styria, 2016) according to their elevation as absolute and relative frequency. Green selection marks the spring horizons.

The diagram above (
Absolute and relative frequency of the elevation
of springs and riparian rights
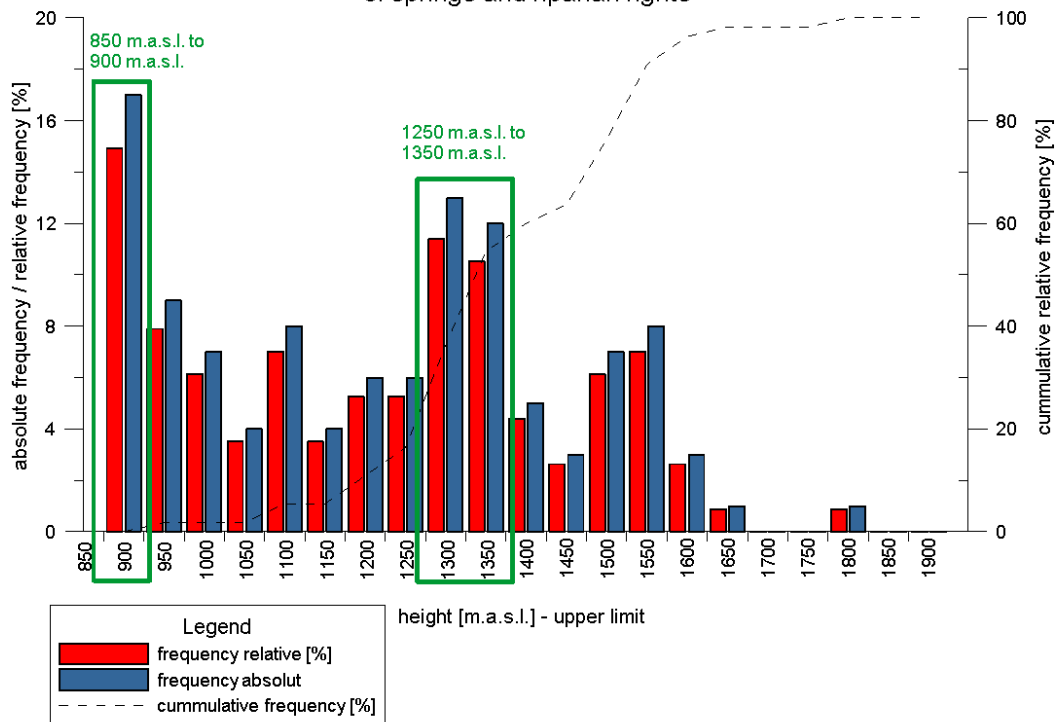
Figure 48) shows the result obtained from frequency analysis using the absolute elevation data for the springs which were reported during field investigation including the riparian rights assigned as springs (Federal Government of Styria, 2016) which are located within the area of the DSGSD Hauser Kaibling.

The diagram shows that the springs occur within preferred horizons. 21.9 % of total 114 analyzed springs and riparian rights assigned as springs are located in an elevation range between 850 m.a.s.l. and 900 m.a.s.l., as well as between 1250 m.a.s.l. and 1350 m.a.s.l.

Figure 49 DSGSD Hauser Kaibling: Springs without riparian rights (Federal Government of Styria, 2016) according to their elevation as absolute and relative frequency. Green selection marks the spring horizons.

If the frequency analysis is just performed on the springs which were reported in course of the field work, then just two spring horizons are present. These are located at an altitude between 1250 m.a.s.l. and 1350 m.a.s.l. as well as between 1450 m.a.s.l. and 1550 m.a.s.l.

9.2. DSGSD MODITZEN AND GROßSÖLK

The diagram (Figure 50) reveals that the springs of the DSGSD Großsölk occur in preferred elevation ranges as so called spring horizons. In this case, 86 % of total 14 springs occur within two horizons. These are situated between 1200 m.a.s.l. and 1300 m.a.s.l. and in a range of 1400 m.a.s.l. up to 1550 m.a.s.l.
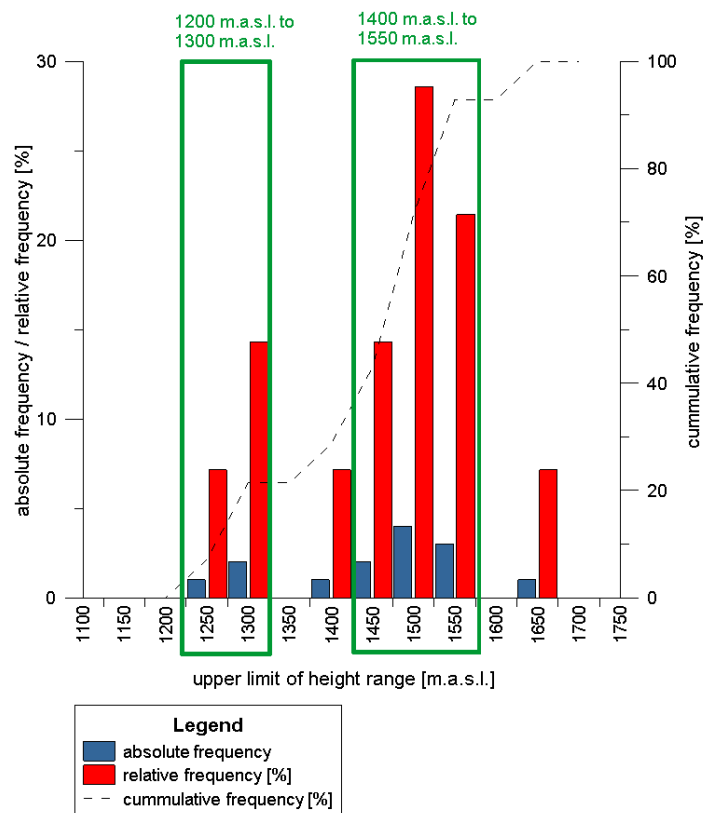
Figure 50: DSGSD Großsölk: Springs accoring to their elevation as absolute and relative frequency. Green selection marks the spring horizons.

For the DSGSD Moditzen it behaves similarly as at the DSGSD Großsölk which is obviously due to the fact that they are located on adjacent mountains. Here are the spring horizons located in an elevation range between 1200 m.a.s.l. and 1300 m.a.s.l. as well as between 1450 m.a.s.l. and 1500 m.a.s.l. Compare Figure 51 below.

Absolute and relative frequency of springs according to their elevation
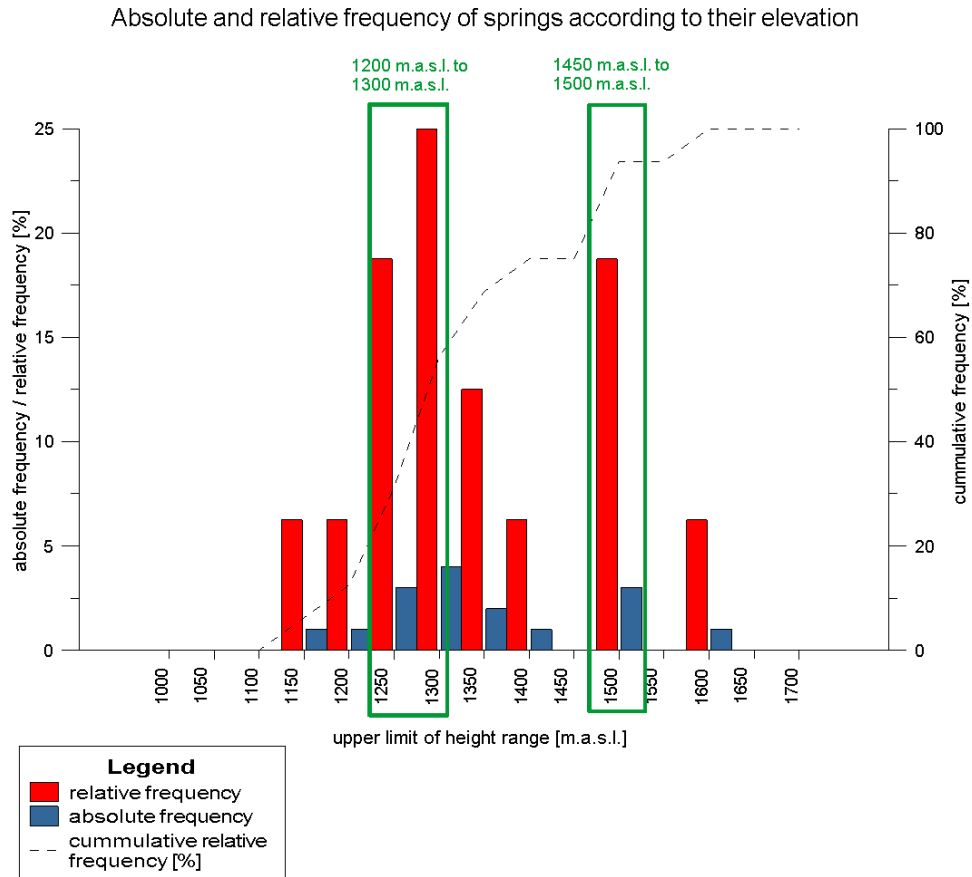
Figure 51: DSGSD Moditzen: Springs according to their elevation as absolute and relative frequency. Green selection marks the spring horizons.

9.3. DSGSD VOETTLECK

Absolute and relative frequency of springs according to their elevation
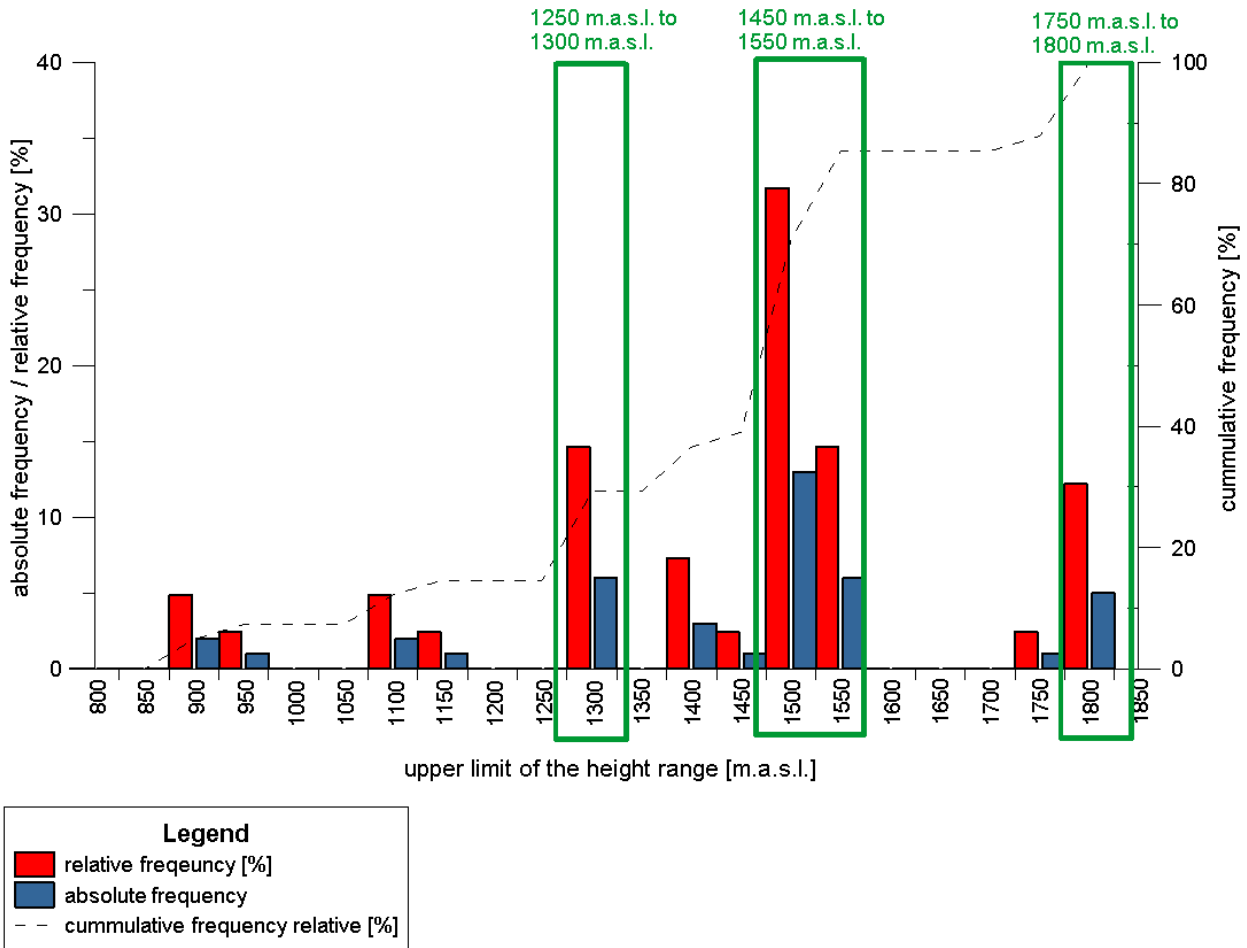
Figure 52: DSGSD Voettleck: DSGSD Moditzen: Springs accoring to their elevation as absolute and relative frequency. Green selections mark the spring horizons (Data has been provided by Bevilaqua (2016) and Oberbichler (2016))

The diagram above (Figure 52) shows the result of the frequency analysis performed on the absolute elevation data for the documented springs during field investigation by Oberbichler (2016) and Bevilaqua (2015) which are located within the DSGSD Vöttleck.

The diagram shows that the springs occur within preferred horizons as well. The majority of the analyzed springs are located in an elevation range between 1250 m.a.s.l. and 1300 m.a.s.l. as well as between 1450 m.a.s.l. and 1550 m.a.s.l.

9.4. COMPARISON OF THE DETAIL MAPPING AREAS

Based on the frequency analysis presented in the previous chapters of each DSGSD, it was determined that the springs occur in so called spring horizons. The results of the frequency are summarized and presented in Table 8. In the profile (Figure 54), the preferred elevation ranges where springs occur are visualized.

Table 8: Summarized results of the frequency analysis of the springs.

Name of DSGSD	Spring horizons			H_{min}	H_{mean}	H_{max}	Δh
	[m.a.s.l]			[m.a.s.l]	[m.a.s.l]	[m.a.s.l]	[m.a.s.l]
Hauser Kaibling	850-900**	1250-1350*/**	1450-1550*	720	1316	1992	1272
Moditzen		1200-1300	1450-1500	1011	1402	1927	917
Großsölk		1200-1300	1400-1550	903	1412	1973	1070
Vöttleck		1250-1300	1450-1550	702	1122	1686	985

result based on the frequency analysis without taking the riparian rights according to the Federal Government of Styria (2016) into account

*** result based on frequency analysis together with the data of the riparian rights (Federal Government of Styria, 2016)*

In comparison of the DSGSDs with each other, it is remarkable that the spring horizons occur at the same or at least at a similar range of elevation (compare Table 8). The first horizon is situated between 1200 (1250) m.a.s.l. and 1300 (1350) m.a.s.l. The second spring horizon shows an elevation between 1450 m.a.s.l. and 1550 m.a.s.l.

In the profiles (Figure 54) of the local test sites is visible that the spring horizons occur at 3 of 4 local testing sites (Hauser Kaibling, Großsölk and Motizen) either in the intermediate part or in the lower part of the DSGSD. The local site Vöttleck show that although the spring horizons are located in the same range of elevation as at the other local test sites, the spring horizons are situated in the upper and intermediate part of the DSGSD. This result could indicate that the DSGSDs Hauser Kaibling, Großsölk and Motitzen have an similar internal structure which indicates a similar type of DSGSD according to its kinematics and formation. Hence it is assumed that the DSGSD Vöttleck shows different underground conditions. This result is plausible compared to the results of the steady-state finite model of groundwater conditions performed by Crosta, et al. (2013) where different internal structur leads to different groundwater conditions. Hence the drainage system possibly shows a different drrainage pattern (springs) at the surface.

The basic phenomenon of an occurring spring horizon can be lead back to either the lithology or potentially the outcrop of discontinuities of a zone of weakness. At geologic boundaries where two different geologic units meet, so called contact springs can often occur. This is a result of

the different hydraulic conductivity / permeability of the meeting rock masses (independent of loose or solid rock). (Hölting and Coldewey, 2005)

This is as well the case of shear zones which typically are less permeable due to the occurrence of fault gauge or fault breccia (Crosta 2013). Therefore the water which infiltrates atop follows the shear zone until it reaches the surface and discharges as spring.

The meeting of geologic units could not be confirmed, neither in the field nor by comparing the location of the reported springs with the geologic map. Hence it can be assumed that the spring horizons occur due to zones of weakness which outcrop in these ranges of elevation. The disintegrated bedrock, that is occurring within the volume affected by DSGSDs, forms possible pathways for the water. At the steeper slope toe the water can finally discharge as spring from the ground. This assumption is at least valid for the spring horizons occurring in the lower part of the DSGSD.

Furthermore, as visible in Figure 54, the DSGSD Vöttleck is mainly built up by a different lithology (Greywackeschist) as the other local test sites (Micaschist). Additionally it is located in the SeT while the DSGSDs Hauser Kaibling, Großsölk and Motitzen are located in the ScT (westernmost part of the Niedere Tauern Range) where the glacier surface of the continuous ice cover of LGM reached up to ca. 900 m.a.s.l. higher than in the SeT. This could be also a possible influence factor, although this has to be proven within further research.
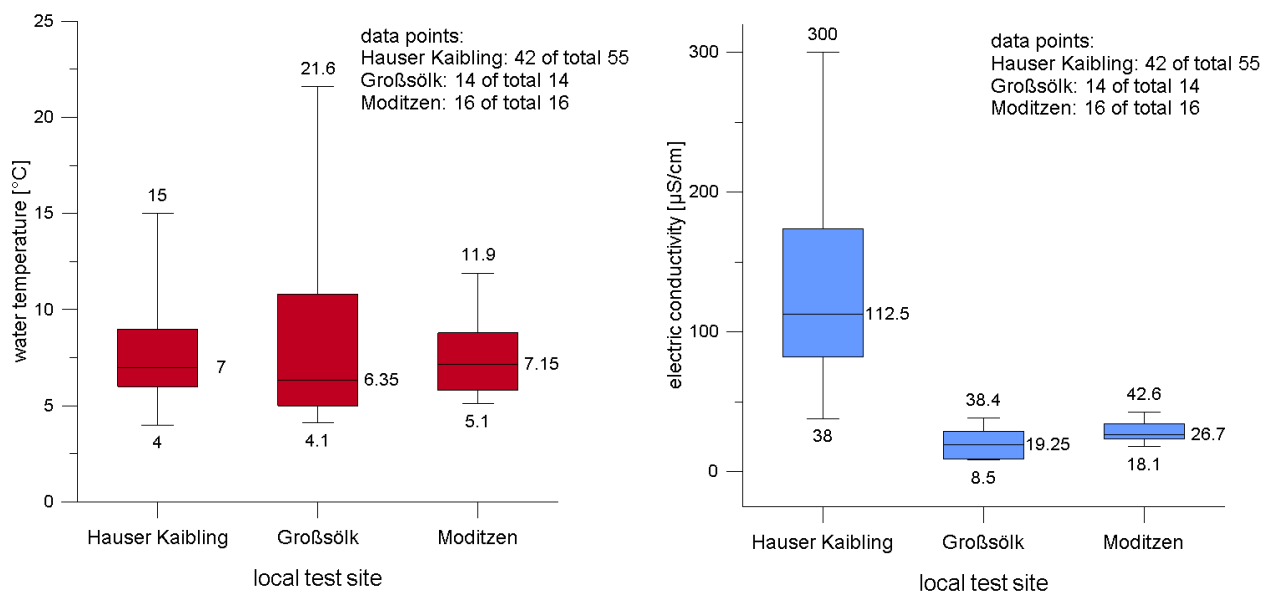
Figure 53: Measured values during field investigation of water temperature and electric conductivity presented as whisker plot with the median, range and outliers if present.

In the diagrams (Figure 53) above, the measured values for electric conductivity and for water temperature are presented as whisker plots with the median as mean value and outliers if present.

The values for electric conductivity lie within the typical range of the crystalline area of the Niedere Tauern Rangen (compare chapter 4.2.1.) The values which were measured at the springs of the DSGSD Hauser Kaibling show higher electric conductivity. This is assumed to be the result of the presence of seams of marble within the catchment area. Compare Figure 25. Low values for electric conductivity, in this area lower than 20 µS/cm, indicate that these springs are influenced by meteoric water and a dilution effect occurs.

The measured water temperature of the spring water mostly lies in a range which is expectable for groundwater (at Moditzen and Hauserkaibling ca. 75%, at DSGSD Großsölk about 50%) and therefore the water possibly flowed through deeper depth of the ground. The springs where higher values (>8°C) were measured are possibly influenced by water which passed through shallow ground depth. Therefore the higher values reflects the impact of solar radiation of summer season. Nevertheless these values have to set into the context with the wheater conditions of this summer, means also lower values for water temperature could origin from water which was circulating in shallow depth.
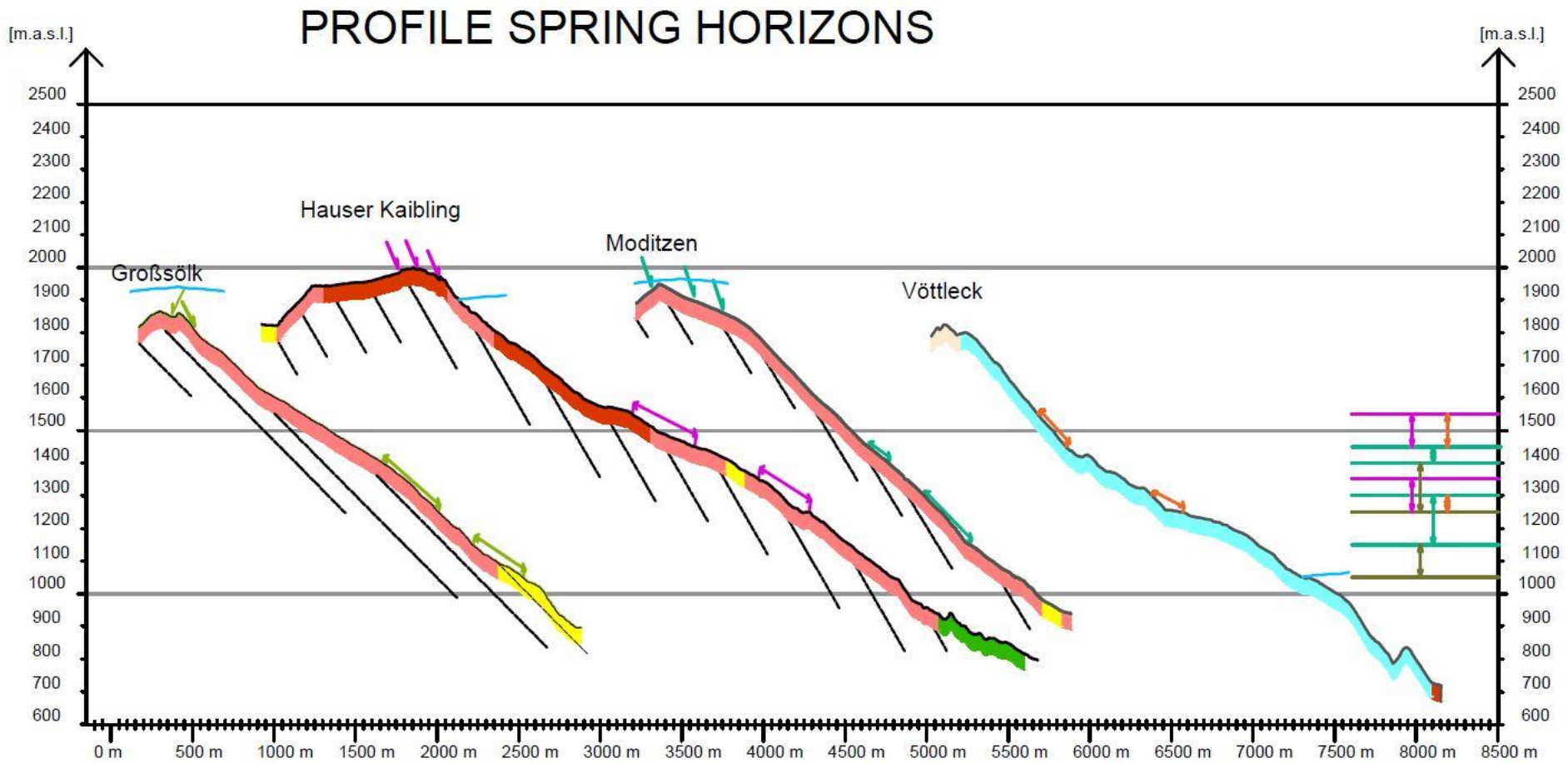
Figure 54: Visualization of the occurring spring horizons based on frequency analysis presented in previous chapters. The spring horizon for the DSGSD Hauser Kaibling is based on the results excluding the riparian rights assigned as springs. The profile is presented two times exaggerated in Y-direction.The arrows at the top near the summits refer to headscarps.

73
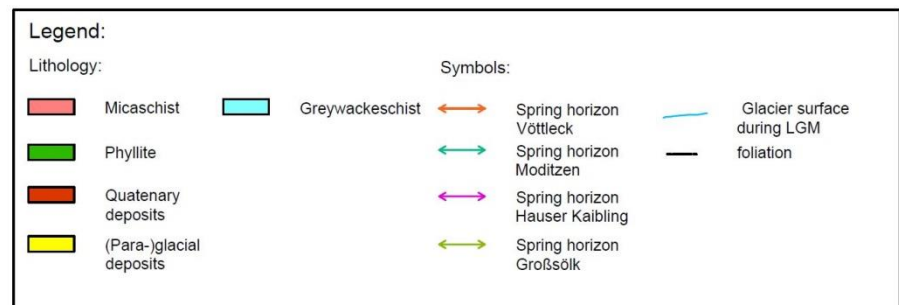
10. CONCLUSION

The following conclusion is based on the results obtained by visual analysis of the provided ALS data as well as statistical analysis of parameters calculated within the GIS platform. Interpretation according the possible influence on drainage system is mainly based on data acquired in the field but include also data provided by the Federal Government of Styria within the platform of GIS Steiermark.

DSGSDs within regional investigation area

Within the styrian part of Niedere Tauern Range 135 assumed DSGSDs exceeding 0.3 km² in extent were detected during visual GIS-Analysis. They cover an area of 207 km² of the Niedere Tauern Range, 204 km² are referred to primary mass movements. Hence 3 km² are assumed to be secondary phenomena which are also bigger than 0.3 km² in extent and were classified as DSGSD. Furthermore 14.6% of the area of primary mass movements is affected by secondary (or even tertiary) movement activity what imply a further segmentation of the DSGSDs.

The majority of the detected assumed DSGSDs within the regional investigation area are located in the norther part of it. 61.5% of the analyzed DSGSDs the northern, northeastern or the northwestern hillside is affected by the mass movement.

The spatial distribution is consistent with the occurrence of schists (micaschist, greywackeschist) and phyllites in this area. These lithologies are, based on the classification (compare chapter 8.4), medium strong to strong rock masses, what refers to UCS values between 25 MPa up to 100 MPa. 67.9%. and therefore the majority of the detected DSGSDs within the Niedere Tauern Range are located within lithologies of this type related to the rock strength. Hence it can be considered that DSGSDs occur preferentially within rock masses of low rock strength.

Furthermore these geologic units are characterized by high anisotropy due to occurring discontinuity networks such as schistosity or joint sets caused by tectonic processes. The influence of the orientation of the mentioned discontinuity- and fault networks is not part of this master thesis and therefore a possible starting point for further studies.

The valley shape within the Niedere Tauern Range is suggested to be U-shaped with oversteepened sidewalls if they were affected by glaciation. Therefore, it can be assumed that the sidewalls of these valleys showed a broken profile due to the influence of several successive glaciation stages. (Compare chapter 3.3.2), what is according to Ambrosi and Crosta (2011) an important factor concerning the formation of DSGSDs. Within the Niedere

Tauern Range, valleys are present which were, according to the Paleogeographic map from Van Husen (1987), not affected by the continuous glacier of any of the glaciation periods of the Quatenary. Nevertheless it has to be considered that these areas were affected by the occurrence of local glaciers and other glacial processes which occur independently of coverage by an ice sheet. These are located in the easternmost part of the Niedere Tauern Range, the Seckauer Tauern.

As the results of the analysis of the relationship of the assumed DSGSDs to the extent of the glacier of the LGM shows, 42 of 135 mass movements are situated in the above mentioned areas which were not covered by the continuous glacier of the LGM.

Therefore glacial processes are assumed to be very important influencing factors (preconditioning) for the possible formation of deep-seated rock failures but according to the analysis no triggering factor. This is underlined by the result that DSGSDs obviously exist also in areas which were not affected by a continuous glacier.

Furthermore it was determined that a relationship between the affected area of DSGSDs and the difference in altitude Δh exist. As the area increases also Δh increases although not at the same scale. Therefore a correlation between the length/width ratio to the area exist. Further it can be assumed that the area is dominated by its lateral extension.

Influence of DSGSDs on the underlying drainage system

Based on results obtained by performing a frequency analysis, it can be considered that springs are occurring in preferred spring horizons. This is assumed to be a result of the heavily disintegrated bedrock typical for the mass volumes which are affected by DSGSDs in particular. The disintegrated bedrock is mostly higher permeable than the basal shear zone. Therefore the water infiltrates atop of the DSGSD, stays above the shear zone and follows either the discontinuities (disintegrated bedrock) or at least the basal shear zone until it reaches the surfaces and discharge as spring (compare Figure 4).

Although the spring horizons lie within the same ranges in all of the local test sites, it is remarkable that in case of 3 local test sites the horizons are situated in the intermediate and lower part of the DSGSD while they are situated at the 4th local test site in the upper and intermediate part. This is assumed to be a result of the internal structure hence 3 of the analyzed sites have possibly similar underground conditions and one has a different structure. Based on the simulation of Crosta, et al (2013), presented in chapter 3.2, the drainage pattern at the surface (springs) is influenced by different underground conditions which are further influencing the groundwater conditions. This is assumed to be a result of differnces in formation

(one or more shear zones) and the hydraulic conductivity (degree of disintegration of the involved rock masses, permeability of the shear zones).

It has to be considered that this is interpretation is simply an assumption of the possible influence of the DSGSDs on the drainage system, based on information acquired about springs within the local test sites which was further set into a context with other researches.

<u>Outline</u>

Based on the numerical results of frequency analysis and on visual intrepretations whch were obtained within this master thesis, already first conclusions were drawn according the two objectives of this work. Nevertheless still many questions remained unanswered.

First of all the influence of the orientation discontinuity- and fault networks on the formation and kinematics of existing DSGSDs within the regional investigation area were not part of this master thesis. Therefore it would be interesting, especially because of the close proximity of the SEMP to the Niedere Tauern Range, to relate the spatial distributions of the DSGSDs to tectonic fault networks. Furthermore the relation to the orientation of discontinuity networks, such as joint sets and schistosity for example would create further interesting results. In particular if the considerations of Agliardi, et al (2013) could be confirmed.

For better understanding regarding the influence of this type of mass movement on the hydrogeologic conditions further studies are recommended.These could include further field investigations with focus on springs again to create a useful dataset where universally valid considerations can derived from.

Therefore to relate the drainage pattern on the surface (springs) to groundwater conditions in the underground possibly geophysical methods could be applied in selected aresa. If possible, as it was already done for example in the Kaunertal (Strauhal, et al 2016), boreholes could give invaluable informations in particular concerning the depth and the properties of shear zones.

11. REFERENCES

Agliardi, F., G. Crosta, and B. Zanchi. "Structural constraints on deep-seated slope deformation kinematics." Engineering Geology (Elsevier) 59, no. 2001 (2001): 83-102.

Agliardi, F., G. Crosta, P. Frattini, and M. Malusà. "Giant non-catastrophic landslides an the long-term exhumation of the European Alps." *Earth and Planetary Science Letters* (Elsevier) 365, no. 2013 (2013): 263-274.

Ambrosi, C., and G. Crosta. "Large sackung along major tectonic features in the Cetnral Italian Alps." *Engineering Geology* 83 (2006): 183-200.

Ambrosi, C., and G. Crosta. "Valley shape influence on deformation mechanisms of rock slopes." *Geological Society, London, Special publications* 351 (2011): 215-233.

Ampferer, O.. "Über einige Formen der Bergzerreißung." *Akademie der Wissenschaften in Wien Mathematisch-Naturwissenschaftliche Klasse Sitzungsberichte*, 1939: 1-14.

Ampferer, O.. "Zum weiteren Ausbau der Lehre von Bergzerreißungen." *Akademie der Wissenschaften in Wien Mathematisch-Naturwissenschaftliche Klasse Sitzungsberichte*, 1940: 51-70.

Austria, Geological Survey. *Webapplikation - Massenbewegungen.* n.d. https://gisgba.geologie.ac.at/ArcGIS/rest/services/AT_GBA_MASSENBEWEGUNGEN/ MapServer (accessed Nov/ 2016).

Ballantyne, C.. "Paraglacial geomorphology." *Quaternary Science Reviews* (Pergamon) 21 (2002): 1935-2017.

Becker, Leander. "Zur Gliederung des Obersteirischen Altkristallins." *Verh. Geol. B.-A.* , no. 2 (Dezember 1981): 3-17.

Bevilaqua. "Massenbewegungen in den Rottenmanner Tauern und hydrogeologische Untersuchungen der Großmassenbewegung am Vötteleck im Paltental (Seckauer Tauern, Steiermark)." Bachelor thesis, Hydrogeologie, Karl-Franzens-Universität Graz, Graz, 2015.

Bidgoli, M. Noorian, and L. Jing. "Anisotropy of strength and deformability of fractured rocks." *Journal of Rock Mechanics and Geotechnical Engineering* (CSRME) 6 (2014): 156-164.

Brown, E. T. 1981. *Rock characterization, testing & monitoring: ISRM suggested methods.* Oxford: Published for the Commission on Testing Methods, International Society for Rock Mechanics by Pergamon Press.

Bryan, K.. "Classification of springs." *The Journal of Geology* 27 (1919): 522-561.

Button, E. A. "Characterization of phyllites for tunneling." *International Journal Rockk Mechanics and Mining Sciences* 41 (2004): 215-220.

Cossart, E., R. Braucher, M. Fort, D. L. Bourlès, and J. Carcaillet. "Slope instability in relation to glacial debuttressing in alpine areas (Upper Durance catchment, southeastern France): Evidence from field data and 10Be cosmic ray exposure ages." *Geomorphology* 95 (2008): 3-26.

Crosta, G., P. Frattini, and F. Agliardi. "Deep seated gravitational slope deformations in the European Alps." *Tectonophysics* (Elsevier) 605 (2013): 13-33.

Crosta, G. "Landslide, spreading, deep seated gravitational deformation: analysis, examples, problems and proposals." *Supplementi di Geografia Fisica e Dinamica Quaternaria* 19 (1996): 297-313.

Cruden, D. M., and D. Varnes. "Landslide Types and Processes." In *Landslides Investigation and Mitigation*, by Keith A. Turner, 36-75. Washington, 1996.

Cruden, D. M. "A simple definition of a landslide." *Bulletin of the International Association of Engineering Geology* 43 (1991): 27-29.

Dramis, F., and M. Sorriso-Valvo. "DSGSDs, related landslides and tectonics." *Engineering Geology* (Elsevier) 38 (1994): 231-243.

Eurock 2014. *Rock engineering and rock mechanics: structures in and on rock masses: proceedings of Eurock 2014. ISRM European Regional Symposium, Vigo, Spain.* Edited by R Alejano. 2014.

Fahrnberger, W. "Morphogenese des Paltentales zwischen Rottenmann und Wald am Schoberpass." Diplomarbeit, Karl-Franzens-Universität Graz, Graz, 2000, 105.

Froitzheim, N., D. Plasienka, and R. Schuster. "Alpine tectonics of the Alps and Western Carpathians." In *The geology of Central Europe*, edited by Tom McCann, 1141-1232. Geolgocial Survey (London), 2008.

Gaidies, F., R. Abart, C. De Captiani, R. Schuster, J. A. D. Connolly, and E. Reusser. "Characterization of polymetamorphism in the Austroalpine basement east of the Tauern

Window using garnet isopleth thermobarometry." *J. metamorphic Geol.* 24 (2006): 451-475.

Gasser, Deta, et al. "Geology of Styria: an overview." *Mitteilungen des naturwissenschaftlichen Vereines für Steiermark*, 2009: 5-36.

Glade, T., and M. Crozier. "The Nature of Landlside Hazard Impact." In *Landslide Hazard and Risk*, by Thomas Glade, Malcolm Anderson and Michael J. Crozier, 43-74. John Wiley & Sons Ltd., 2005.

Harbor, J. M. "Development of glacial-valley cross sections under condition of spatially variable resistance to erosion." *Geomorphology* 14 (1995): 99-107.

Harbor, J. M. "Numerical modelling of the development of U-shaped valley by glacial erosion." *Geological Society of American Bulletin* 104 (1992): 1364-1375.

Hausegger, S., and W. Kurz. "Cataclastic faults along the SEMP fault system (Easter Alps, Austria) - A contribution to fault zone evolution, internal structure and paleo-stresses." *Tectonophysics*, 2013: 237-251.

Hermann, S. "Initial stage of DGSD (deep-seated grvitational slope deformation) as a source of rockfall, landsliedes and debris flow - case studies from national park Sölktäler, Austria." *Internationales Symposium INTERPRAEVENT 1996.* Gamisch-Partenkirchen, 1996. 409-418.

Hermann, S. "Tiefreichende Hangdeformationen im Kristallin der Niederen Tauern." Dissertation, Karl-Franzens-Universität Graz, Graz, 1997, 191+36.

Hermann, S., and L. Becker. "Gravitational spreading ridges on crystalline basement of the Eastern Alps (Niedere Tauern mountain range)." *Mitt. Österr. Geol. Ges.* 94, no. 2001 (August 2003): 123-138.

Hermann, S., G. Madritsch, H. Rauth, and L. Becker. "Modes and Structural Conditions of Large Scale Mass Movements (Sackungen) on Crystalline Basement Units of the Eastern Alps (Nieder Tauern, Austria)." *Mitt. naturwiss. Ver. Steiermark* 130 (2000): 31-42.

Hoek, E., and E. T. Brown. "Practical estimates of rock mass strength." *International Journal of Rock Mechanics and Mining Science* 34, no. 8 (1997): 1165-1186.

Hölting, Bernward, and Wilhelm G. Coldewey. *Hydrogeologie: Einführung in die Allgemeine und Angewandte Hydrogeologie.* München: Elsevier GmbH, 2013.

Huang, A., J. Lee, Y. Ho, Y. Chiu, and S. Cheng. "Stability monitoring of rainfall-induced deep landslides through pore pressur profile measurements." *Soil and Foundations* 52, no. 4 (2012): 737-747.

Hungr, O., S. Leroueil, and L. Picarelli. "The Varnes classification of landslide types, an update." *Landslides* 11 (2014): 167.

Hutchinson, J.N. "General report: Morphological and geotechnicak parameters of landslides in relation to geology and hydrogeology." *Landslides - Proceedings of the fifth international symposium on landslides.* Rotterdam: A.A.Balkema, 1988. 3-35.

Ivy-Ochs, S., et al. "Chronology of the last glacial cycle in the European Alps." *Journal of quaternary science*, 2008, 6-7 ed.: 559-573.

Keil, M., and F. Neubauer. "Initiation and development of a fault-controlled, orogen-parallel overdeepened valley: The upper Enns Valley, Austria." *Austrian Journal of Earth Sciences*, 2009: 80-90.

Kellerer-Pirklbauer, A., H. Proske, and V. Strasser. "Paraglacial slope adjustment since the end of the Last Glacial Maximum and its long-lasting effects on secondary mass wasting processes: Hauser Kaibling, Austria." *Geomorphology* (Elsevier) 120, no. 2010 (2010): 65-76.

Kolle, R. „Geotechnische Analyse Zur Rezenten Großrutschung Kleinsölk" *(Stmk.)*, Diplomarbeit, Karl-Franzens-Universität Graz, Graz, 1997.

Lang, H.-J., J. Huder, P. Amann, and A. M. Puzrin. *Bodenmechanik und Grundbau.* Vol. 8. Springer Berlin Heidelberg New York, 2007.

Lieb, G. "Zur spätglazialen Gletscher- und Blockgletschergeschichte im Vergleich zwischen den hohen und niederen Tauern." *Mitteilungen der Österreichischen Geographischen Gesellschacht*, 1987: 5-27.

Maatsura, S., S. Asano, and T. Okamoto. "Relationship between rain and/or meltwater, pore-water pressure and displacement of a reactivated landslide." *Engineering Geology* 101, no. 1-2 (2008): 49-59.

Madritsch, G. P. "Aktive und inaktive Massenbewegungen in den Wölzer Tauern (Lachtal, Pustertal und Umgebung)." Diplomarbeit, Karl-Franzens-Universität Graz, Graz, 1999.

Mattheß, G., and K. Ubell. *Allgemeine Hydrogeologie - Grundwasserhaushalt: Mit 83 Tabellen.* 2. Berlin [u.a.]: Bomtraeger, 2003.

McColl, S. "Paraglacial rock-slope stability." *Geomorphology* 153-154 (2012): 1-16.

Metz, K. "Der geologische Bau der Wölzer Tauern." *Mitt. naturwiss. Ver. Steiermark* 106 (1976): 51-75.

Nemcok, A, J. Pasek, and J. Rybar. "Classification of Landslides and Other Mass Movements." *Rock Mechanics* 4 (1972): 71-78 .

Oberbichler, D. "Digitale Klassifizierung von Massenbewegungen in den Seckauer Tauern und hydrogeologische und strukturgeologische Untersuchung der Großmassenbewegung am Vöttleck." Bacherlor thesis, Hydrogeologie, Karl-Franzens-Universität Graz, Graz, 2016, 58.

Pfingstl, S, W. Kurz, R. Schuster, and C. Hauzenberger. "Geochronological constraints on the exhumation of the Austroalpine Seckau nappe (Eastern Alps)." *Austrian Journal of Earth Sciences* 108, no. 1 (2015): 172-185.

Prinz, H., and R. Strauß. *Abriss der Ingenieurgeologie.* 4. bearb. Müchen: Spektrum, Akademischer Verlag, 2006.

Rauth, H. "Bergzerreißung und Talzuschub am Beispiel Brennkogel - Gulling / Steiermark." Diplomarbeit, Karl-Franzens-Universiät Graz, Graz, 1996, 65.

Schellhorn, Christian. „Gefügeanalyse Und Mechanik Der Hangdeformation Zinken-Ebeneck : (Kleinsölktal, Steiermark)", Diplomarbeit, Karl-Franzens-Universität Graz, Graz, 2001.

Schmid, S. M., B. Fügenschuh, E. Kissling, and R. Schuster. "Tectonic map and overall architecture of the Alpine orogen." *Eclogae geol. Helv.* (Birkhäuser Verlag) 97 (2004): 93-117.

Schön, J. H. *Physical properties of rocks: A workbook.* Amsterdam [u.a.]: Elsevier Science, 2011.

Strauhal, T., S. Loew, M. Holzmann, and C. Zangerl. "Detailed hydrogeological analysis of a deep-seated rockslide at Gepatswch reservoir (Klasgarten, Austria)." *HYDROGEOLOGY JOURNAL* 24, no. 2 (2016): 349-371.

Styria, Federal Government of. *Digitaler Atlas Steiermark - Gewässer und Wasserinformation.* n.d. www.gis.steiermark.at (accessed 08 2016).

Tollmann, A. *Geologie von Österreich.* Vol. 1. 3 vols. Wien: Franz Deuticke, 1977.

U.S. Geological Survey. "Landslide Types and Processes." *Factsheet*, 2004.

Untersweg, T., and A. Schwendt. "Die Quellen der Blockgletscher in den Niederen Tauern." *Berichte der wasserwirtschaftlichen Planung*, 1995: 1-76.

Van Husen, D. *Die Ostalpen in den Eiszeiten (with paleogeographic map of the last glaciation 1 : 500.000. Die Ostalpen un ihr vorlagn in der letzten Eiszeit (Würm).* Wien: Geologic Survey of Austria, 1987.

Van Husen, D. "Quaternary Glaciations in Austria." *Developments in Quarternary Science*, 2011: 15-28.

Van Husen, D. "Geologic Processes during the Quaternary." *Mitteilungen der Österreichischen Geologischen Gesellschaft* 92 (2000): 135-156.

Varnes, D. J. *Slope Moveement Types and Processes.* Special Report 176: Landslides: Analysis and Control, Washington D.C.: TRB, National Research Council, 1978, 12-33.

Weidner, S., M. Moser, and E. Lang. "Geotechnische und kinematische Analyse des Talzuschubes Gradenbach (Kärnten/Österreich)." *Jahrbuch der geologischen Bundesanstalt*, 2011: 17-60.

Zangerl, C. "Vortrag Erdwissenschaftliches Kolloquium." *Tiefreichende Massenbewegungen - Geologie und Hydrogeologie.* KFU , 2017.

Zangerl, C., et al. "Methodischer Leitfaden zur prozessorientierten Bearbeitung von Massenbewegungen." *Geo.Alp* 5 (2008): 1-51.

Zezere, J. L., R. M. Trigo, and L. F. Trigo. "Shallow and deep landslides induced by rainfall in the Lisbon region (Portugal): assessment of relationships with the North Atlantic Oscillation." *Natural Hazards and Earth System Sciences* (European Geosciences Union) 5 (2005): 331-344.

Zischinsky, U.. "Über Bergzerreißung und Talzuschub." *Geologische Rundschau* 58 (1969a): 974-983.

Zischinsky, U. "Über Sackungen." *Rock Mechanics* 1 (1969b): 30-52.

LIST OF TABLES

LIST OF FIGURES

APPENDIX

App. Table 1: Assumed DSGSDs obtained from GIS-Analysis of the ALS-data which exceed the threshold value of 0.3 km².

number	Name	formation	exposi-tion	glacier surface	part of the NT	area	Data of the polygon-centroid		
							X coordinate	Y coordinate	altitude
		chronolgy	[°]	[m.a.s.l.]		[km²]	UTM 33N	UTM 33N	[m.a.s.l]
DSGSD_1	Gaishorn/Trieben	primary	3	1050	SeT	6.7	463410.5	5258187.09	1122.14
DSGSD_2	Gaishorn/Treglwang	primary	3	1000	SeT	8.06	466342.95	5257202.77	1238.33
DSGSD_3	Huehnerkogel	primary	261	0	SeT	1.06	465611.47	5254552.99	1441.05
DSGSD_4	Huehnerkogel	primary	343	0	SeT	0.4	467238.73	5254854.34	1569.79
DSGSD_5	Dobritschgrabenbach	primary	304	0	SeT	0.99	466130.95	5252599.12	1321.64
DSGSD_6	Grünkarbach	primary	333	0	SeT	0.32	469382.83	5255992.84	1206.22
DSGSD_7	Gruenkarbach	primary	83	0	SeT	0.53	469348.92	5253951.09	1655.67
DSGSD_8	Rosseggbach	primary	315	0	SeT	1.29	468666.79	5254381.55	1629.05
DSGSD_9	Gruenkarbach	primary	292	0	SeT	0.38	469927.59	5254582.38	1424.89
DSGSD_10	Hintertriebental	primary	221	0	SeT	0.54	467275.16	5251028.05	1334.16
DSGSD_11	Triebental	primary	237	1050	RoT / SeT	4.07	462197.67	5256707.75	1329.87
DSGSD_12	Vordertriebental	primary	21	0	SeT	0.5	463830	5254131.03	1277.35
DSGSD_13	Hohentauern	primary	288	0	SeT	1.59	461955.69	5252719.74	1563.51
DSGSD_14	Riedlgraben	primary	337	0	SeT	0.48	464469.45	5239529.23	1583.89
DSGSD_15	Wald am Schoberpass	primary	39	0	SeT	1.59	474046.72	5254675.23	1195.85
DSGSD_16	Wald am Schoberpass	primary	16	0	SeT	0.75	475306.33	5254586.89	1006.86
DSGSD_17	Unterwald	primary	51	0	SeT	0.48	476011.53	5254088.01	949.34
DSGSD_18	Unterwald	primary	6	0	SeT	0.68	476642.66	5253270.59	987.09
DSGSD_19	Doerfl	primary	14	0	SeT	2.83	478341.92	5251628.17	1174.32
DSGSD_20	Kalwang	primary	11	0	SeT	0.48	481381.33	5251555.22	885.2
DSGSD_21	Obere Liesingau	primary	47	0	SeT	0.75	482350.72	5250591.81	932.4
DSGSD_22	Hagenbach	primary	346	0	SeT	0.94	482823.91	5249171.37	1032.29
DSGSD_23	Hagenbach	primary	138	0	SeT	0.31	481403.91	5249190.72	1055.13
DSGSD_24	Mutern in Stmk	primary	332	0	SeT	0.42	487210.07	5247696.58	955.49
DSGSD_25	Kammern im Liesingtal	primary	6	0	SeT	0.35	491024.43	5248137.22	771.08
DSGSD_26	Moetschendorf	primary	19	0	SeT	0.41	496016.26	5246112.08	971.6
DSGSD_27	Rabenkoppe	primary	10	0	SeT	0.32	476032.8	5249530.19	1560.87
DSGSD_28	Rabenkoppe	primary	358	0	SeT	0.55	475319.6	5250423.91	1265.55
DSGSD_29	Kerschkern	primary	233	0	SeT	0.42	470235.72	5248406.57	1911.7

DSGSD_30	Ingeringerbach	primary	260	0	SeT	0.46	475608.41	5238714.09	1278.21
DSGSD_31	Ingeringerbach	primary	289	0	SeT	0.38	476119.55	5240425.2	1362.19
DSGSD_32	Papstriegel	primary	277	0	SeT	0.59	478538.22	5240284.72	1702.87
DSGSD_33	Timmersdorf	primary	9	0	SeT	0.55	497300.94	5245423.35	1011.49
DSGSD_34	Timmersdorf	primary	346	0	SeT	1.07	497994.6	5246040.96	863.7
DSGSD_35	Hennerbach	primary	307	0	SeT	0.97	492511.63	5245289.04	1155.82
DSGSD_36	Feistereralm	primary	25	0	SeT	0.5	477112.48	5249635.19	1485.97
DSGSD_37	Pischingbach	primary	90	0	SeT	0.74	478870.19	5249038.02	1418.51
DSGSD_38	Lärchkogel	primary	57	1150	RoT	0.76	459103.27	5257546.98	1314.45
DSGSD_39	Trieben	primary	63	1080	RoT / SeT	2.33	460660.06	5258380.02	1008.8
DSGSD_40	St. Lorenzen i.P.	primary	44	1125	RoT	1.07	459018.05	5259651.14	911.84
DSGSD_41	Schrattnerkogel	primary	173	0	RoT	0.31	44485166	5247477.23	1630.42
DSGSD_42	Schrattnerkogel	primary	178	0	RoT / WoT	1.48	446015.99	5247316.17	1597.79
DSGSD_43	Schattneralm	primary	328	1700	RoT	1.39	446204.34	5251389.23	1454.38
DSGSD_44	Regenkarspitze	primary	274	1730	RoT	0.82	450367.23	5248839.5	1806.3
DSGSD_45	Saurüssel	primary	219	0	RoT	0.43	456845.89	5243978.46	1555.96
DSGSD_46	Reiteralm	primary	324	1925	RoT	0.4	451049.35	5251759.84	1718.31
DSGSD_47	Bruderkogel	primary	199	0	RoT	0.33	45509133	5248260.99	1889.38
DSGSD_48	Bruderkogel	primary	272	0	RoT	0.71	455875.07	5247713.95	1851.62
DSGSD_49	Seegupf	primary	248	1450	RoT	1.91	451540.56	5258758.32	1555.7
DSGSD_50	Kohlmeisriedel	primary	13	0	RoT	0.45	455270.85	5250702.75	1837.4
DSGSD_51	Kraberg	primary	194	1610	RoT	0.46	451490.39	5247006.7	1603.68
DSGSD_52	Schattnerzinken	primary	204	1760	RoT	0.33	449041.8	5248005.58	1603.45
DSGSD_53	Rottenmann	primary	10	1250	RoT	3.98	450666.5	5262369.73	1099.48
DSGSD_54	Rottenmann	primary	18	1185	RoT	1.15	454420.89	5261985.54	869.26
DSGSD_55	Wieden	primary	30	1440	RoT	4.95	440516.14	5264488.17	967.77
DSGSD_56	Wieden	primary	19	1425	RoT	1.32	442322.72	5263006.91	1101.47
DSGSD_57	Wieden	primary	3	1350	RoT	7.93	445540.35	5262976.51	1071.59
DSGSD_58	Oppenbach	primary	320	1280	RoT	0.89	446663.96	5259695.18	1272.07
DSGSD_59	Rottenmann	primary	24	1160	RoT	0.88	455222.47	5260010.75	1277.04
DSGSD_60	Bergbau	primär	69	1450	RoT	0.79	459158.34	5255111.39	1313.42
DSGSD_61	Gulling	primary	321	1800	RoT / WoT	6.23	444889.42	524880137	1542.14
DSGSD_62	Steinwandkogel	primary	256	1750	RoT	0.82	452683.83	5250124	1714.28
DSGSD_63	Rotleitenkoppe	primary	207	1800	RoT	0.38	449104.01	5252510.73	1807.01
DSGSD_64	Pleschnitzzinken	primary	139	19950	ScT	0.9	414546.26	5246777.57	1481.33
DSGSD_65	St.Nikolai im Sölktal	primary	73	2060	ScT	0.71	42723111	5241694.5	1481.89
DSGSD_66	Ochsenriegel	primary	66	2050	ScT	0.78	426436.77	524263124	1450.25
DSGSD_67	Zinken-Zwieflerseen	primary	29	2100	ScT	0.36	428950.55	5234410.52	1635.52
DSGSD_68	Großsölk - Zinken	primary	62	1925	ScT	3.3	422643.63	5248048.66	1387.9
DSGSD_69	Kleinsölk	primary	288	1950	ScT	4.59	420520.56	5247015.67	1524.75

DSGSD_70	Schusterstuhl	primary	65	2025	ScT	0.4	422375.52	5243183.58	2004.84
DSGSD_71	Niederlabeck-Moaralm	primary	45	1895	ScT	0.57	409587.74	5247551.8	1513.51
DSGSD_72	Hochwurzen	primary	269	2060	ScT	1.09	396485.19	5245747.69	1407.94
DSGSD_73	Gössenberg	primary	346	1875	ScT	3.28	412031.56	5251145.31	996.76
DSGSD_74	Planai	primary	339	1950	ScT	10.34	402905.23	5248845.84	1304.38
DSGSD_75	Hauser Kaibling	primary	350	1900	ScT	13.12	407281.83	5249594.24	1315.63
DSGSD_76	Fleischkögel	primary	103	1900	ScT	3.07	418627.87	5248210.89	1390.44
DSGSD_77	Schladminger Alm	primary	294	1980	ScT	1.66	416222.54	5246282.63	1608.39
DSGSD_78	Fleischkögel W	primary	289	1890	ScT	0.67	416762.51	5248872.76	1386.16
DSGSD_79	Hühnerkogel	primary	82	1885	ScT	0.54	414759.93	5249205.29	1441.75
DSGSD_80	Guschen-Schneiden	primary	286	2100	ScT	1.65	396628.03	5242461.15	1514.34
DSGSD_81	Boringeralm	primary	284	1370	WoT	1.2	441808.14	5258268.81	1227.19
DSGSD_82	Elferkogel-Lantschern	primary	319	1540	WoT	1.19	433969.77	5260441.96	933.17
DSGSD_83	Stubenberg-Plattental	primary	145	1800	WoT	0.67	449266.22	5238492.65	1681.05
DSGSD_84	Sonneck	primary	182	1650	WoT	0.63	448208.61	5240786.61	1504.66
DSGSD_85	Mirzlzinken	primary	73	1900	WoT	0.98	433226.83	5231588.91	1826.93
DSGSD_86	Kampel-Fuchsriedel	primary	295	1750	WoT	0.9	431689.8	5253713.75	1542.17
DSGSD_87	Schaumberg	primary	326	1850	WoT	1.19	431565.77	5247869.18	1449.14
DSGSD_88	Huberwald	primary	72	1750	WoT	0.76	433199.89	5250539.65	1312.54
DSGSD_89	Hahnalpl	primary	123	1990	WoT	0.45	436288.6	5241641.88	1553.54
DSGSD_90	Mooseck	primary	344	1950	WoT	1.95	438482.22	5245588.03	1554.8
DSGSD_91	Kreuzberg	primary	278	1930	WoT	1.07	439844.12	5247068.18	1715.98
DSGSD_92	Hühnereck	primary	298	1800	WoT	4.66	434924.75	5248633.28	1500.88
DSGSD_93	Zachenschöberl	primary	2	1685	WoT	0.69	431117.45	5256397.03	1478.4
DSGSD_94	Fuchsriedl-Fuchsberg E	primary	114	1690	WoT	0.75	433085.89	5253869.2	1468.68
DSGSD_95	Hochrettelstein	primary	261	1685	WoT	0.33	441474.29	5254146.71	1628.28
DSGSD_96	Bröckelalm	primary	347	2025	ScT	0.97	420288.64	5244981.84	1479
DSGSD_97	Stubeggsattel	primary	358	1710	WoT	0.74	429432.39	5256588.69	1260.17
DSGSD_98	Karlspitz	primary	307	1750	WoT	0.64	430321.98	5254623.61	1649.85
DSGSD_99	Hahnalpl	primary	7	1930	WoT	1.58	436438.47	5243823.53	1519.89
DSGSD_100	Schaabspitze	primary	2	1690	WoT	0.74	435153.57	5253556.88	1183.03
DSGSD_101	Edelweißspitze	primary	211	1650	WoT	0.56	437213.9	5255676.22	1536.71
DSGSD_102	Pendleseck	primary	4	1675	WoT	1.17	429499.61	5258673.32	1236.56
DSGSD_103	Brennkogel	primary	167	1800	RoT / WoT	0.67	444115.47	5249642.4	1580.41
DSGSD_104	Brennkogelsattel	primary	167	1900	RoT / WoT	0.65	443011.94	5249051.55	1538.18
DSGSD_105	Hintergullingspitz	primary	131	1920	WoT	1.01	441656.12	5248452.97	1716.27
DSGSD_106	Gulling	primary	206	1700	WoT	0.3	445063.41	5252187.23	1400.49
DSGSD_107	Hochwurzen	primary	349	2025	ScT	3.73	396714.81	5248243.44	1134.86
DSGSD_108	Kochofen	primary	346	1850	ScT	1.57	419195.3	5253078.08	943.22
DSGSD_109	Speiereck	primary	92	1950	ScT	1.15	422604.17	5246187.97	1696.47
DSGSD_110	Moditzen	primary	11	1950	ScT	1.82	424415.23	5246372.3	1401.75

DSGSD_111	Riesnerkrispen	primary	45	1850	WoT	0.61	432843.26	5246763.74	1312.87
DSGSD_112	Jausenkogel	primary	4	2030	WoT	0.87	429287.89	5243050.11	1461.88
DSGSD_113	Speikkopf	primary	15	1990	WoT	0.57	438365.8	5242574.55	1437.98
DSGSD_114	Rindereck	primary	62	1880	WoT	1.39	442665.48	5237766.38	1706.4
DSGSD_115	Brennkogel	primary	355	1780	WoT	0.56	444324.01	5251497.93	1456.77
DSGSD_116	Brennkogel	primary	326	1850	WoT	3.02	442980.45	5250422.41	1647.34
DSGSD_117	Kreuzkogel	secondary	345	1900	RoT / WoT	1.52	443099.39	5248055.43	1698.48
DSGSD_118	Windlucken	primary	346	1850	RoT	0.9	444255.48	5248330.28	1610.27
DSGSD_119	Redlgraben	primary	226	1550	WoT	1.28	442595.82	5255430.85	1549.84
DSGSD_120	Elferkogel	primary	0	1510	WoT	1.48	435185.2	5260259.69	1028.27
DSGSD_121	Hofkogel	primary	44	1500	WoT	1.43	450554.7	5240526.37	1425.19
DSGSD_122	Hühnerkogel	primary	41	0	WoT	0.86	445652.36	5239082.28	1981.72
DSGSD_123	Schwarzkogel	primary	359	1885	ScT	1.22	410555.19	5249501.8	1345.11
DSGSD_124	Brandwall-Predlalm	primary	330	1440	WoT	2.07	438673.91	5259816.28	1129.39
DSGSD_125	Fuchsriedl-Fuchsberg	primary	296	1690	WoT	2.17	432512.57	5254945.58	1394.19
DSGSD_126	Schupfenberg	primary	320	1810	WoT	5.17	423786.91	5255238.82	1097.81
DSGSD_127	Schöttl	primary	251	1660	WoT	1.23	445782.03	5234511.44	1529.95
DSGSD_128	Bärengrube	primary	305	1700	WoT	0.87	451143.52	5236865.45	1787.93
DSGSD_129	Hainzl-Wasserkogel	primary	9	1780	WoT	0.36	444567.81	5246329.7	1884.77
DSGSD_130	Stubenberg-Hofkogel	primary	318	1680	WoT	0.89	448495.46	5239392.23	1768.25
DSGSD_131	Kleiner Zinken	primary	334	1800	WoT	0.88	450649.23	5236124.87	1983.54
DSGSD_132	Scharnitzfeld	primary	166	1830	WoT	0.67	446192.35	5240053.99	1814.36
DSGSD_133	Kochofen	primary	346	1860	ScT	7.21	417290.4	5251283.35	1228.86
DSGSD_134	Vordertriebental	primary	212	0	SeT	0.44	464360.02	5255255.68	1354.74
DSGSD_135		primary	92	2100	ScT	0.55	395152.61	5242845.47	1606.95

App. Table 2: Mass Movements which exceed 0.3 km² in extent but were not classified as DSGSD.

number	Name	formation	X coordinate	Y coordinate	altitude	area
			Data of the polygon-centroid			
		chronology	UTM 33N	UTM 33N	[m.a.s.l]	[km²]
int_1	Gaishorn	secondary	467143.56	5257225.51	1252.9	1.2
int_2	Gaishorn	secondary	465443.46	5258356.97	852.5	0.33
int_3	Gaishorn	secondary	467343.44	5256405.93	1455.5	0.48
int_4	Gaishorn	secondary	464675.46	5257847.82	1047.4	0.45
int_5	Gaishorn	secondary	465183.66	5256936.59	1353	1.34
int_6	Triebental	secondary	461746.64	5257109	1119.6	1.11
int_7	Triebental	secondary	462103.2	5256225.78	1230.4	0.78
int_8	Wald am Schoberpass	secondary	474165.95	5254760.33	1135.8	1.29
int_9	Vorberg	primary	443809.71	5260928.05	1255.3	0.46
int_10	Lassing	secondary	445465.76	5261582.7	1526.4	0.3
int_11	Wieden	secondary	445649.31	5263301.27	967.3	2.09
int_12	Wieden	primary	452297.96	5261514.34	1215.6	0.33
int_13	Höllensteinalm	primary	403074.23	5242374.19	2007.3	0.37
int_14	Hochwurzen	secondary	396578	5247450.43	1451.7	0.33
int_15	Schwarzkogel	primary	411014.33	5247847	1330.4	0.45
int_16	Großsölk-Ebeneck	secondary	422961.38	5248608.69	1130.8	0.56
int_17	Moditzen	secondary	424927.73	5246144.8	1349.5	0.41
int_18	St.Nikolai im Sölktal	primary	426890.48	5240865.01	1435.8	0.59
int_19	Hochwurzen	primary	398860.33	5246698.68	1080.1	0.6
int_20	Hauser Kaibling	secondary	408804.58	5248831.93	1405.2	1.01
int_21	Hochwurzen	primary	398364.32	5247328.89	1213.7	0.84
int_22	Gössenberg	primary	413061.47	5249515.8	1324.9	0.65
int_23	Elmeck-Kleinsölk	primary	421135.33	5249340.06	1121.6	0.42
int_24	Brandwall-Mitteregg	primary	440121.85	5257767.87	1357.8	0.31
int_25	Halserkogel-Moarkogel	secondary	446038.15	5234631.2	1635.2	0.31
int_26	Roßalmspitz	primary	441179.06	5235242.49	1660.6	0.48
int_27	Bröckelalm	secondary	420177.35	5245041.04	1419.3	0.56
int_28	Hahnalpl	secondary	436197.58	5244379.9	1335.5	0.41
int_29	Fuchsriedl-Fuchsberg	secondary	432460.08	5255285.54	1252	0.36
int_30	Kochofen	secondary	416130.3	5251542.45	1037.8	0.93
int_31	Kochofen	secondary	417599.73	5251820.45	1102.4	1.97
int_32	Kleinhansl	primary	444642.69	5242102.75	2041.3	0.41

App. Table 3: List of the DSGSDs obtained by literature research. Mass movements which are displayed in grey font were not affirmed in course of the GIS-Analysis. (GBA refers to Geologische Bundesanstalt – Geological Survey of Austria)

ID	name	main reference	further references
1	Ahrnspitze - Oberkar - Großsölktal	Hermann (1997)	GBA, 03.10.2016
2	Niedereck - Knalltal	Hermann (1997)	
3	Schusterstuhl - Strickertal	Hermann (1997)	GBA, 03.10.2016
4	Lafenberg - Schlagerwald - Sattental	Hermann (1997)	
5	Dromaispitz - Kolblacke - Kleinsölk	Hermann (1997)	
6	Moditzen - Großsölktal	Hermann (1997)	
7	Speiereck - Strickertal	Hermann (1997)	GBA (2016); Hermann, S.W. (1996); Hermann and Becker. (2003)
8	Ebeneck - Großsölktal	Hermann (1997)	GBA (2016); Hermann, S.W. (1996, 2002); Hermann, S.W. and Becker, L.P. (2003);
9	Zinken - Kleinsölktal	Hermann (1997)	
10	Schladmingeralm - Sattental	Hermann (1997)	GBA (2016); Hermann, S.W. (2002)
11	Galsterbergalm - Sattental	Hermann (1997)	
12	Ochsenkarhöhe - Sattental	Hermann (1997)	
13	Kochofen - Fleischkögel - Kleinsölktal	Hermann (1997)	GBA (2016); Hermann, S.W. (1996. 2002); Hermann, S.W. and Becker, L.P. (2003)
14	Lafenbergal - Kleinsölktal	Hermann (1997)	
15	Hahnlberg - Kleinsölktal	Hermann (1997)	GBA, 03.10.2016; Hermann (1996, 2002); Hermann and Becker(2003);
16	Mittereck - St.Nikolai im Sölktal	Hermann (1997)	
17	Scheibenkogel - St.Nikolai im Sölktal	Hermann (1997)	GBA, 03.10.2016; Hermann, S.W. (2002)
18	Sonntagskarzinken - Obertal	Hermann (1997)	
19	Vorderer Wildkarstein - Untertal	Hermann (1997)	GBA (2016) Hermann and Becker (2003); Hermann (2002)
20	Mandelspitze - Riesachtal	Hermann (1997)	
21	Placken - Riesachtal	Hermann (1997)	GBA (2016); Hermann, S.W. (2002)
22	Zachenschöberl - Niederöblarn	Hermann (1997)	
23	Planai - Schladming - Ennstal	Hermann (1997)	GBA (2016) Hermann and Becker (2003); Hermann (2002)
24	Hauser Kaibling - Haus - Ennstal	Hermann (1997)	GBA (2016) Hermann and Becker (2003); Hermann (2002)
25	Hühnerkogel-Scharnitzgraben	Madritsch (1999)	GBA (2016); Madritsch (1999)
26	Hoher Zinken - Bärental	Madritsch (1999)	GBA (2016); Madritsch(1999)
27	Jauriskampel - Edelweißwand	Madritsch (1999)	GBA (2016) Madritsch (1999)
28	Reiteralm	GBA (2016)	
29	Hochwurzen	GBA (2016)	
30	Höllermahd	GBA (2016)	

ID	name	main reference	further references
31	Hochfeldmandl	GBA (2016)	
32	Guschen	GBA (2016)	Hermann and Becker (2003)
33	Sonntagskarzinken	GBA (2016)	Hermann and Becker (2003); Hermann (2002)
34	Niederlabeck	Hermann and Becker (2003)	Hermann and Becker (2003); Hermann (2002); GBA (2016)
35	Ebeneck - Westflanke	Hermann and Becker (2003)	Hermann (1996, 2002); Hermann and Becker (2003); Kolle (1997); GBA 2016); Schellhorn (2001)
36	Niedereck - Ostflanke	GBA (2016)	
37	Zinken - Ochsenkopfalm	Hermann (1996, 2002)	Hermann (1996, 2002); Hermann and Becker (2003); GBA (2016); Schellhorn, Ch. (2001)
38	Moditzen	GBA (2016)	Hermann, S.W. (1996, 2002); Hermann Becker (2003)
39	Brennkogel	Rauth (1996)	GBA (2016)
40	Hintergulling	Hermann and Becker (2003)	GBA (2016)
41	Jaklitschbergrutschung - Wolfsgraben	Fahrnberger 2000	GBA (2016) Hermann, S. (2002)

DATA AQUIRED BY FIELD INVESTIGATION

The in the table used numbering for the type of spring and its meaning:

Type of spring	
protected	1
unprotected - natural	2
protected - with overflow	3
protected - water protection area	4
drainage pipe + natural spring	5
drainage pipe	6
protected - water protection area and overflow	7
surficial water channel	8

App. Table 4: Parameters and Data for springs at DSGSD Hauser Kaibling.

Name	X	Y	Z	Q	eC	T	Type
	UTM 33N	UTM WGS84	[m.a.s.l.]	[l/s]	[µS/cm]	[°C]	
HK_01	406945	5248192	1778	-	-	-	2
HK_02	406286	5248284	1552	0.2-0.5	50.2	6.4	1
HK_03	406208	5248449	1493	0.5-1.0	115.45	4.9	1
HK_04	406174	5248482	1469	0.2-0.5	140.95	5.25	1
HK_05	406218	5248502	1487	<0.2	108.9	6.3	1
HK_06	406246	5248507	1496	0.2-0.5	84.4	7	1
HK_07	406306	5248519	1514	0.2-0.5	82.4	6.4	1
HK_08	406306	5248519	1514	0.5	74.5	5.6	1
HK_09	405764	5248590	1285	-	-	-	2
HK_10	405750	5248791	1285	0.5-1.0	88.7	7	1
HK_11	405754	5248740	1283	-	-	-	2
HK_12	405747	5248768	1282	0.5-1.0	83.5	7.7	1
HK_13	405748	5248751	1281	-	-	-	2
HK_14	406899	5249733	1179	0.2-0.5	63.1	9.7	1
HK_15	406222	5249772	1197	-	-	-	2
HK_16	408657	5248999	1440	-	-	-	2
HK_17	408489	5249001	1503	-	-	-	2
HK_18	408646	5248320	1560	<0.2	44.9	7.4	1
HK_19	408512	5247797	1589	0.2-0.5	122.1	5.1	1
HK_20	408500	5247748	1602	0.2-0.5	121.2	5.1	1
HK_21	409004	5248407	1384	1.0-2.0	224.7	5.5	3
HK_22	408924	5248655	1381	-	44.5	11.6	1
HK_23	408988	5248747	1349	0.2-0.5	43.6	11.3	1
HK_24	409021	5248763	1338	-	-	-	5
HK_25	409029	5248684	1336	0.5-1.0	105.5	13.3	1
HK_26	409070	5248622	1333	0.5-1.0	169.6	9.8	1
HK_27	409087	5248344	1327	0.2-0.5	163.1	11.4	6
HK_28	409089	5248289	1323	-	-	-	2
HK_29	407119	5250256	1052	-	-	-	5
HK_30	409068	5247781	1307	-	-	-	2
HK_31	409277	5248829	1253	0.2-0.5	190.5	15.4	4

Name	X	Y	Z	Q	eC	T	Type
	UTM 33N	UTM WGS84	[m.a.s.l.]	[l/s]	[µS/cm]	[°C]	
HK_32	409200	5249314	1220	2.0-5.0	139	5.6	3
HK_33	407871	5249721	1207	0.2-0.5	151.6	9	3
HK_34	407708	5248674	1537	0.5-1.0	180.1	4.3	1
HK_35	407708	5248695	1527	1	181.1	4.6	4
HK_36	407695	5248772	1497	0.5-1.0	197.8	5.4	3
HK_37	407005	5250570	906	2.0-5.0	96.7	8.2	5
HK_38	407357	5248988	1494	0.5-1.0	81.1	5.5	3
HK_39	407355	5248896	1529	1.0-2.0	150	5.8	3
HK_40	407082	5248838	1538	0.5-1.0	300	4.7	3
HK_41	407086	5248820	1549	0.5-1.0	38.4	7.5	1
HK_42	406856	5249181	1414	<0.2	65.3	5.5	6
HK_43	407446	5249528	1351	5.0-10.0	189.1	8	3
HK_44	406189	5249439	1309	0.2-0.5	56.3	5.6	1
HK_45	406209	5249434	1315	0.5-1.0	94.7	5.7	1
HK_46	406231	5249529	1277	<0.2	95.5	6.7	1
HK_47	408260	5249098	1499	<0.2	199	9	3
HK_48	409016	5249179	1294	0.2-0.5	109.6	7.8	5
HK_49	408914	5249334	1312	1.0-2.0	95.5	7.3	1
HK_50	407929	5249412	1282	0.5-1.0	135.2	5.8	1
HK_51	408147	5249649	1260	0.2-0.5	230	12.3	1
HK_52	408142	5249628	1267	1.0-2.0	211	11.5	7
HK_53	406990	5249704	1209	0.2-0.5	173.7	11.7	7
HK_54	406924	5249735	1176	-	-	-	2
HK_55	407336	5250296	1081	-	-	-	2

App. Table 5: Parameters and Data for springs at DSGSD Großsölk.

Name	X	Y	Z	Q	eC	T	Type
	UTM 33N	UTM 33N	[m.a.s.l.]	[l/s]	[µS/cm]	[°C]	
GS_01	422504	5247845	1445	<0.2	15.4	8	2
GS_02	422144	5248359	1486	<0.2	11	7.3	2
GS_03	422144	5248417	1486	<0.2	8.5	21.6	2
GS_04	422083	5248262	1510	<0.2	8.5	15.9	2
GS_05	422084	5248251	1512	<0.2	9.1	10.8	2
GS_06	423196	5247599	1238	na	35.8	14.3	2
GS_07	421870.2	5247860.1	1620	0.2-0.5	9.1	5	2
GS_08	423084	5247560	1298	0.5-1.0	38.4	6.5	2
GS_09	423180.2	5247658.2	1257	na	26.6	4.2	2
GS_10	422945.3	5247474.6	1377	2.0-5.0	31.8	4.1	2
GS_11	422619.8	5247768.3	1435	2.0-5.0	28.8	4.5	6
GS_12	422042	5248029.8	1548	0.2-0.5	10.6	6	2
GS_13	422467	5247803.1	1467	0.2-0.5	23.1	6.2	2
GS_14	422550.7	5247709.8	1464	0.2-0.5	23.5	5.6	2

App. Table 6: Parameters and Data for springs at DSGSD Moditzen.

Name	X	Y	Z	Q	eC	T	Type
	UTM 33N	UTM 33N	[m.a.s.l.]	[l/s]	[µS/cm]	[°C]	
MOD_01	424606.3	5246733.4	1196	<0.2	25.3	8.8	2
MOD_02	424270	5246739	1248	na	18.1	9	2
MOD_03	424264.1	5246758.9	1236	na	34.2	7.2	2
MOD_04	424396	5246707	1250	0.2-0.5	42.6	6.7	2
MOD_05	424499	5246613	1271	0.5-1.0	23.2	7.1	2
MOD_06	424645	5246518	1288	1.0-2.0	36.8	5.7	2
MOD_07	424657.6	5246500.4	1286	na	36.9	5.8	2
MOD_08	424414	5246490	1350	na	24.7	6.8	2
MOD_09	424686	5246500.5	1277	na	22.7	6.7	2
MOD_10	424809	5246269	1311	na	30.6	8	2
MOD_11	424733	5246887	1100	0.2-0.5	33.8	7.7	2
MOD_12	424415.9	5246473.9	1356	na	31	8.1	2
MOD_13	424514	5246118	1474	<0.2	28.1	5.4	2
MOD_14	424521.5	5246076.3	1478	<0.2	21.5	9.3	2
MOD_15	424024	5246151	1589	<0.2	24.6	5.1	2
MOD_16	424593.9	5246037.8	1461	1.0-2.0	23.9	11.9	2